



TECHNISCHE
UNIVERSITÄT
WIEN

Vienna University of Technology

Diplomarbeit

New Design of an Ion Source Control Software and Investigations of Ion-Induced Electron Emission from LiF

ausgeführt am

Institut für Angewandte Physik
der
Technischen Universität Wien

unter Anleitung von

Univ.-Prof. Dr. Friedrich Aumayr
und **DI Gregor Kowarik**

durch

Kai Iskratsch

Matrikelnummer: 9525885

Stumpergasse 24/3

1060 Wien

Wien Oktober 2009

Abstract

The present thesis describes the new Control Software for the Electron Cyclotron Resonance Ion Source (ECRIS) SOPHIE, the changes that were made to the setup of the Ion Source (IS), and the measurements performed for Ion-Induced Electron Emission (IIEE) from a Lithium Fluoride (LiF) crystal under ion impact.

The SOPHIE ECRIS, has been in use for a few years now and became an important tool for the workgroup. Over the last years people have collected a list of possible improvements, requests for changes and bugs for the software and the IS. The first part of the work was to design a completely new control software, which is based on that feedback. Also some hardware changes had to be implemented to improve working with the IS.

While Electron Emission (EE) from conductors has been studied a lot in the past 20 years using different experimental setups and theoretical models, the IIEE from insulators is still a rather fresh area. Some recent works measured EE from LiF under impact of Highly Charged Ions (HCI) using the electron emission statistics method. The aim of this work was to validate that a current method can be used for total electron yield measurements on insulators as well. Compared to conductors where the current method was used very successfully, insulators have the problem of a strongly reduced charge transport. If the charge cannot be transported away from the impact position fast enough the ion current will not work and the target will just get charged.

But heating of the insulator improves the mobility of the ions in the ionic crystal (ionic conductance). If the experiments can be done with a hot enough target and low enough ion currents, then we might be able to reach a state where charge is transported away with at least the same speed as the impacting ions create it. This would allow measuring the target current and avoid getting charging effects on target, while for the duration of an individual ion-induced electron emission event (typically some $10^{-12}s$) the target would still behave as an insulator.

The basis for these experiments was the already existing EYE experiment. Due to high blind currents with the existing filament-based target heating system, we had to design a new target holder without any direct contact between target and the heating wires. To estimate the reliability of these measurements simulations in SIMION were made.

Measurements were performed for singly and multiply charged Argon (Ar) and Xenon (Xe) ion impact on LiF . In the case of Ar projectiles good agreement with the emission yields obtained by the electron statistics technique was found. For multiply charged Xe ions ($1 \leq q \leq 7$) data on electron emission yields are presented for the first time.

Kurzfassung

Die vorliegende Diplomarbeit beschreibt die Entwicklung der neuen Kontrollsoftware für die Elektron-Zyklotron-Resonanz Ionen Quelle (engl. Electron Cyclotron Resonance Ion Source (ECRIS)) SOPHIE, die notwendigen Änderungen am Labor Aufbau, und die durchgeführten Messungen zur Ionen-induzierten Elektronenemission (IIEE) von einem Lithium Fluorid (LiF) Kristall unter Beschuss mit einfach und mehrfach geladenen Ionen.

Die ECRIS SOPHIE ist jetzt seit einigen Jahren im Betrieb und wurde in dieser Zeit ein wichtiges Werkzeug für die Arbeitsgruppe. Während dieser Zeit hat sich aber auch eine Liste mit Vorschlägen für mögliche Verbesserungen und Wünschen für Änderungen für die Kontrollsoftware sowie für die Hardware der Quelle angesammelt. Deshalb war der erste Teil der Arbeit die Entwicklung einer neuen Kontrollsoftware für die Ionenquelle, die auf diesem Feedback aufbaut. Unterstützend dazu wurden auch einige Änderungen an der Hardware der Ionenquelle durchgeführt um die Arbeit mit SOPHIE zu vereinfachen.

Während die Ionen-induzierte Elektronenemission von leitenden Oberflächen in den letzten 20 Jahren mit Hilfe verschiedener experimenteller Methoden und theoretischer Modelle sehr gründlich untersucht wurde, ist die IIEE von Isolator Oberflächen noch ein recht neues Forschungsgebiet. Kürzlich wurde die Elektronen Emission (EE) von LiF unter Beschuss mit hochgeladen Ionen (engl. Highly Charged Ions (HCI)) erfolgreich mit Hilfe der Elektronenstatistikmethode gemessen. Deshalb befasst sich der zweite Teil dieser Arbeit mit der Überprüfung, ob die einfachere Strommessmethode auch für die Messung der totalen Elektronenemissionsausbeute (engl. yield) γ auf Isolatoroberflächen eingesetzt werden kann. Verglichen mit Leitern bei denen die Strommessmethode sehr erfolgreich eingesetzt wurde, haben Isolatoren das Problem einer stark reduzierten Leitfähigkeit. Wenn aber die Ladung nicht schnell genug vom Einschlagsort abtransportiert werden kann, wird kein Ionenstrom zustande kommen und das Target wird sich elektrisch aufladen.

Für Ionenkristalle erhöht sich aber die ionische Leitfähigkeit mit der Temperatur. Das eröffnet die Möglichkeit, dass bei ausreichend hoher Temperatur und kleinen Ionenstrahlintensitäten, sich ein Zustand einstellt, in dem die Ladung mindestens so schnell wieder abtransportiert wird wie die einschlagenden Ionen die Ladung auf dem Target erzeugen. Damit wäre es möglich, den Targetstrom zu messen und Ladungseffekte am Target zu vermeiden, während sich das Target aber für die Dauer eines einzelnen Elektronenemissionsereignissen (üblicherweise einige $10^{-12}s$) wie ein Isolator verhält.

Die Grundlage für diese Experimente war das bereits existierende EYE Experiment. Aufgrund der hohen Leckströme mit der original Targetheizung, mussten wir einen neuen Targethalter designen ohne jeglichen direkten Kontakt zwischen dem Target und der Hei-

zung. Die Zuverlässigkeit der Messungen mit der geänderten Apparatur wurde mit Hilfe von Simulationen in SIMION überprüft.

Zum Abschluss wurden Messungen für die IIEE yields γ von LiF bei Beschuss mit einfach und mehrfach geladenen Argon (Ar) und Xenon (Xe) Ionen durchgeführt. Für Ar Ionen wurde eine gute Übereinstimmung mit existierenden Yield Daten, welche mit der Elektronenstatistikmethode gemessen wurden, gefunden. Für mehrfach geladene Xe Ionen ($1 \leq q \leq 7$) wurde erstmalig der totale Elektronenemissionsausbeute präsentiert.

Contents

Abstract	iii
Kurzfassung	v
1 Introduction	1
1.1 General Remarks and Structure of the Thesis	1
1.2 State of the Art and Motivation	5
1.3 Ion Induced Electron Emission	7
1.3.1 Introduction	7
1.3.2 Kinetic Emission	8
1.3.3 Potential Emission	8
2 Experimental Setup and Methods	11
2.1 ECR-Ion Sources	11
2.2 SOPHIE	12
2.2.1 SOPHIE Hardware	14
2.3 SOPHIE Control Software	18
2.3.1 Introduction	18
2.3.2 Program Details	19
2.3.3 Configuration of the Software	27
2.4 Augustin Lab Setup	30
2.4.1 Changes made during this work	32
2.5 The EYE	37
2.5.1 The Current Measurement Method	37
2.5.2 Setup of Electron Yield Experiment (EYE)	39
2.5.3 Changes made during this work	42
2.5.4 Validation of the Measurements	43
3 Results	49
3.1 Ar^{q+} on LiF	49
3.2 Xe^{q+} on LiF	58

3.3 Estimation of the Error	61
4 Conclusions and Outlook	63
Acknowledgements	65
Bibliography	66
A Appendix	73
A.1 List of used or reserved I/O Connectors	73
A.2 CAD Drawings	75
A.2.1 CAD Drawings for the Faraday Cups	75
A.2.2 CAD Drawings for the Indirect Heated Targetholder	81

List of Figures

1.1	Impact of an HCI - processes leading to PE	9
1.2	Differences in PE for conductors and insulators	10
2.1	Operation principle of an ECRIS	11
2.2	Schematic picture of SOPHIE	13
2.3	Photo of SOPHIE	14
2.4	Photo of the SOPHIE racks	15
2.5	Connections between the control PC and the SOPHIE hardware	17
2.6	NX works as an additional layer over the X - Windows protocol	18
2.7	Screenshot of the main-window of the control software	21
2.8	Scope tab in 2nd window of the software	22
2.9	Measure/load spectrum tab in 2nd window	23
2.10	Peak detection tab of the 2nd window	24
2.11	Fit peaks tab in the 2nd window	25
2.12	Schematic drawing of the Augustin Lab setup	31
2.13	Augustin Lab seen from above	32
2.14	Faraday-cup in both positions in the CF-35 4 way cross	34
2.15	Exploded view drawing of the Faraday-cup	35
2.16	Ar Spectrum measured in the new Faraday Cup	35
2.17	Photo of the assembled Faraday-cup	36
2.18	Electrodes in EYE in different states	38
2.19	CAD picture of the EYE setup	39
2.20	Photo of the Mesh used in EYE	40
2.21	Targetholder originally used in EYE	41
2.22	The 3 States in ISA and EYE Measurements	42
2.23	New targetholder CAD images	44
2.24	Schematic picture of the Targetholder	44
2.25	Temperature simulation of the new targetholder design	45
2.26	Influence of increasing charge on the target	45
2.27	Currents measured for varying mesh potential	46
2.28	Currents measured for varying collector potential	46

2.29	Yield dependency on ion current for different temperatures	47
2.30	Yields over time for different ion currents	48
3.1	Transparency c' for the different Ar projectile energies	50
3.2	Dependency of the yield γ_2 on transparency c	51
3.3	Yields for Ar Ion Impact on LiF	53
3.4	Ionisation energies and potential energies for different charge states of Ar and Xe	54
3.5	Direct comparison of the yields form LiF for Ar^+	55
3.6	Direct comparison of the yields form LiF for Ar^{3+}	56
3.7	Direct comparison of the yields form LiF for Ar^{6+}	56
3.8	Transparency c' for the different Xe projectile energies	58
3.9	IIEE yields for Xe Ion Impact on LiF	59
3.10	Comparison of the measured yields γ between Ar and Xe projectiles of the same charge state.	60

Listings

2.1	Example for saved Output Settings	22
2.2	Contents of IO.csv	28
2.3	Example for an IO-Abstraction configuration section in Sophie.conf	29
2.4	Example for a section configuring a VISA serial device in Sophie.conf	29
2.5	Example for a section configuring a DAQ input device in Sophie.conf	29
2.6	Example for gases.csv	29
2.7	Example for Fit.conf	30

1 Introduction

1.1 General Remarks and Structure of the Thesis

This thesis was carried out in the research group of Professor F. Aumayr at the “Institut für Allgemeine Physik”¹ of the Vienna University of Technology. The experimental parts were mainly supervised by DI Gregor Kowarik as part of his PhD thesis.

While no new experiment was built during this thesis, still about any part that is needed to setup a new experiment had to be executed during this thesis, from the solicitation of quotations for power supplies, over designing parts in CAD Software to assembling these parts and developing the control software.

Parts of the work on the Electron Yield Experiment (EYE) were done in collaboration with Elisabeth Gruber who was working on her bachelor thesis [1].

The basic design for the new Control Software was presented in a short talk at the ITS-LEIF Winterschool in March 2009, and some early results for the IIEE from LiF measured with the current method were presented by Gregor Kowarik in a poster [2] in May 2009 at the 4th Annual Meeting of the EU network ITS-LEIF.

Goals

The main goals of this thesis were

- Designing and programming a new control software for the Electron Cyclotron Resonance Ion Source (ECRIS) SOPHIE, and working on improvements for the whole workflow with the Ion Source (IS). This included lots of smaller tasks like sizing and then ordering replacements for the magnet power supplies, designing new Faraday cups for the 3 beam lines which can be moved in and out of the beam, testing a field calibration for the sector magnets, and adding flow measurements for the magnet water cooling.

¹renamed to “Institut für Angewandte Physik” (english name “Institute of Applied Physics”) on Oct 1st, 2009

- Modifying the existing EYE experiment to be able to work with an insulating target, and doing simulations and measurements to validate if and under what parameters the current method with a collector can be used for measuring Ion-Induced Electron Emission (IIEE) from insulators too.
- measuring IIEE yields for singly and multiply charged Argon (Ar) and Xenon (Xe) ions on Lithium Fluoride (LiF).

Structure

The written thesis is split into 3 chapters, **1 Introduction** which consists of some general information, motivation plus a short theory chapter on IIEE. **2 Experimental Setup and Methods** describes the experiment setups and methods used for this thesis. And finally **3 Results** shows the results produced during the experiments.

Contents of the CD

Folder	Subfolder	Contents
CAD	EYE	Solidworks 2009 CAD files for the redesign of the targetholder, including the thermal simulation
CAD	SOPHIE	Solidworks 2009 CAD files for the moving Faraday cup design
Software	SOPHIE Control	LabVIEW 8.6 Source Code of the SOPHIE Control Software. Load the project file with LabView.
Software	Scripts	The scripts used for a few automatic tasks on the Control Computer for SOPHIE
Software	Kernel Modules	The sources for the manually compiled kernel modules used on the Control Computer
Software	Documentation	Documentation for the new Control Software
Data	Measurements	raw Measurement Data of the IIEE measurements
Data	Evaluation	Kaleidagraph files with the evaluated Data
Thesis		electronic form (pdf) of this thesis
Thesis	Latex	latex sources for this thesis
Thesis	Figures	Kaleidagraph files and other original files for the figures that were created new for this thesis

Shorts and acronyms

This is a complete list of the acronyms and short forms used in this thesis.

Ar Argon

<i>Ar^{q+}</i>	Argon ions in (different) charge states q
BL	beamline
CAD	Computer Aided Design
COB	classical over-the-barrier (model)
csv	comma separated values - a file format that stores data separated by comma or sometimes other separation characters
DVI	Digital Visual Interface - a video interface standard used mainly for connecting LCD Displays to Computers
DAQ	Data Acquisition
ECR	Electron Cyclotron Resonance
ECRIS	Electron Cyclotron Resonance Ion Source
EE	Electron Emission
eV	electron Volt - an energy unit used in atomic, nuclear and particle physics. It equals the energy that a single unbound electron gains when it is accelerated by a potential difference of 1V
EYE	Electron Yield Experiment : the existing experiment for measuring IIEE built by Michael Brunmayr during his master thesis [3]
HA	Hollow Atom
HCI	Highly Charged Ions
HV	high voltage
IIEE	Ion-Induced Electron Emission
IS	Ion Source
KE	Kinetic (electron) Emission
<i>LiF</i>	Lithium Fluoride
PE	Potential (electron) Emission
PTFE	polytetrafluoroethylene - usually known by the brand name Teflon
QP	quadrupole magnet

RN	Resonant Neutralisation
RS232	recommended standard 232 - a standard serial interface, which was used on all computers in the past, now getting more and more replaced by USB, but it is still widely used in communication between computers and lab equipment
SE	secondary electrons
SM	sectormagnet
SOPHIE	SO urce for P roduction of H ighly charged I ons using ECR : the ECRIS of the AG Aumayr built by Ernst Galutschek during his PhD thesis [4]
SSH	secure shell - is an encrypted network protocol that allows secured access to remote shells
SVN	subversion - is a version control system, that maintains current and older versions of files, and allows multiple users to work on the same project
USB	Universal Serial Bus - Serial Bus Interface used on computers since 1996
UHV	Ultra High Vacuum
XDMCP	X Display Manager Control Protocol : the X - Windows Protocol that allows to run a graphical session on a remote computer (for more details see [5])
Xe	Xenon
Xe^{q+}	Xenon ions in (different) charge states q

Symbols

These Symbols for physical properties have been used in this thesis

- e - electron charge
- q - charge state of the ion (not the actual charge $q * e$)
- n - number of electrons
- γ - electron yield
- E - energy
- E_{kin} - Kinetic energy
- E_{pot} - Potential energy

1.2 State of the Art and Motivation

ECRIS are widely used for different applications like in high energy physics where they are used for production of high quality ion beams for particle accelerators, medical applications where they are used in cancer treatment, and in semiconductor industry. The ECRIS design derived from Electron Cyclotron Resonance (ECR) plasma heating used in fusion experiments, and soon got an important spot as IS in experiments that required stable beams of single and multiply charged ions.

An ECRIS for use in research with different experiments connected to it, requires a lot flexibility. The source usually has to be able to produce stable beams with good intensity from ions of different atoms or molecules, and should be able to produce ions with different charge states and different energies for each experiment. This requires controlling multiple parameters in the source, which can lead to a lot of time spent optimising the source parameters. Today computers are usually used to control these parameters, also other tasks like measuring spectra and evaluating them get much easier with the help of computers.

For efficient work this requires a software that is intuitive and can help the people working with the ion source to be more productive.

SOPHIE is the modern all permanent magnet 14.5 GHz ECRIS at the “Institut für Allgemeine Physik” of the Vienna University of Technology [6]. It was originally controlled with the CODIAN Software by J. Bundesmann [7]. In its current position in the Augustin Lab SOPHIE is connected to 3 beamlines which hold the MUSIC (MULTipurpose Solid-target Irradiation Chamber), the quartz crystal microbalance and the EYE experiments.

Ion-surface interaction has been an important research for some time now. Detailed knowledge of the different processes involved with these interactions is especially important for fusion research, where plasma wall interaction plays an important role. Sputtering yields [8, 9] and electron emission coefficients [10] are important criteria for selecting wall materials for fusion experiments and future reactors. But fusion research is not the only field for which ion-surface interactions are relevant. In nanostructuring of surfaces by highly charged ion impact different ion induced irradiation defects in the forms of pits [11] and hillocks [12] have been observed recently. Another rather new research topic that involves ion-surface interaction is capillary guiding of ion beams [13, 14, 15].

Like mentioned before ion-surface interaction involves multiple processes. When ions interact with solid targets the surface can be modified (sputtering, nanostructuring), the ion can be backscattered, or photons, electrons and other secondary particles (target atoms & ions) can be emitted. For this thesis the focus lies on electron emission, which is described in more detail in the next section 1.3.

IIEE from conducting surfaces has been widely studied experimentally in the last 20 years [16, 17, 18, 10], and theoretical models for both emission paths, depending on either kinetic- [19] or potential energy [20] of the projectile ions, have been found that are in good

agreement with the experiments. [21]

Contrary to that IIEE from insulators is still a rather fresh topic and there is only few data available yet. One reason for this is that, IIEE on insulators is a bit more complicated to study experimentally.

The impact of ions transports positive charges to the surface and the emitted electrons also leave positive charge behind, which when not removed fast enough will lead to charging up of the target and influence the electric fields around it. This in turn will effect the flight paths of the charged particles in the experiment. Since the emitted electrons are mostly rather low in energy their emission can be easily influenced by even small charges on the surface.

Conducting target surfaces had no problem with this, as they were simply put on a predefined potential (usually ground potential) and all charge that was created in the target on ion impact was immediately transported away by normal electrical conductance.

But insulators like alkali halides have only a small ion-based conductance that is very low at normal temperatures. At higher temperatures the ionic conductance increases mainly due to the improved mobility of the ions in the crystal.

This means IIEE experiments on insulators have to be executed at a state with high enough target temperature and low enough ion currents to reach an equilibrium state, where charge in the insulator is transported away as fast as new charge is created by ion impact, to avoid building a charge on the target that influences the experiment.

Recently successful IIEE measurements for LiF and CaF_2 crystals have been done using an electron statistics detector[22]. This raised the question if it would also be possible to use the simpler setup for the current method to measure emission yields for insulators.

The decision was made to modify the EYE experiment built and used during the master thesis of M. Brunmayr [3], to allow measurements on insulators and to test if the current method with a collector can really be used for insulator measurements too.

The first measurements on the new setup with insulator targets (mostly covered in [1]), indicated that it should be possible to use the current method with high enough target temperature and ion currents under a certain threshold, which depends on the target temperature. So further measurements were made during this thesis to compare γ for Ar impacts on LiF to older data available in [23, 24].

1.3 Ion Induced Electron Emission

1.3.1 Introduction

Impact of ions on solid surfaces leads to several different processes:

- emission of electrons (IIEE)
- emission of photons
- emission of atoms and ions (sputtering)
- backscattering of the projectile ions
- defect-production on the surface

While the other topics are also interesting topics of research, only the emission of electrons is relevant for this work. Electron emission from surfaces is a phenomenon that is not special to ion impact, it can also be observed on impact of other projectiles (including photons).

We can generally define the total emission yield γ for a projectile impacting on a surface as:

$$\gamma = \frac{N_{e^-}}{N_i} \quad (1.1)$$

where N_{e^-} is the number of electrons emitted into the half space in front of the target and N_i is the number of impacting projectiles. In the case of the IIEE these projectiles are the ions.

Electrons emitted by IIEE can be split into kinetic electron emission (KE) [25] and potential electron emission (PE) [26].

KE produces electron emission based on the kinetic energy of the projectile ion (depending on mass and velocity), while PE produces emission based on the potential energy of the ion (depending on the charge state and element).

The actual Electrons emitted by these two mechanisms are not distinguishable, so experiments can just measure the total emission yield γ . The only way to investigate these two components separately is to select conditions under which one process dominates the emission completely and the other process is negligible. To measure nearly pure KE E_{kin} has to be high (fast impact velocity) [27] while keeping E_{pot} very small (low charge state), near pure PE is observable with impact velocities slower than the threshold velocity for KE and very high charge states where ($E_{pot} \gg E_{kin}$) [28, 29, 30].

1.3.2 Kinetic Emission

For kinetic emission a part of the kinetic energy of the projectile is used to excite the emitted electrons. The actual excitation can happen because of different mechanisms. If energy transfer is at least equal to the work function W_Φ of the electrons, an emission event can occur. For direct ion-electron interaction a minimal threshold velocity v_{th} can be defined under which no emission should be found.

$$v_{th} \approx \frac{1}{2}v_F \left(\sqrt{1 + \frac{W_\Phi}{E_F}} - 1 \right) \quad (1.2)$$

With E_F the Fermi Energy and v_F the Fermi velocity [25]. But emission can also be observed below this threshold velocity. This sub-threshold KE can be explained e.g. by a promotion model. In this model the target atom and the projectile ion form a short lived quasi-molecule in which some electron energy levels can be promoted to higher energy levels, and during the decay of that state emission can occur[25, 17, 31].

Starting from the threshold velocity the KE yield shows approximately a linear behaviour with v , which in a simplified picture corresponds to the ion exciting multiple electrons along its path through the target till the kinetic energy gets too low. Only a part of these sub surface excited electrons can reach the surface and get emitted, because the penetration depth for ions is usually higher than the mean free path L for electrons. Insulators usually show higher KE yields than conductors because of the higher mean free path for electrons in insulators.[32]

1.3.3 Potential Emission

Especially Highly Charged Ions (HCI) carry a high potential energy which gets released when the ion approaches a surface and gets neutralised (see Fig. 1.1). The following will be just a short introduction to PE and the involved processes. More details can be found elsewhere e.g. [33, 34].

Contrary to KE which only happens on impact and inside the solid, PE processes start already when the ion gets close to the surface.

The interactions outside the solid consist of (cf. Fig. 1.1):

- *Image Charge Acceleration*: The acceleration created by the image charge leads to a minimum impact velocity.
- *Hollow Atom (HA) formation*: When the Ion is close enough to the surface, electrons are captured by Resonant Neutralisation (RN) and other Auger-type processes into the outer shells of the ion, leading to the formation of the so called Hollow Atom (HA) [35]

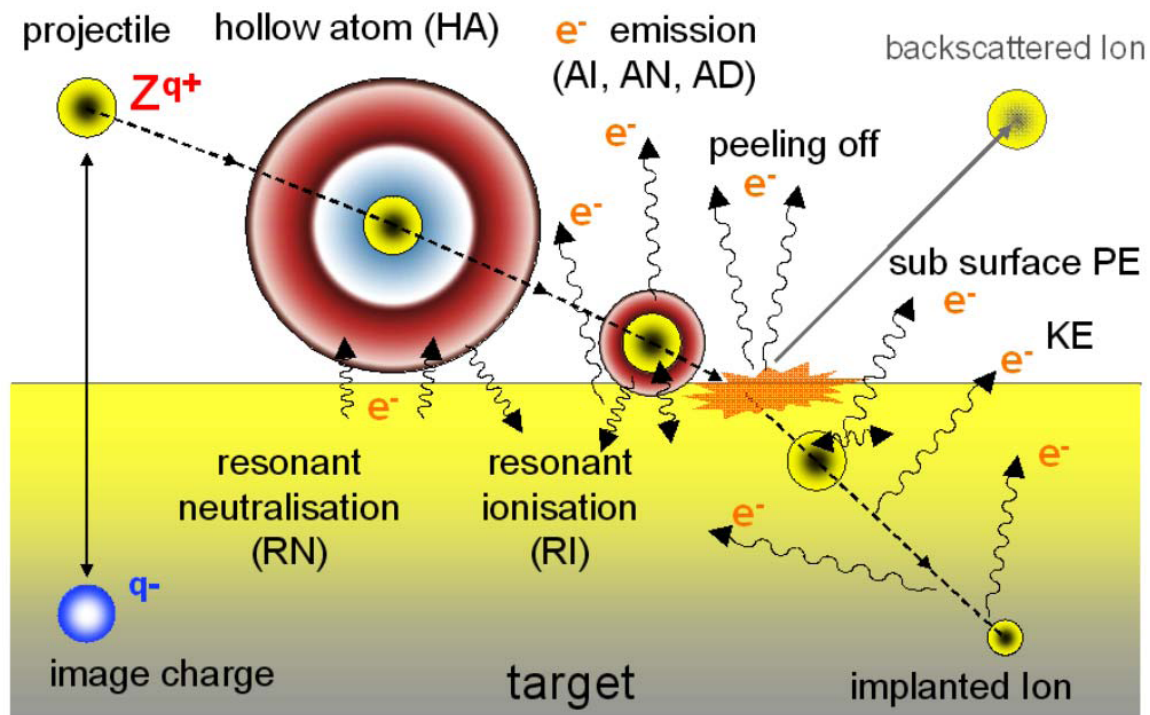


Figure 1.1: Impact of an HCI - processes leading to PE. In this picture the horizontal dimension represents time. [32]

- *HA decay*: During the de-excitation of the HA electrons are emitted, this increases the charge state and leads to a new electron capture phase. Through repetition of this process the number of emitted electrons can be higher than the initial charge state of the ion.

When the ion enters the solid the electrons in the Rydberg-states are peeled off, which leads to emission again. The final part of the interaction then happens inside the solid when the remaining free vacancies are filled in Auger Processes.

For conductors the classical over-the-barrier model (COB) [20] gives a theoretical explanation for the PE, which is in good agreement with the experiments. [29, 36],

First measurements for HCI impact on insulators showed surprisingly high yields γ which were also very dependent on impact angle. Simulations made based on a COB for insulators showed that the HA phase is happening later, when the ion is already closer to the surface, due to the increased binding energies in the target. The shorter HA phase leads to a smaller electron emission above the surface, but the projectile also enters the solid in a higher charge state, which equals higher remaining potential energies. This leads to more Auger processes happening inside the target, and inside the solid each single Auger electron can be multiplied by secondary electrons (SE) cascades. Due to the larger mean free path in the insulators also a higher part of these secondary electrons can escape from the target. (cf. Fig. 1.2)

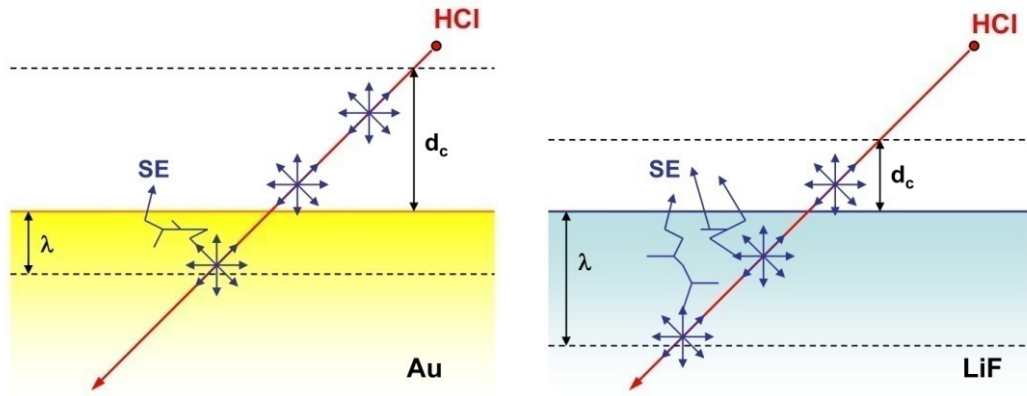


Figure 1.2: The differences in PE between Au and LiF arise from different critical distance d_c for RN, different escape depth λ for the electrons and different numbers of SE for the auger electrons. [22]

In this way the higher electron yields for HCl induced Electron Emission (EE) from *LiF* as compared to an *Au* target could be successfully explained, despite the higher binding energies for electrons in *LiF* than in *Au*. [22].

2 Experimental Setup and Methods

2.1 ECR-Ion Sources

Electron Cyclotron Resonance Ion Sources (ECRIS) are used in many laboratories to produce high quality ion beams for a wide range of experiments and applications. [37, 38] Fig. 2.1 shows a schematic view of a typical ECRIS.

An ECRIS produces ions from a magnetically confined plasma which is heated via Electron Cyclotron Resonance (ECR). For confinement usually an axial mirror field is superimposed by a radial multipole field, which results in a magnetohydrodynamical stable “minimum B” field. [40]

The injected microwaves are resonantly absorbed by the plasma electrons in an area where the microwave frequency coincides with the gyro motion frequency ω_{ECR} of the electrons in the magnetic confinement field B_{ECR} . The area where the resonant condition is true and the absorption happens (called the ECR zone) is a closed surface around the centre of the plasma. [37]

$$\omega_{ECR} = \frac{e}{m_e} B_{ECR} \quad (2.1)$$

The plasma inside an ECRIS is a typical non equilibrium plasma. There are two energy

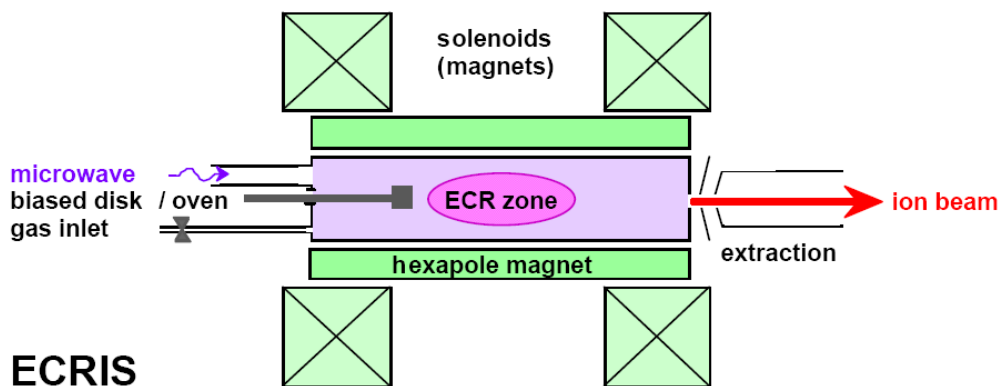


Figure 2.1: Operation principle of an ECRIS. [39]

populations for electrons, one of a cold (about 20eV) species and a hot population which has a tail reaching up to 100keV or even higher, while the ion energies in the plasma are just a few eV. This non equilibrium state aids the production of ions in higher charged states because there are some fast electrons that have enough energy to produce highly charged ions with sequential electron impact ionisation.

On the other side mainly charge exchange processes are lowering the charge states again. Since the pressure is a factor for these processes a lower working pressure can reduce the effects of charge exchange.

The confinement time for both electrons and ions is a critical factor for creating higher charge states, this makes the shape of the magnetic field important. Especially the hot electrons have fast velocities and need good confinement to avoid losing too much energy in collisions with the walls of the plasma chamber. The plasma ions are rather slow and usually less affected by the magnetic field. The not so good confinement for the ions makes it easier to extract them. When designing the magnetic field it also has to be considered that this magnetic field also needs to build the ECR zone around the centre of the plasma, to allow the resonant heating with microwaves of the right frequency.

The ion source is usually on positive high voltage to allow extraction of the ions to experiments at ground potential. The extraction is done by a simple electrode system, in many cases an "Accel-Deccel" system consisting of 3 electrodes (inner electrode on positive source potential, middle electrode on a negative suppressor potential and the outer electrode on ground potential) is used to obtain a parallel and intense ion beam.

Often also a so-called "Biased" electrode on the opposite side of the extraction is used to influence the production of electrons and ions.

Using a mix of 2 gasses (the working gas and a 2nd "lighter" gas) can aid the production of ions in higher charge states.

More detailed information about ECRIS can be found in the books and articles[41, 42, 37] .

2.2 SOPHIE

SOPHIE (**SO**urce for **P**roduction of **H**ighly charged **I**ons using **ECR**) is the 14.5 GHz ECRIS at the "Institut für Angewandte Physik" of the Vienna University of Technology. SOPHIE was built during the PhD thesis of Ernst Galutschek [4, 6], and has been in use for some years now with different experiments at the 3 beam lines.

SOPHIE uses an all-permanent magnetic field setup for the creation of the magnetic confinement, based on 4 permanent magnet rings and a Halbach-type hexapole magnet with 80mm outer diameter. Two of the rings are axial and the other 2 are radially magnetised providing the axial mirror field with a maximum of about 0.9T. Microwaves with frequencies between 12.75 and 14.5GHz are created by a thin film oscillator, and amplified

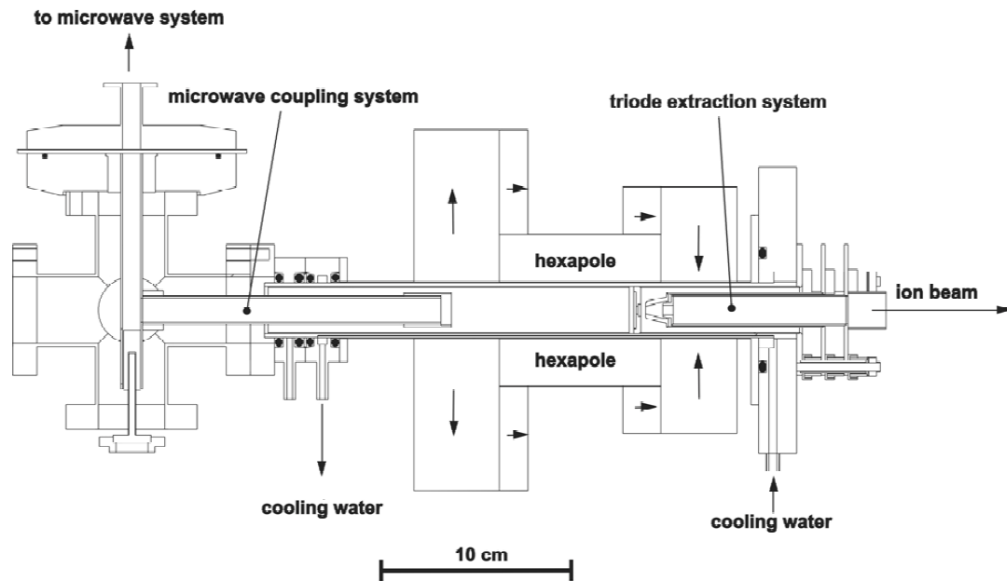


Figure 2.2: Schematic picture of SOPHIE. [4]

by a travelling wave tube amplifier with up to 300W amplification power. These microwaves are transported at ground potential by a wave guide and coupled into the vacuum chamber through a polytetrafluoroethylene (PTFE) window, the wave guide coupling system inside the vacuum chamber is also used as the biased electrode.

For supplying the working gas for the plasma, SOPHIE also has 2 gas inlets with pre-chambers and a pressure regulation for these pre-chambers, which allows the operation with a single gas or the mix of two gases at well defined pressures in the plasma chamber. There is no real limitation which gas can be used, as long as the connectors can be fitted to the gas inlets (the standard connectors are made for Minican gas containers).

This shows that SOPHIE has quite a few parameters that can be changed to optimise the plasma for the production of the ions. Here is a list of them:

- *Gas*: SOPHIE has 2 gas inlets with connectors for laboratory gas in Minicans.
- *Source Potential* (U_{Source}): This is the potential that is applied to the plasma chamber of the source. Since the beam lines and experiments are usually operated at ground voltage (except if you want to decelerate the ions), this potential together with the ion charge also defines the energy of the ions in the experiments.
- *Suppressor Voltage* ($U_{Suppressor}$): The additional voltage for the “Accel-Deccel” extraction system. It is used to shape the electric field at the extraction electrode.
- *Bias Voltage* (U_{Bias}): the Bias voltage which allows to change some of the plasma parameters.

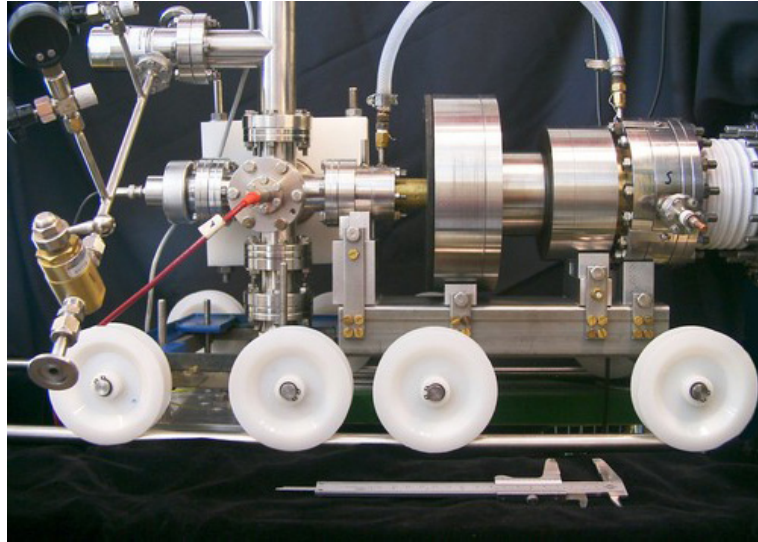


Figure 2.3: A photo of SOPHIE. [4]

- *Pressure in the Main-chamber:* Currently the pressure regulation for the gas inlet Gas 2 is connected to the main-chamber pressure so we can directly control which pressure we want in the plasma chamber. (for gas mixing the pressure regulator should be connected to the pre-chamber pressure, to allow setting the pressures for both pre-chambers independently)
- *Microwave Frequency:* The Microwave Frequency can be adjusted between 12.75 and 14.5 GHz by adjusting a voltage input for the microwave generator.
- *Microwave Power:* The Microwave Amplifier can be controlled to amplify the microwaves to a power between a minimum of a few W and a maximum of 300W.

2.2.1 SOPHIE Hardware

This should be just a short introduction into the hardware needed to operate SOPHIE to help the understanding of the new control software. Most of this hardware is located in the 2 racks, but some elements have to be in other locations, like the bias power supply which is located in the high voltage (HV) cage under SOPHIE.

Fig. 2.4 shows a Photo of the 2 racks. The left rack houses from the top to bottom:

- the pressure measurement for the SOPHIE pressure gauges and the manual switch for the BL valves, the gauge controller for the pre-chamber pressures is on the left, the controller for the main-chamber in the middle.
- the microwave amplifier
- the oscillator with the SOPHIE Cooling Water Interlock (which turns off the oscillator power if there is no cooling water flow)

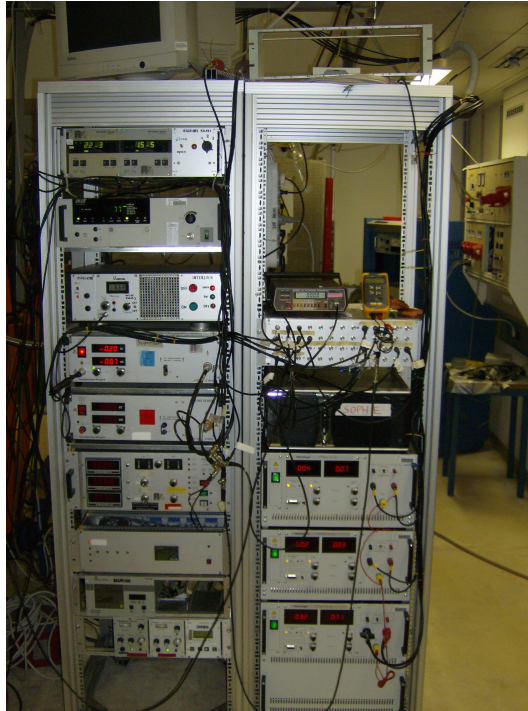


Figure 2.4: Photo of the SOPHIE racks

- the voltage source for the suppressor electrode
- the voltage source for the source potential (currently not in use)
- the controls for the old SM & QP power supply
- the interlock that interrupts HV when the cage around SOPHIE is opened and watches the pressures.
- the controllers for the turbomolecular pumps
- the controllers for the regulating valves that control the gas inlets.

In the right rack are from the top to the bottom:

- not really visible on the picture, but on top of this rack is the polarity changer box for the first sector magnet
- the pico-ammeter (on the picture a multimeter is next to it)
- the bnc connector board (which offers BNC connectors to the I/O channels of the 2 DAQ cards)
- the control computer
- the power supply(current source) for the first quadrupole

- the current source for the second quadrupole
- and the power supply (current source) for the first sector magnet

Other important hardware controls outside these racks are:

- power supply for the bias voltage, since this voltage is added/subtracted to the source potential this power supply is in the HV cage below SOPHIE.
- the currently used power supply for the source potential, which is just below SOPHIE.
- the power supply for the 2nd sector magnet plus the electronics box needed to control it (mounted in one of the wall panels)
- cooling water + flow measurement for the 2 sector magnets.

Fig. 2.5 shows how all these components are connected and controlled by the computer. The connectors for the 2 Data Acquisition (DAQ) cards (NI PCI-6034E and NI PCI-6703) are on the BNC connector board. The first 8 BNC connectors represent the digital I/O ports of the 6703 card, the next 16 BNC plugs correspond to the 16 analogue out channels of the same card, and the next 16 BNC connectors link to the 16 analogue in connectors of the 6034E card. The digital connectors of the 6034E analogue in card are currently not on the BNC board.

The microwave amplifier and the current sources for the first sector magnet and the quadrupoles are connected to the computer by RS232 serial connections. Most other devices are controlled by analogue control signals (-10V – 10V range) from the analogue out card. The digital IO lines are used for controlling the two polarity changer boxes, the valves for the pneumatic moved Faraday cups (described later in section 2.4.1) and the beamline valves, as well as for reading the status of the flow switches (which are placed in the cooling water cycles for the two sector magnets). The analogue inputs are connected to the pico-ampere meter (which is used to measure the ion currents on the Faraday cups or on different apertures), the current measurement for the plasma current, multiple pressure measurements, and the signal of the magnetic field calibration (which is still in early testing).

Additionally there are three inputs and outputs reserved as user channels, which can be used for controlling and monitoring different voltage signals.

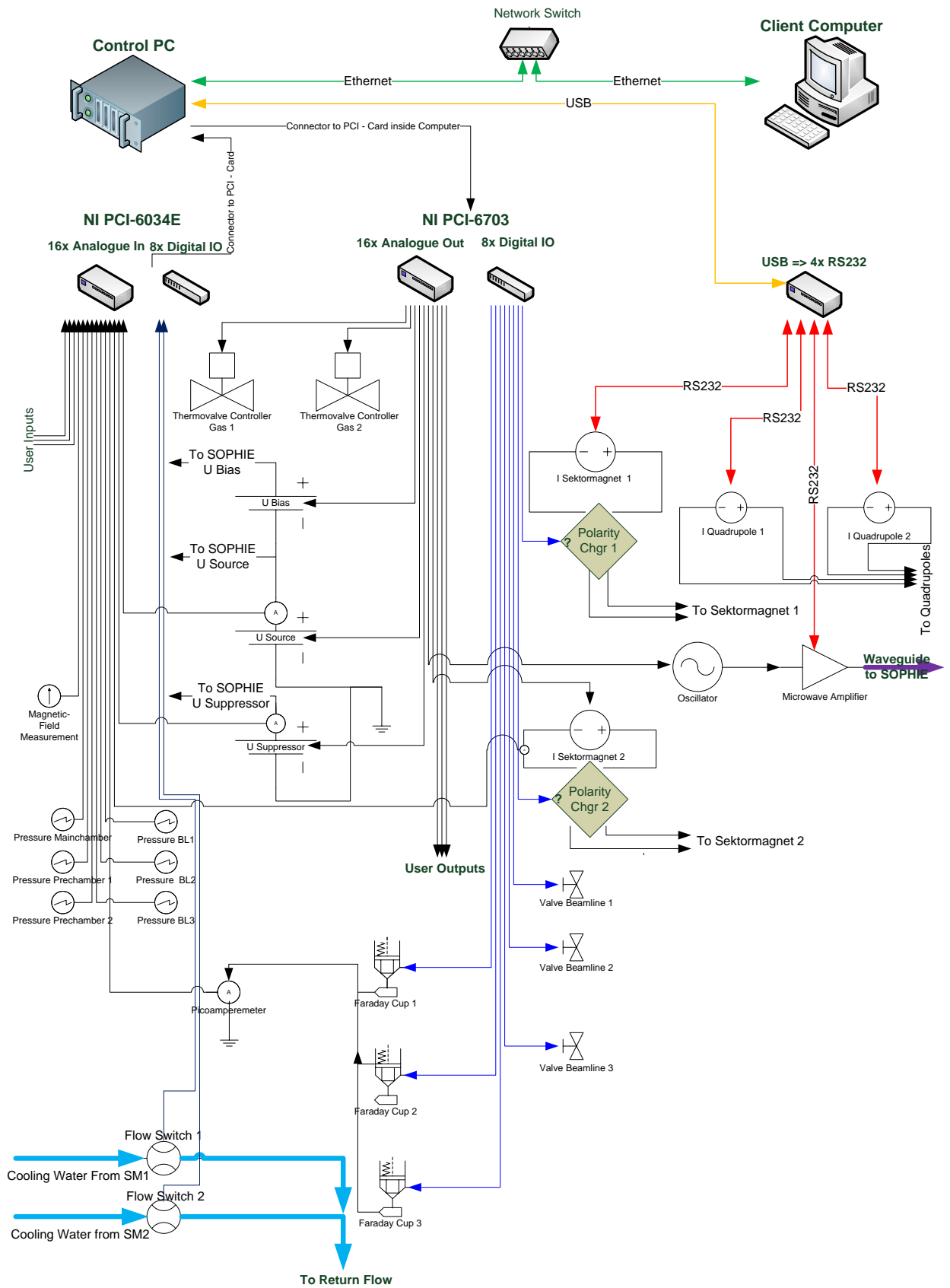


Figure 2.5: Connections between the control computer and the hardware parts of SOPHIE. Arrows indicate direction of connections, colour indicates type of connection. (black = analogue, blue = digital, special interfaces use other colours and are labelled)

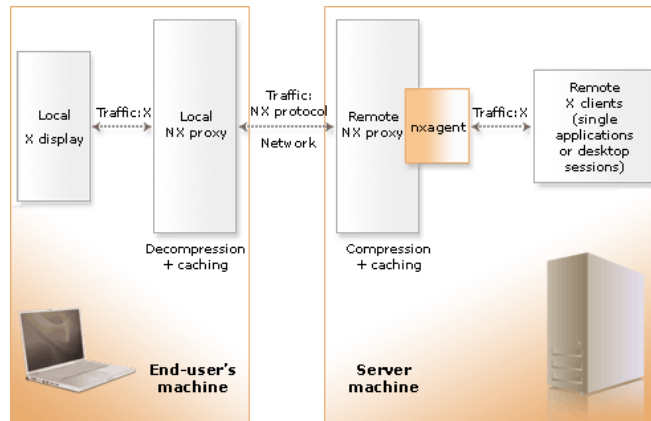


Figure 2.6: NX works as an additional layer over the X - Windows protocol. [43]

2.3 SOPHIE Control Software

2.3.1 Introduction

One big part of this thesis was designing a completely new control software for SOPHIE. The reasons for wanting a completely new software were mainly:

- the wish for a more intuitive user interface
- the old software was not developed at our institute so we had no source code for it, and therefore we were not able to change and improve it
- the old software used an old LabVIEW version and there was no guarantee how much longer we could run that software on a future computer.

After some discussions it was decided that we want a software that is implemented in LabVIEW (version 8.6), which should run on a new computer under Linux operating system and should be running on a dual 22" TFT - monitor setup for a good visual display of all parameters. Since we had some problems finding Digital Visual Interface (DVI) cables that were long enough to connect the computer in the rack directly to the monitors on the control table, we decided to use a 2 computer setup. The computer on the control desk is connected via a NX¹ client - server connection to the control computer in the rack (see Fig. 2.6). This setup also allows controlling SOPHIE from any other computer that has an NX client installed.

The control computer in the rack uses an Intel Core 2 Duo processor with 3GHz, 2GB DDR2 RAM, an ATI Radeon 2400 graphics card on a mainboard based on the Intel P45 chipset (Asus P5Q Pro). We reused the two DAQ boards from the old computer for the

¹NX is a remote desktop protocol that is based on X - Windows System connections. It adds a layer that handles compression and caching on top of the X - Windows protocol, additionally NX wraps the connections in secure shell (SSH) sessions for encryption and authentication. Like with XDMCP the whole application is running on the server computer and only the display and user interaction part is handled on the client computer. More details are available under [43]

analogue and digital I/O channels, and added a USB to 4x RS232 serial hub for connecting the devices that need serial input.

The Linux version used is OpenSUSE 11.1 as it is one of the Linux versions officially supported by National Instruments for LabVIEW and their NIDAQmx DAQ drivers. The kernel had to be compiled manually after doing a back port of the driver for the USB to RS232 hub from a staging kernel. (So exchanging the kernel is not recommended unless you really know what you do).

On this Linux system a nomachine² NX free edition server was installed (the open source freeNX from the OpenSUSE repository had some graphic problems with labview, so I switched to the free edition of the closed source product). Further important software installed is LabVIEW 8.6, NI-KAL 1.10, NI-DAQmx 8.01 and NI-VISA 4.5.

The computer also runs a cron³ script that automatically creates a backup of the whole system once a week, and keeps these files for a limited time. The job also copies the backup data with rsync⁴ to the client, vice versa the client also copies a backup of his system to the control computer. With only small changes to the rsync command the script can be modified to use a external hard-disk as backup storage medium instead.

For security reasons it might be a good idea to use a separate network between the client and the control computer, without direct connection to the outside for the control computer. It would be possible with installing a 2nd network card on the client to keep the client still connected to the Internet, and even a NAT⁵ configuration with a iptables⁶ based firewall on the client would be possible to still allow accessing the Internet from the control computer without allowing outside access to the control computer (and it would also remove the need for one ipaddress in the institute ip range).

2.3.2 Program Details

The software is developed and maintained in the subversion (SVN) repository of the workgroup. The current version of the software can be checked out from the url:

<http://eapp42.iap.tuwien.ac.at/repo/SOPHIE/trunk/Computer/SOPHIE%20Control%20Software/>

²www.nomachine.com

³cron is a time based job scheduler on Unix-like operating systems. It offers options to let jobs run automatically at a certain time and date, and is often used for doing system maintenance jobs automatically

⁴rsync is an open source program that provides incremental file transfer and can be used to synchronise data between directories, it can be used with directories on same computer but also works over the network. <http://samba.anu.edu.au/rsync/>

⁵Network Address Translation (NAT) is a technique that allows a private network to access the internet over one router or a computer working as a router. This router masquerades the ipaddresses inside the private network, the outside network can only see the router, but computers from inside the private network can still access the outside network/internet

⁶iptables is the program that allows the configuration of the firewall, which is integrated into the linux kernel

The new software uses multitasking, which means the DAQ Input and Output routines are running in the background without being interrupted by User Interface events. Also the two main windows are both running in separate tasks. To communicate between all these tasks a simple communication stack based on global variables is used. All critical write accesses to these global variables and to output devices are synchronised with semaphores⁷, to make sure that only one task at a time writes to that variable or device.

A basic hardware abstraction layer is implemented in the program to allow easy exchange of hardware components in the future, the program sees all hardware accesses as so called IOABSTR - tasks, which are defined in the configuration file, a simple change in that file can reconfigure which channel on the DAQ card a device is connected to, which scaling is used or even switch a device from being connected to a serial port to an analogue output or the other way round.

The user interface is split into 2 windows (one for each screen), the main window on screen one (see Fig. 2.7) shows a schematic drawing of the ion source and the beam lines and has the input and data display fields placed on it to allow the user to directly see which part of the setup he is modifying, and what value is displayed there.

The main window also has a "Shutdown SOPHIE on exit" toggle, which can be used to select if the click on the exit program button below that, will first set all output values to 0 and turn off microwave power (by switching the microwave amplifier to standby mode) before exiting the software, or if the ion source should continue running (by default shutdown is selected).

Additionally there are some options in the application menu, "Preferences" opens the preferences window which allows configuring some basic hardware settings, "Save Current Out Values" allows saving the values of all outputs to a file (see Listing 2.1) which can be loaded again later with "Load Output Values" to restore the same settings, "Reinit VISA Device" will pop up a dialogue which allows the user to select which VISA serial devices should be reinitialised, this can be helpful in case that communication to a device connected to a serial port is not working anymore and might save you from restarting the whole program. The final 2 options "Exit Program" and "Shutdown SOPHIE" both end

⁷In computer science a semaphore is a protected variable or data type. It is often used as a flag for locking/unlocking resources, which only one process should access at a time.

A typical workflow with semaphores looks like this:

- Each process calls a function to acquire access to the semaphore before it does any access to the protected resource.
- The acquire semaphore function only returns immediately if no other process has an open access to the semaphore. If another process has currently acquired the semaphore that function will wait till the semaphore gets available again.
- Once the process has acquired semaphore access, it is free to access the protected resource.
- When no more access to the protected resource is needed the process calls the release semaphore function which makes it free for the next process to acquire it.

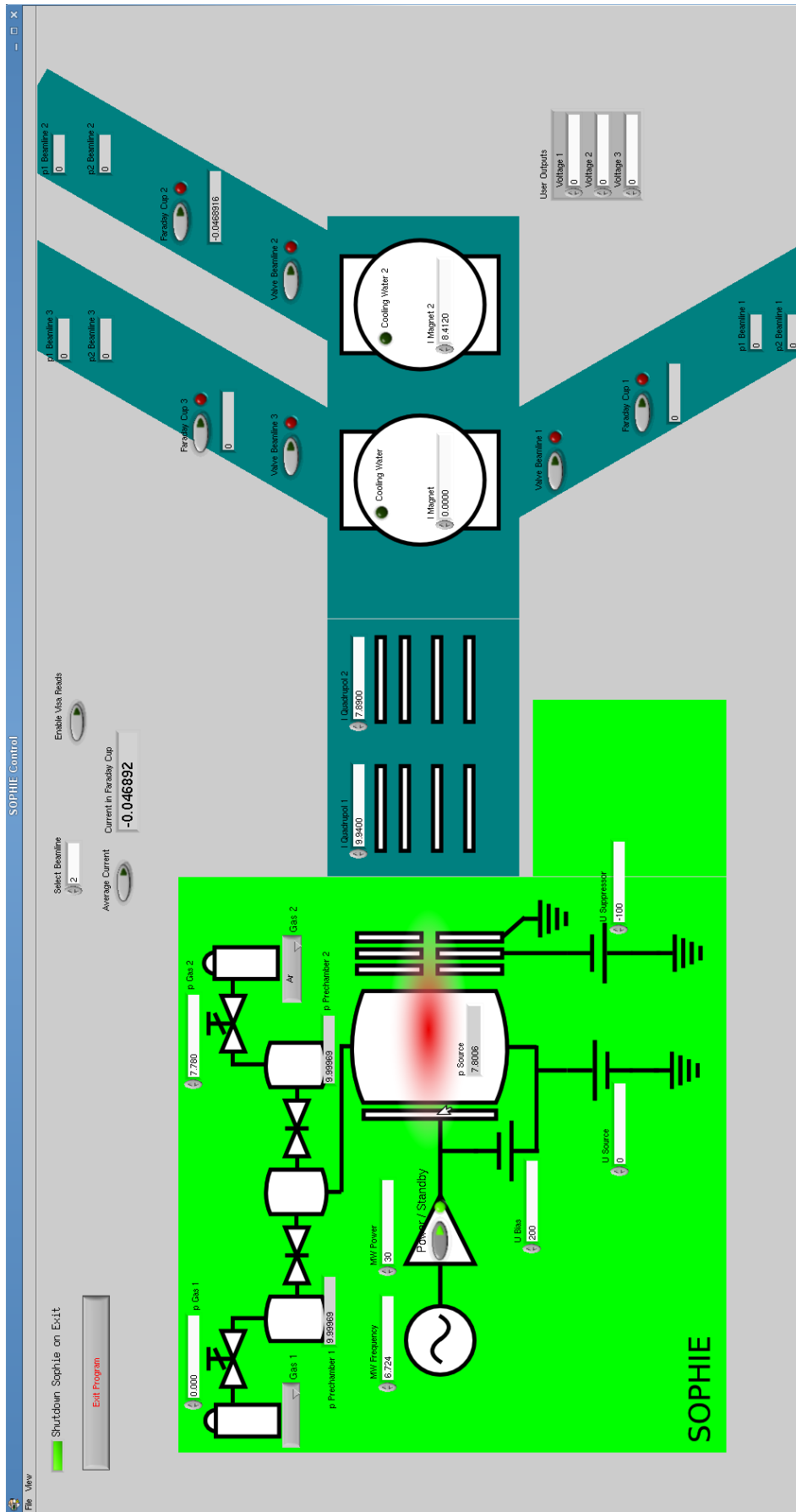


Figure 2.7: Screenshot of the main-window of the control software

Listing 2.1: Example for saved Output Settings

```
[Values]
Out U Source=1000.000000
Out U Suppressor=-100.000000
Out U Bias=-300.000000
Out I Sektormagnet 1=9.5800000
Out I Sektormagnet 2=0.0000000
Out I Quadrupol 1=3.1000000
Out I Quadrupol 2=2.5800000
Out MW Power=49.0000000
Out MW Frequency=6.68900000
Out USER1=0.0000000
Out USER2=0.0000000
Out USER3=0.0000000
Out Pressure Gas 1=0.0000000
Out Pressure Gas 2=7.35000000
Select Beamline=3.0000000
Gas 1=0.0000000
Gas 2=0.0000000
```

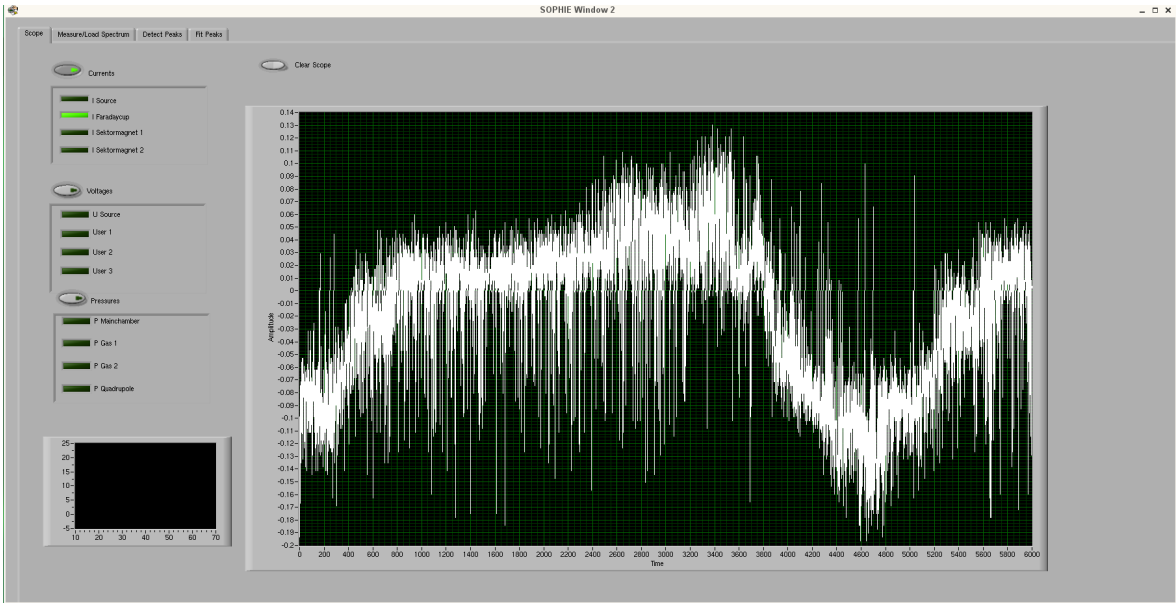


Figure 2.8: Scope tab in 2nd window of the software

the program, but the shutdown option first sets all output values to 0 and switches the microwave amplifier to standby mode.

The window on the 2nd screen has four tabs. Tab one has a configurable scope on it, tab 2 is for measuring or loading spectra, the 3rd tab is for peak detection and the last one for the peak fitting.

The scope tab (Fig. 2.8) has on the left border controls that allow the user to select what is displayed in the big scope display. All data captured via the DAQ devices is stored in arrays, so when you switch the scope on you should already see the data of the last few minutes (if you have not cleared scope data recently). Data points from the analogue DAQ devices are captured approx every 20msec, but since the capture is not really done in a real time operation the scale on the time axis does not show absolute time values. Data from devices that are connected to the serial interfaces is only captured every 500msec to avoid causing waits for data output on these serial lines (this value could probably be lowered a bit) and only when “enable VISA Reads” is selected (if that is not selected then no reads for

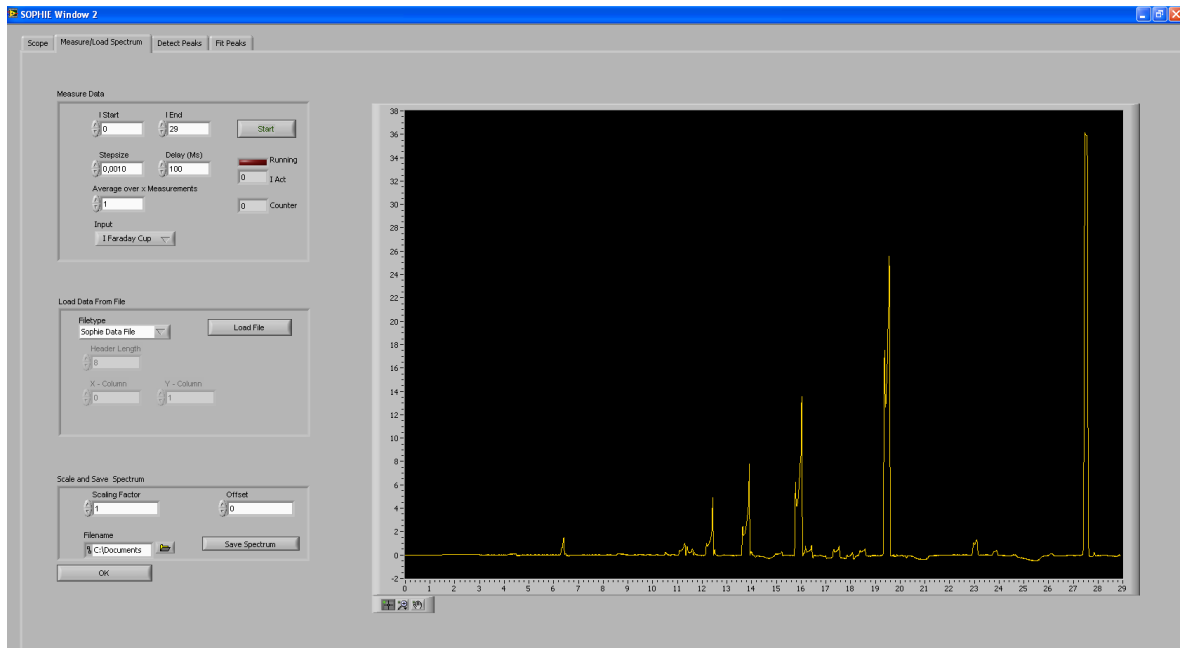


Figure 2.9: Measure/load spectrum tab in 2nd window

data capture are done on serial lines). This means the 6000 points timescale corresponds to approximately 2 minutes for the analogue inputs, and to about 50 minutes time on the serial channels.

The measure/load spectrum tab (Fig. 2.9) allows the user to measure a spectrum or load a previously measured spectrum. Then the data can be scaled, an offset value can be added, and the spectrum can be saved (with all the modifications).

For measuring a spectrum the user can set start and end points as well as step size and the delay to wait between setting the new current and measuring the value. If needed averaging over multiple measured values can be selected and also another input channel can be used. The measurement can be stopped at any time by clicking the start button again, the data measured till that time will stay in the display and can be further processed. This allows you to manually stop the measurement in the case that you set the end point too high.

The data displayed in the window is scaled in real time by the values in the corresponding controls.

When finished with loading or measuring press the "OK" button to switch to peak detection on the currently displayed data, a simple tab switch will not change the graphs and data that is displayed in the detect peaks and fit peaks tabs, this means tab switching can be used at any time to compare the spectrum that is displayed in the other tabs to a newly measured one (or even to one that is still in the process of getting measured).

The next tab is the user interface for the peak detection (Fig. 2.10), it shows the graph and the detected peaks marked by small circles in it, a configurable low pass filter can be applied to the spectrum to reduce noise before the detection, and the detection algorithm

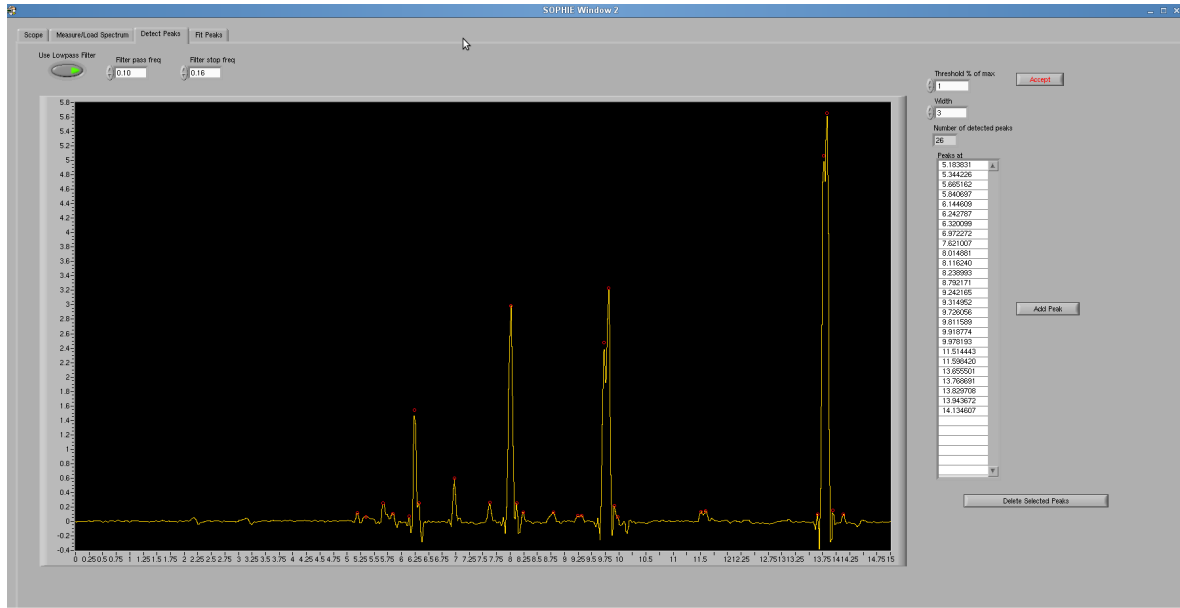


Figure 2.10: Peak detection tab of the 2nd window

can be modified by the parameters threshold and width. “Threshold” configures how big the peak has to be compared to the highest measured value to be still considered as a peak, and “width” is a parameter that sets how many neighbouring points are considered in the peak detection (if you have very sharp peaks then you should not set the width too high).

Any change to the parameter values for the low pass filter or the parameters for peak detection will be instantly applied, which allows seeing the effects of it immediately.

Also there are the options to manually delete or add peaks, if you use these then make sure you do not modify any of the automatic detection parameters after this, or your manual changes will be lost with the automatically started new detection run.

The final tab in the 2nd window has the interface for the peak fitting algorithm. To get a first fit only the extraction voltage and the gas types should be needed as input parameters, but there is a lot more room for interaction to refine the fits, get more information about the fit and save the fit.

The experimental setup in the Augustin lab uses a 60° sectormagnet (SM) setup for ion selection (more details about the setup in the next section 2.4). In such a setup the ions are exposed to the magnetic field in the SM. The deflection in the magnetic field is proportional to the Field \vec{B} (which is proportional to the current in the magnet I_{SM}) and to \vec{v} (which is proportional to $\sqrt{\frac{m}{q}}$).

Because of this the fitting algorithm works with a linear fit between the $\sqrt{\frac{m}{q}}$ and the magnet current I_{SM} , with the 2 fit parameters a and b .

$$I_{SM} = b * \sqrt{\frac{m}{q}} + a \quad (2.2)$$

It works in a few modes depending on how much manual fit data the user provided.

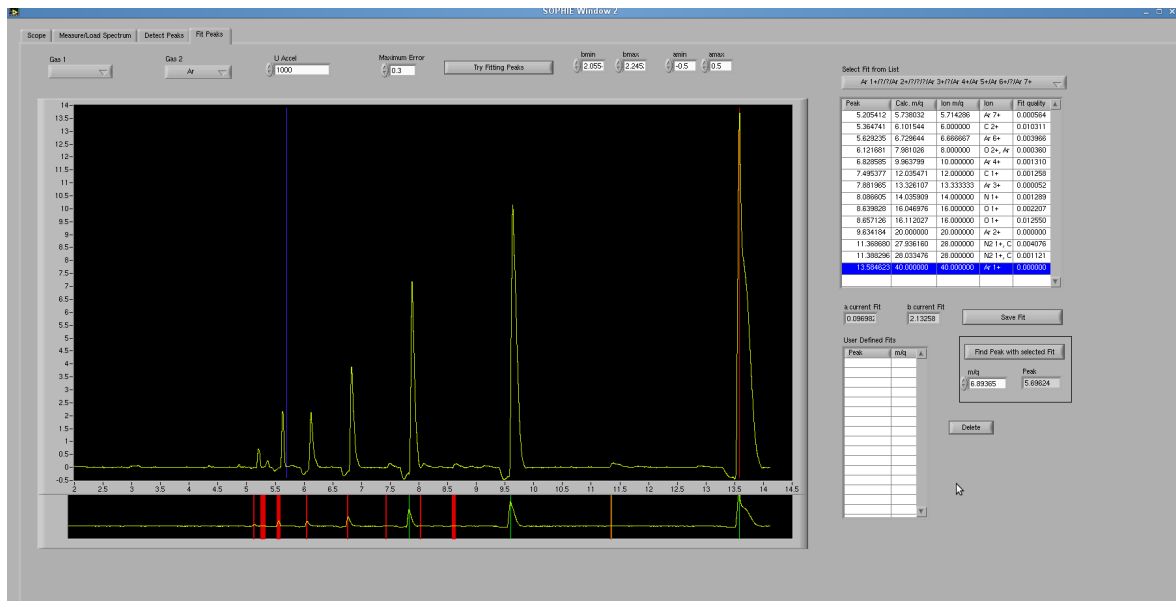


Figure 2.11: Fit peaks tab in the 2nd window

Without any manually fitted points it calculates all possible fits, using each possible combination of 2 peak positions and then tries out ion $\frac{m}{q}$ values for these and calculates the fit parameters then. To reduce the amount of calculations these parameters are checked against upper and lower boundaries based on the extraction voltage, and all combinations that do not fit these are discarded before calculating the fits for the other peaks and the fit error. Without this step the calculation time would increase exponentially with the number of detected peaks. Configuring these boundaries narrow should improve the time needed for the first fully automatic fit, but if the boundaries are set too narrow then the program might discard the right fit and not be able to find an automatic guess. (more on the configuration of the fit can be found in the next section 2.3.3).

For each of these remaining possible fits a fit error is calculated and then fits are sorted based on that fit error and some extra rules (if the peak for a charge state of an element is missing between two visible charge states a penalty is added internally to the ranking for this possible fit, and some other rules). The fit which ends up on top is automatically selected and the table is filled with that data, the other fits are stored in a list and added to the select box. The user can then switch between all the remaining fits with the select box above the table.

On a click into the first 2 columns in the table the peak corresponding to the clicked table row will be marked with a green line in the graph. If there exists a fit for it already, then the magnet current for the fitted $\frac{m}{q}$ value is displayed by a red line. The distance between these lines shows how good the fit for this peak is, the same information about the quality of the fit is also displayed in the graph window below the main graph. It shows for all peaks either a green line if the fit is perfect or a red box with a width that corresponds to the fit error. That small graph should give you a fast overview on how good the fit overall

is, but it is not a perfect visualisation: in cases with many peaks close to each other that graph might look worse than the fit is in reality since these boxes might overlap and look like one big box.

When the user wants to manually refine the fit then he can click in columns 3 to 5 of the table in the row for the point, which he wants to fit manually. This will again display the lines like in the first 2 columns, but also bring up a dialogue window which allows the user to define a manual fit for this peak. When that window is closed with the "OK" button that manual fit will appear in the lower table, and from that point on the software will do fitting based on that manual fit. The manual fit can be deleted again with the delete button or by selecting cancel in the manual fit dialogue for that point (it has to be reopened first, to delete the fit this way).

As soon as the user selects a single peak only fits that include that point are considered, with 2 manual fits the user fully defined the fit and the software only calculates the $\frac{m}{q}$ values and fit quality for the other peaks (but will not consider any other fits), when the user defines more than 2 points then this over defines the fit and the software tries to optimise the fit by variation so that the fit quality for the user defined points is as good as possible.⁸.

If the user is happy with the fit he can save that fit, which automatically creates an extra file named same as the spectra with the ".fit" extension added. When that spectrum is loaded in the future that fit will also be automatically loaded and shown in the peak detect and fit tabs. Additionally the fit parameters are appended to a beam line specific csv file (saved under the config path), this file is created to help optimising the upper and lower borders for the fit parameters for this beam line. Finally the user gets asked if he also wants to save the fit as a comma separated values (csv) file, if the user selects to do so the same data that is displayed in the table in the user interface is saved in an csv file, which can be opened with a spreadsheet application for further evaluation.

There is also an area in this tab of the user interface that allows calculating the magnet current for a $\frac{m}{q}$ ratio after a fit for the spectrum has been found. To use this you can either just enter the $\frac{m}{q}$ ratio in the control for it, or you can use the find peak button which will pop up a window which lets you select the ion from a select box. In both cases the corresponding magnet current is marked in the spectrum by a blue line and the value is

⁸In detail with one point defined by a manual fit, the software still uses about the same method like without user defined fits, but the one defined point improves the situation. Only those combinations of 2 peaks are used, that include the one for which a user peak has been defined have to be considered. And for these combinations only for the 2nd peak the different values for the possible ions have to be tested against the fit boundaries. With that one assignment between that one peak and a $\frac{m}{q}$ value the problem gets simplified from 4 variable parameters down to 2 variable dimensions which should improve calculation times a lot. With the 2nd manual fit assignment there is no variable parameter left and the fit is fully manually defined. Any further assignment over defines the problem and adds the need for finding the optimal fit parameters again, which is then done by variation of the parameters over the parameter space within the limits that come calculating the fit parameters for all combinations of 2 peaks out of the manual fits and taking minima and maxima of these.

shown in a indicator next to the control where you can enter the $\frac{m}{q}$ value.

2.3.3 Configuration of the Software

The Control Software uses a few configuration files which are all text files and can be edited with a simple text editor. The main hardware configuration can also be edited in software with the preferences window. It is highly recommended to make a backup of any configuration file before changing it. The software uses NI-DAQMx tasks for the analogue in and output operations, these required tasks can be created in the preferences window too. (National Instruments has still not released a Linux version of the user interface for creating or modifying these tasks outside the application, like they have for windows. So currently the only way to configure these tasks is the preferences window).

All configuration files are in the config subdirectory of the source or the compiled application. Building the application will copy the configuration from the source directory to the build directory, so make sure that you loose no changes when you compile the application.

IO.csv

The program uses abstract names for each IO task, each of these tasks is seen as a separate operation by the IO-Abstraction layer. The file `config/IO.csv` (Listing 2.2) includes a list that defines what tasks exist. The task names follow the simple convention that they start with "In" for input tasks, "Out" for output tasks, "DI" for digital input and "DO" for digital output then follows the real task name.

This file is a central configuration file, therefore changes can have big effects. Be careful with changes.

Sophie.conf

`config/Sophie.conf` is the main configuration file which configures the hardware for the IO-Abstraction tasks and some parameters for hardware devices.

It uses the LabVIEW config file format, which is a text file split in sections that are started by the section name in square brackets (like [Test]), followed by key=value pairs for the options in this section, the section continues until the next section start is found.

In this special file there is one section for each IO-Abstraction task (see Listing 2.3) defined in `IO.csv`, and additionally a section for each VISA-Device (see Listing 2.4) that is used, and a section for each used DAQ Input device (see Listing 2.5).

When saving the settings in the preferences window, the program will automatically create this file with all these sections using the values that are currently displayed in the preferences window, so make sure all is configured correctly before saving preferences. (it is also always useful to make a backup of the working settings before changing them).

Listing 2.2: Contents of IO.csv

```
"IOABSTR Name (don't change)"
"Out U Source"
"Out U Suppressor"
"Out U Bias"
"Out I Sektormagnet 1"
"Out I Sektormagnet 2"
"Out I Quadrupol 1"
"Out I Quadrupol 2"
"Out MW Power"
"Out MW Frequency"
"Out Pressure Gas 1"
"Out Pressure Gas 2"
"Out USER1"
"Out USER2"
"Out USER3"
"In Pressure Gas 1"
"In Pressure Gas 2"
"In Pressure Mainchamber"
"In I Plasma"
"In U Source"
"In Faraday Cup"
"In Magnet Field Sensor"
"In USER1"
"In USER2"
"In USER3"
"In Pressure Quadrupole"
"In Pressure Sektor 1"
"In Pressure Sektor 2"
"In MW Reflected Power"
"In I Sektormagnet 1"
"In I Sektormagnet 2"
"DI Coolingwater 1"
"DI Coolingwater 2"
"DO Beamline 1 Valve"
"DO Beamline 2 Valve"
"DO Beamline 3 Valve"
"DO Beamline 1 FCup"
"DO Beamline 2 FCup"
"DO Beamline 3 FCup"
"DO MW Transmit"
"DO Switch Sektormagnet 1"
"DO Switch Sektormagnet 2"
```

Any changes made to this file or in the preferences window require the program to be restarted before they are applied.

gases.csv

The config file gases.csv contains a tabulator separated list of the data for the gas selection box, and which ions can be found when the gas is selected. The program uses this file to build the list of possible ions for $\frac{m}{q}$ peaks.

The first column holds a symbol for that gas that should be displayed in the select boxes, for some gases there are multiple lines which all contain possible ions that can be found when this gas is selected. The 2nd column is the highest possible charge state for that ion that should end up in the lists (for background gases that might be lower than the real maximum possible charge state, since higher charge states might not be visible in spectra anymore), the 3rd column is the atomic mass, the 4th column the name of the ion (without any charge states, the program automatically creates that ion in the charge states from 1 to the max visible charge state), and if the 5th column shows a 1 then that gas is considered a standard background gas that might be visible in any spectrum even without selecting that gas (these will be added automatically to any lists of possible peaks, be careful to not define too many standard background gases, since too long lists of possible peaks might slow down automatic fitting).

Listing 2.3: Example for an IO-Abstraction configuration section in Sophie.conf

```
[In I Plasma]      #this starts the section which configures the IO-Abstraction task for 'IN I Plasma'
DAQ=TRUE          #this means that this IOAbstraction task uses NiDAQmx, if the task uses a VISA Device or there
                 #is no hardware present for it then set this to False
DAQTaskName=""   #this holds the name of the NiDAQmx Task that is used for setting the output value, for a
                 #input task this should not be set, just use DAQDeviceName and ChannelNumber for input tasks since input
                 #devices are read all channels at same time with a single read command.
DAQPhysName=""   #this can be used to set the physical device name for a NiDAQmx task, but that is only needed
                 #to create the Task so this is often not set.
DAQDeviceName=Dev2 #this line is used to configure which device DAQ read tasks use.
ChannelNumber=8   #this config setting is used for DAQ read tasks to configure which channel of the device is
                 #used
VISAResName=""   #if a this IO-Abstraction task refers to a VISA serial device then the resource name has to be
                 #filled in here.
VISAInitCommand="" #if an initialisation command is needed for a device connected to a serial port before sending
                 #the real command then it gets added here
VISACommand=""   #this holds the real command that is send to the serial interface for VISA serial devices, use
                 #typical printf formatting for values, tasks that only accept Boolean values use %b as formating code.
ScalingFactor=1.000000 # scaling factor is the factor with which the value gets multiplied (scaled) before
                 #being sent to the output, or for inputs this is the value that the input value gets multiplied by. before
                 #it is used in the program
Offset=0.000000  #this allows to set an offset value that is added after the multiplication (scaling) and
                 #before being used in output or as input value
Min=0.000000     #this sets the minimum value accepted by the IO-Abstraction task (for outputs it is the full
                 #value before being scaled to the voltage range)
Max=10.000000   #this is the maximum value accepted by this IO-Abstraction task
TrueValue=""     #binary commands sent to serial devices often use different syntax for their true and false
                 #values. this option and the next one allow to set which value is sent for True and which is sent for False
FalseValue=""
```

Listing 2.4: Example for a section configuring a VISA serial device in Sophie.conf

```
[ASRL2::INSTR]   #this starts the section that configures the VISA device with the resource
                 #name ASRL2::INSTR (2nd serial device)
Baud Rate=9600.000000 #this sets the baud rate for the communication
Data Bits=8.000000  #the data bits for the communication (can be 7 or 8 depending on the device
                 #that is connected)
Parity=0.000000    #how many parity bits are used
Stop Bits=10.000000 #a value of 10 means 1 stop bit
Termination Char=10.000000 #the ASCII code for the line termination char
Read Buffer Size=4096.000000 #size for the read buffer
Device Init Commands="VOLT 16\0A" #any commands that are sent for initialising the device. In this case the
                 #voltage output is set to maximum that we get into current limited mode.
Checksum/Parity=0.000000 #is any checksum or parity used in communication. 0=no checksum or parity,
                 #1=checksum, 2=parity
Line Break=0.000000 #which line break mode is used: 0=Linefeed, 1=carriage return, 2=CR+LF
Wait for Answer=FALSE #will the device connected to the serial port send an answer to output
                 #commands that i have to wait for?
```

Listing 2.5: Example for a section configuring a DAQ input device in Sophie.conf

```
[Dev2]           #this starts the section that configures the DAQ input device Dev2
DAQmx Device Name=Dev2 #the DAQmx name of the device
NumberOfChannels=15.000000 #how many channels has this device
TaskName="Read Dev2"  #name of the task that reads all channels of this device
```

Listing 2.6: Example for gases.csv

```
'H'      1      1      'H'      1
'D'      1      2      'D'      1
'H'      1      2      'H2'     1
'He'     2      3      'He-3'   1
'He'     2      4      'He'     1
'C'      6      12     'C'      1
'N'      7      14     'N'      1
'N'      1      28     'N2'     1
'O'      8      16     'O'      1
'O'      1      32     'O2'     1
'Ne'     10     20     'Ne'     1
'Ar'     18     40     'Ar'     1
'H2O'    1      18     'H2O'    1
'H2O'    1      17     'OH'     1
'CO2'    1      44     'CO2'    1
'CO2'    1      28     'CO'     1
'CH4'    1      16     'CH4'    1
'CH4'    1      15     'CH3'    1
'CH4'    1      14     'CH2'    1
'CH4'    1      13     'CH'     1
'Xe'     54     129   'Xe-129'
'Xe'     54     131   'Xe-131'
'Xe'     54     132   'Xe-132'
'Xe'     54     134   'Xe-134'
```

Listing 2.7: Example for Fit.conf

```
[BL1]
Factor Bmin=0.065
Factor Bmax=0.071
[BL2]
Factor Bmin=0.0
Factor Bmax=0.1
[BL3]
Factor Bmin=0.065
Factor Bmax=0.071
```

Fit.conf

The file `config/Fit.conf` saves the configuration for the extraction voltage dependence of the boundaries for the fit parameters a and b for each beamline (BL). Since a only showed minimal dependence on the extraction voltage only values for b are stored currently.

The format is again a LabVIEW config file format, the 3 sections in the file are named BL1, BL2 and BL3 for the 3 beamlines. Each section has a factor for the min ($f_{b_{min}}$) and the max ($f_{b_{max}}$) values for b which when multiplied with the square root of the extraction voltage should give the upper and lower boundaries for the fit parameter b .

The Fit is made based on the equation

$$I_{magnet} = b * \sqrt{\frac{m}{q}} + a \quad (2.3)$$

with the boundaries

$$b_{min} = f_{b_{min}} * \sqrt{U_{Source}} < b < b_{max} = f_{b_{max}} * \sqrt{U_{Source}} \quad (2.4)$$

$$a_{min} = -0.5 < a < a_{max} = 0.5 \quad (2.5)$$

Current Values.dat

This file is not exactly a config file, but it is used to automatically store the current output settings for each output value while the program is running. This allows automatic recovery of the last settings in case of a program crash. It is updated automatically every few minutes and the format is the same as the format that is used to manually save settings (see Listing 2.1). When the software gets started it checks if this file is present, and if it exists the user gets the option to load the last settings.

2.4 Augustin Lab Setup

In the Augustin Lab SOPHIE is first connected to a quadrupole magnet (QP) lens that is used for shaping and focusing the ion beam, and 2 sectormagnets (SMs) which are used for ion separation based on $\frac{m}{q}$ ratio and for the selection of the 3 beamlines (BLs).

Ion separation (or more correctly $\frac{m}{q}$ ratio separation) for the experiments is done by a

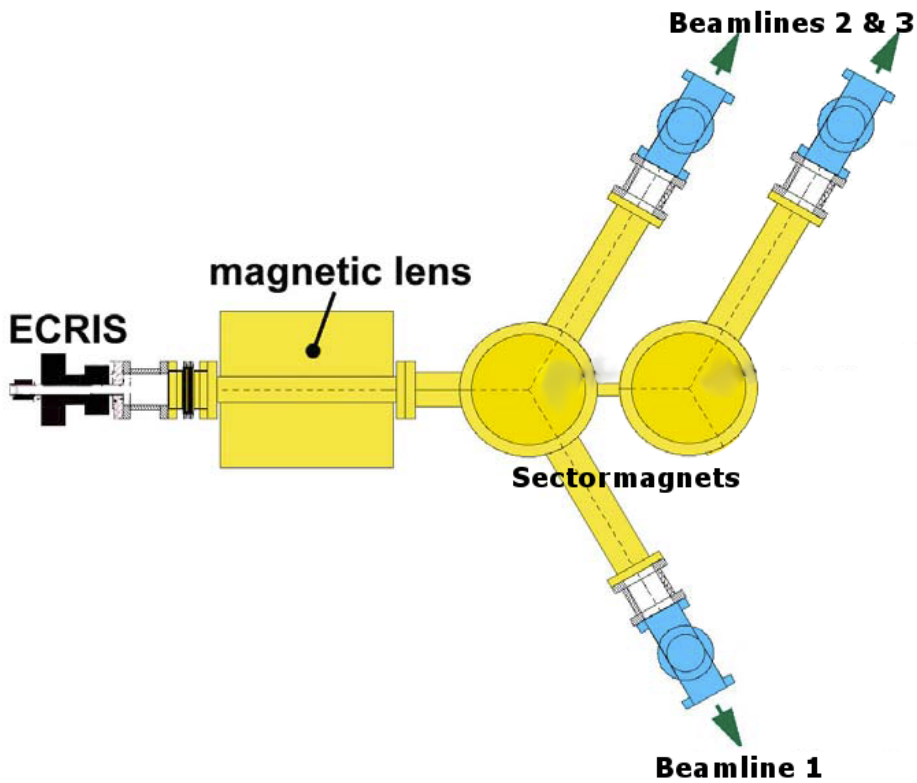


Figure 2.12: Schematic drawing of the Augustin Lab setup

combination of the SM and the mass separation aperture that is the first thing in each BL right after the SM, and only allows a small part of the spectrum to pass. By selecting the current on the sector magnet the magnetic field inside the SM changes, this modifies the trajectories of the ions and by selecting a specific current only the “wanted” ion will pass through the SM and the mass separation aperture.

To find the needed current usually a spectrum is measured in a Faraday cup⁹ or on an Aperture (if no cup is available) behind the mass separation. The control software (described in section 2.3) offers the options to measure and evaluate spectra.

⁹A Faraday cup is a metal cup used to measure ion or electron currents in vacuum. While the most simple version is just a metal cup, most setups come with an aperture in front and a suppressor electrode between the aperture and the cup to keep secondary electrons inside the cup

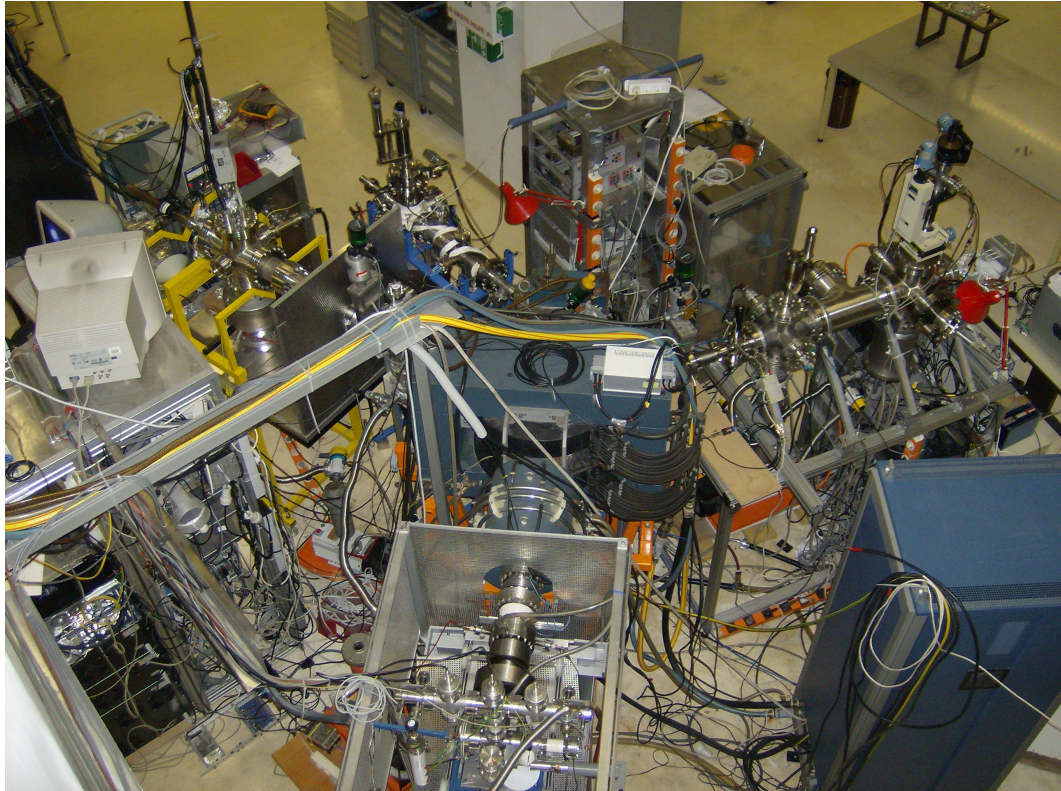


Figure 2.13: Augustin Lab seen from above

Fig. 2.12 shows the basic setup of the IS, the magnets, and the beamlines. Each BL connects to one experiment, BL 1 is linked to the MUSIC (MULTipurpose Solid-target Irradiation Chamber), BL 2 which is the single one at the second magnet connects to the Quartz Crystal Microbalance Experiment, and BL 3 leads to the EYE experiment which is described in more detail in section 2.5.

MUSIC is a multipurpose chamber with a collimation track in which irradiation experiments concerning nanostructuring and capillary guiding are executed. The Quartz-crystal microbalance allows measurements of very small mass changes of the target and is used for measuring of sputtering or implantation effects.

2.4.1 Changes made during this work

As part of this thesis some changes were made to the Augustin setup to supplement the introduction of the new Control Software.

First the power supplies for the primary sectormagnet (SM) and the quadrupole magnet (QP) were replaced by new high precision power supplies. We also added relay based switch boxes to the setup to allow reversing the current direction, to switch between the beamlines, without manual rewiring for changing polarity. The second SM has other values for inductance and resistance that differ quite a lot from the values for the primary sector magnet. Therefore the second magnet needs a completely different relation between voltage

and current (the second magnet seems to have more windings which leads to a higher resistance and so higher a required voltage, while this also increases the inductance so that it needs less current).

When calculating the dimensions for the new power supply we found out that a power supply that can deliver enough current for the first SM to reach the magnet field design goal (the requirement was set that operation with Xe^+ ions at 6keV energy should be possible with the new setup) and enough voltage for the second SM to reach the same goal, would have increased the costs even more. We then decided to change the original plan which was one power supply for both beamlines, and only replace the power supply for the primary SM, and still keep using the lab power supply for the 2nd sector magnet. This also brings the advantage that we now could apply a small current on the primary SM to try compensate the remanence field in SM 1 when we are measuring on BL 2.

During these measurements for IIEE from LiF under impact of Xe ions I had the chance to verify that the new magnet power supplies meet the design goal, and can deliver high enough current, to the magnet to be able to deflect Xe^+ ions with 6keV into the beamlines. That goal was reached easily, it was also possible to select Xe^+ ions with 6.5keV and the maximum of the magnet power supply was still not reached, but 6.5kV is the maximum voltage that the power supply connected to SOPHIE can deliver so that was the end of this testing, and the SM power supply passed the test for the design goal.

Until now most spectra for ion identification were usually just measured on apertures in the beamlines which brings the disadvantage that peaks might be formed as double peaks (when the beam is best aligned to the aperture the measured current is lower than with slightly worse alignment since more ions can pass the aperture), and due to the bigger size of the apertures peaks also tend to be broader than on Faraday - cups.

To improve this Faraday cups for the use in each BL have been designed that can be moved pneumatically into the beam. The pneumatic linear movers that were used in this design allow a defined movement between two positions with a fixed distance of 1in (2.54cm).

In the design of the cup these 2 positions have been used for one position with the cup centred inside the ion beam and a neutral position where a wide hole is in the centre of the beam (the design also allows the addition of an aperture in front of the hole). The base part of the cup assembly is directly connected to the mover which keeps it at ground potential, the real cup is mounted in a ceramics liner inside the lower central hole of the base part and is held in place by a screw. In front of the cup a suppressor electrode, and an aperture with a 4mm front opening are mounted insulated with Al_2O_3 split bushes to allow putting a negative voltage on the suppressor and measuring the current on the aperture and the current in the cup separately. The cup, the aperture and the electrode are connected to the 3 connectors on the electric feedthrough.

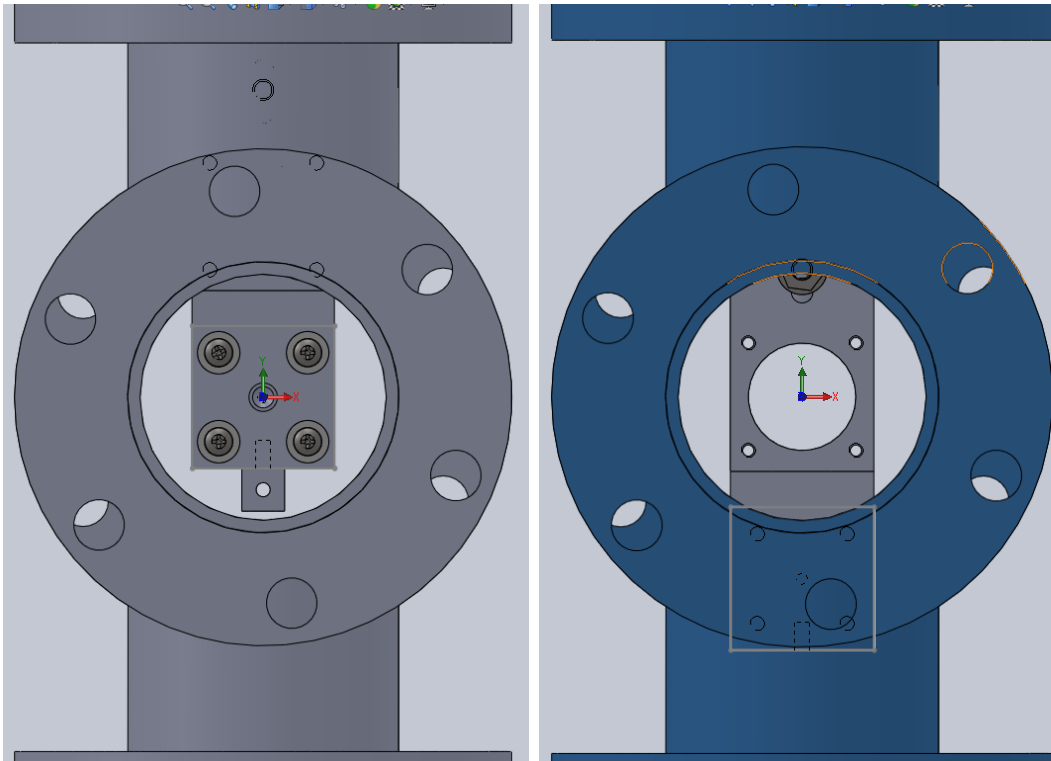


Figure 2.14: Faraday-cup in both positions in the CF-35 4 way cross

The whole cup design is optimised to fit into a CF-35¹⁰ 4 way cross piece with the pneumatic mover on one end and the feedthrough for the electrics on the other open flange. Since all three beamlines use CF-35 flanges in the parts closer to the SM this makes it easy to add these into all 3 beamlines.

The first cup has been mounted in BL 1 and has been successfully used to measure spectra (see Fig. 2.16) and for optimising the beam settings.

¹⁰CF is short for ConFlat, which is a norm for Ultra High Vacuum (UHV) flanges. 35 specifies the diameter.

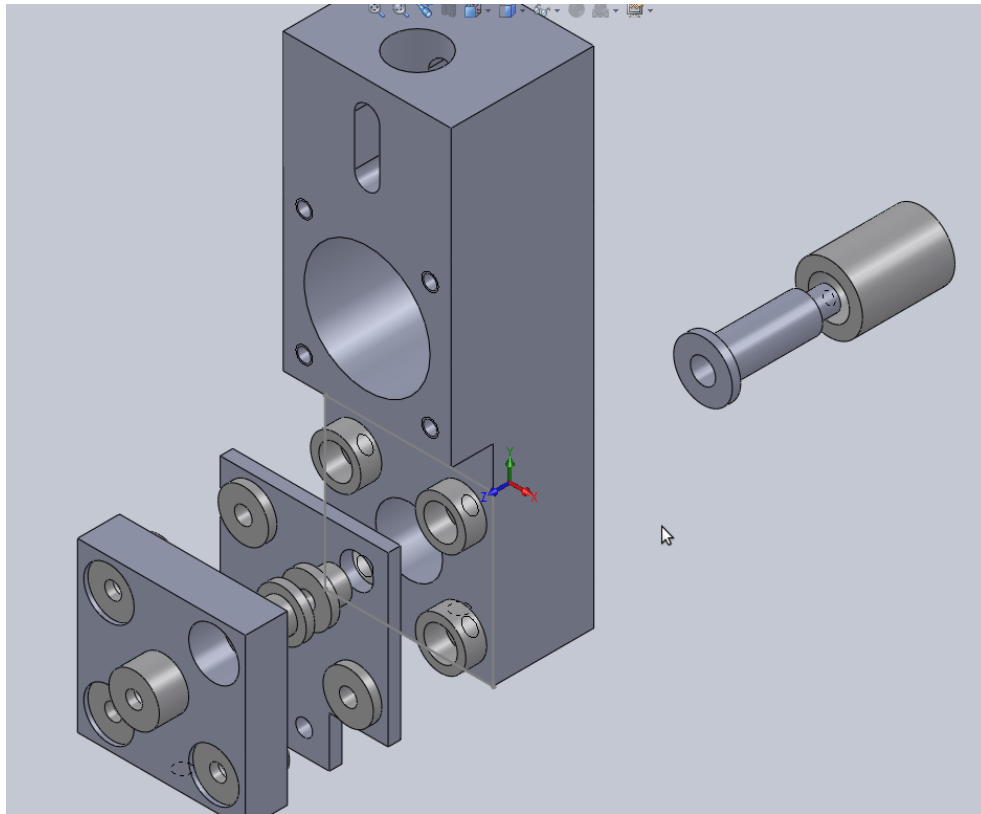


Figure 2.15: Exploded view drawing of the Faraday-cup

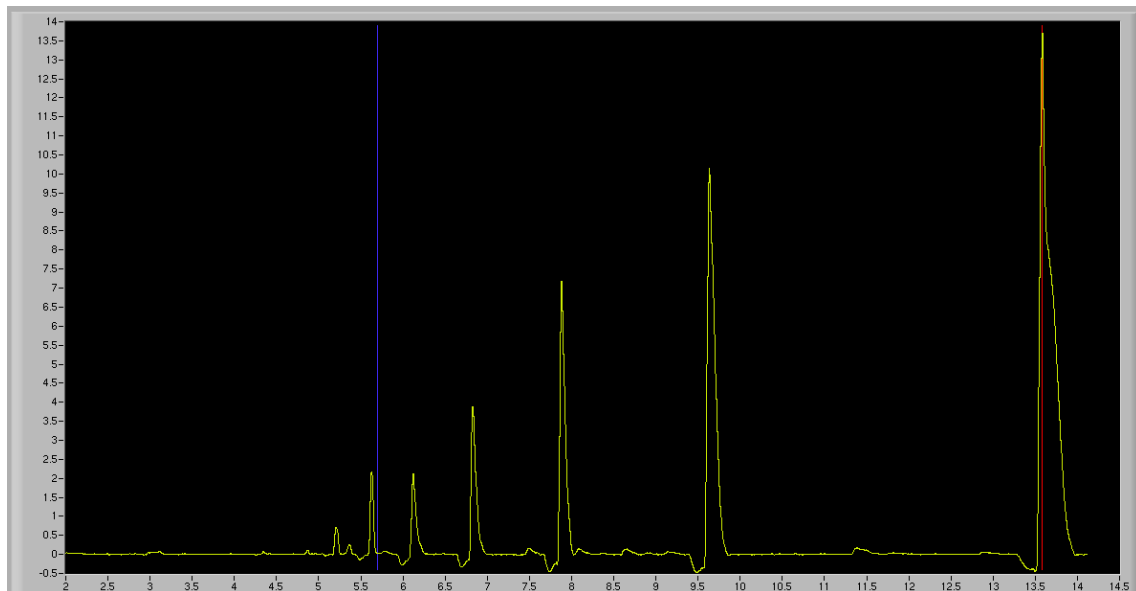


Figure 2.16: Ar 1kV $\frac{m}{q}$ Spectrum measured in the new Faraday Cup, without any suppressor voltage. The peaks for Ar^+ up to Ar^{7+} can easily be identified (from right to left), the smaller peaks in between are Nitrogen, Oxygen and Carbon Peaks from the background gases.

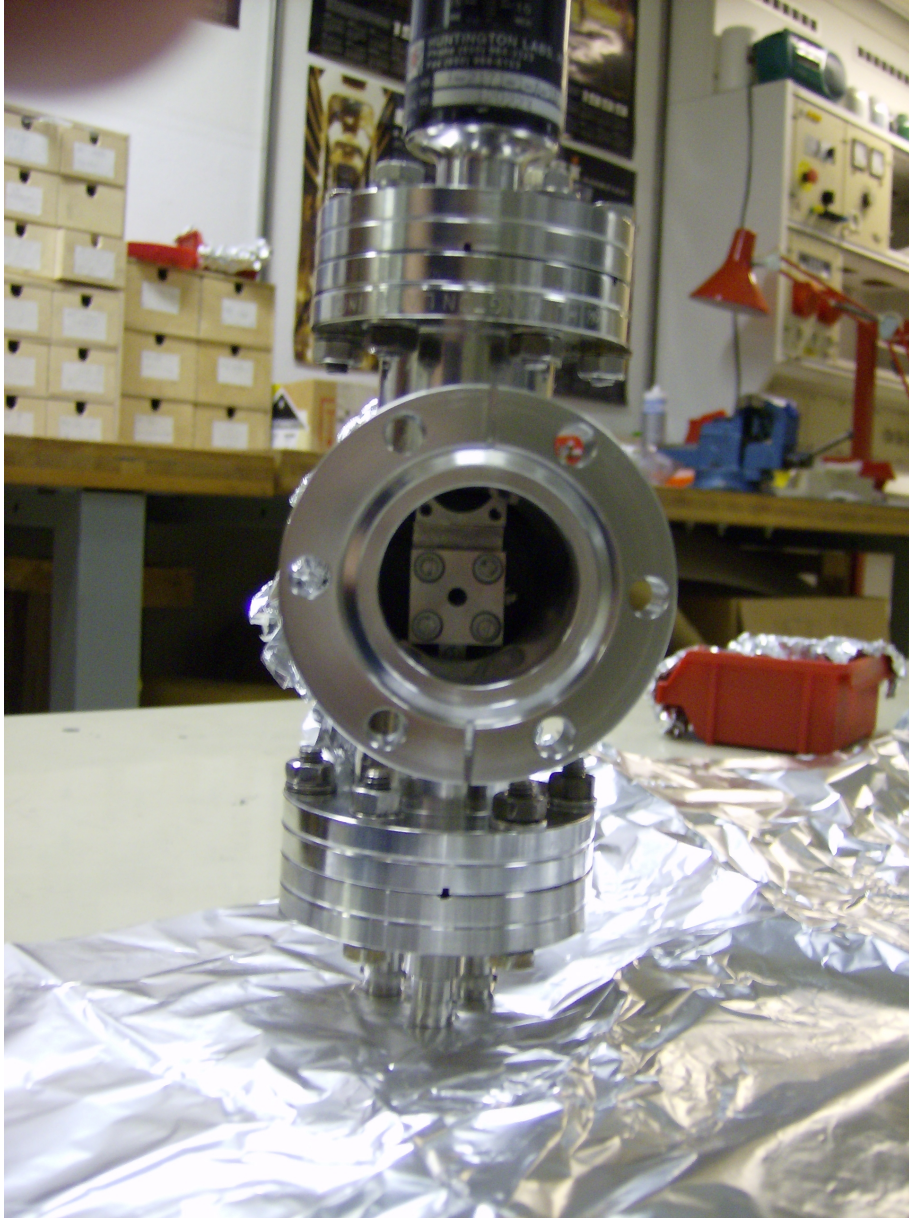


Figure 2.17: Photo of the assembled Faraday-cup

2.5 The EYE

The Electron Yield Experiment (EYE) is an experimental setup to measure total Ion-Induced Electron Emission (IIEE) using the current method with an additional collector for improved accuracy.

2.5.1 The Current Measurement Method

The current method measures the total electron emission yield γ by simple current measurements. For this a setup is used with a target and a mesh around it (see Fig. 2.18). The target is set to ground potential and the current which is needed to keep the target at ground potential (or in case that you want to decelerate the beam at the defined deceleration potential) is measured. The electrostatic potential of the mesh is altered during the measurement.

The target current is measured for two states of the mesh potential, I_T^+ where the mesh is charged positively against the target to siphon all emitted electrons away, and I_T^- for which the mesh is charged negatively against the target to repel the electrons back to the target. For ions with the charge state q this leads to the total electron yield γ :

$$\gamma = q \frac{I_T^+ - I_T^-}{I_T^-} \quad (2.6)$$

This is the most simple setup for a current measurement, but comes with the disadvantage that both I_T^- and I_T^+ often are rather high while the difference between these 2 values stays small which can increase the systematic error of the measurement. Especially for measurements with HCl where the error in the measurement of the difference also gets multiplied with a higher charge state this can lead to rather high errors.

A simple idea to solve that problem is adding another electrode (the collector) around the mesh and measuring the current of the emitted electrons directly (Fig. 2.18 shows a simulation of such a setup in the two states). Some electrons will collide with the mesh and not reach the collector, but if the mesh has a high enough transparency then most electrons can reach the collector and the geometry factor for the amount of electrons passing the mesh can be used as correction in the equations used to calculate the yield. It is also possible to calculate the yield based on the current measured on the mesh using the complementary geometry factor for the amount of electrons that hit the mesh.

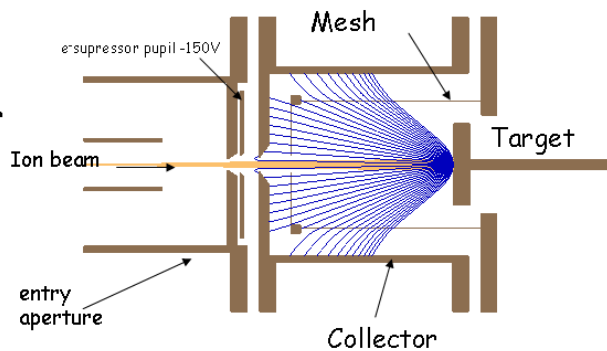
So with such a setup there are 3 ways to calculate the total emission yield γ based on measuring currents on target only, target & collector, and target & mesh. With I_T^- and I_T^+ being the currents for the 2 states on the target, I_C^- and I_C^+ the currents on the collector, I_M^- and I_M^+ the currents on the mesh and c the geometric transparency factor of the mesh we get:

Bias voltages states

state "+"

nearly all electrons (blue) reach collector

Collector	+50V
Mesh	+20V
Target	0V



state "-"

electrons are not allowed to leave target

Collector	-30V
Mesh	-60V
Target	0V

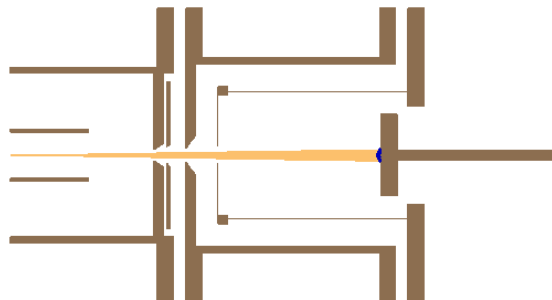


Figure 2.18: Electrodes in EYE in different states - SIMION simulations for the states + and minus in the EYE chamber are shown. In the state - the electrons are all repelled back to the target while in the state + nearly all of them reach the collector. (taken from [3])

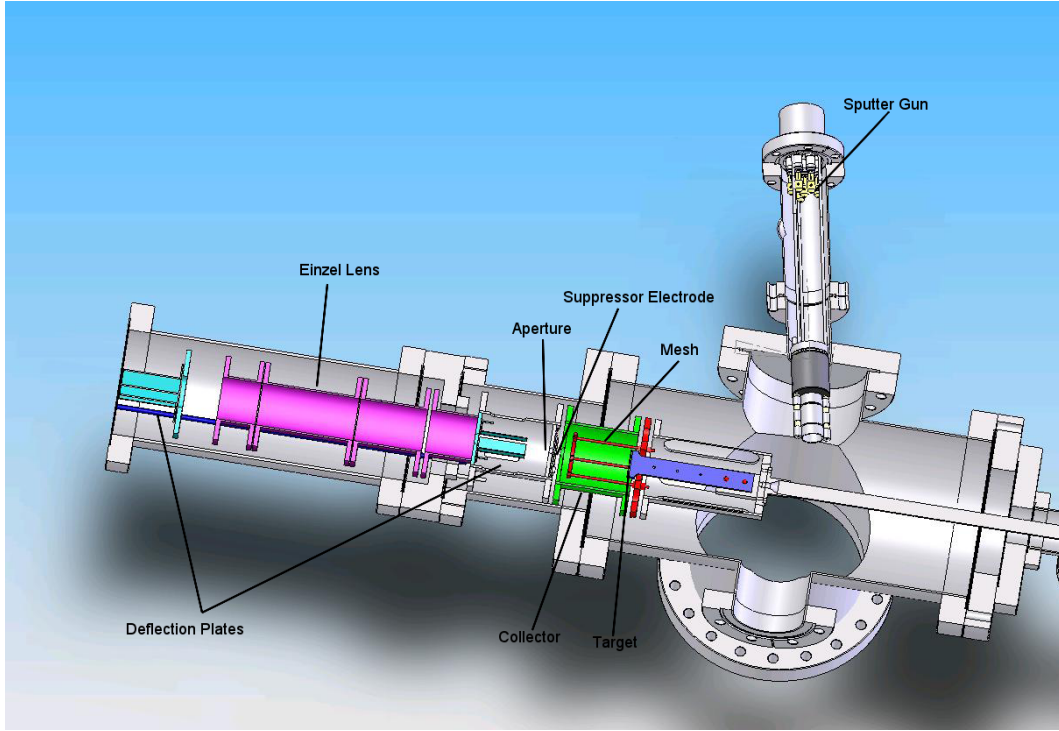


Figure 2.19: CAD picture of the EYE setup. [3]

$$\gamma_1 = q \frac{I_T^+ - I_0}{I_0} \quad (2.7)$$

$$\gamma_2 = \frac{q}{c} \frac{I_C^+ - I_C^-}{I_0} \quad (2.8)$$

$$\gamma_3 = \frac{q}{1-c} \frac{I_M^+}{I_0} \quad (2.9)$$

with I_0 defined as $I_0 = I_T^- + I_C^- + I_M^-$ in the 3 equations for calculating the yield.

When using this method with insulators the main problem is very obvious, the method includes measuring the current needed to keep the target at a defined potential, so the target needs enough conductivity to allow measuring this current. For insulators this can only be reached by heating them enough to get the ion based conductance up.

2.5.2 Setup of EYE

The current measurement method has been in use for a long time now with conducting targets worldwide, also there have been a few previous experiments for measuring IIEE with the current measurement method at the "Institut für allgemeine Physik". The direct ancestor of the EYE Setup was the ISA Experiment [44], which had some influence on the design of EYE and the control and evaluation software from ISA is still used with EYE.

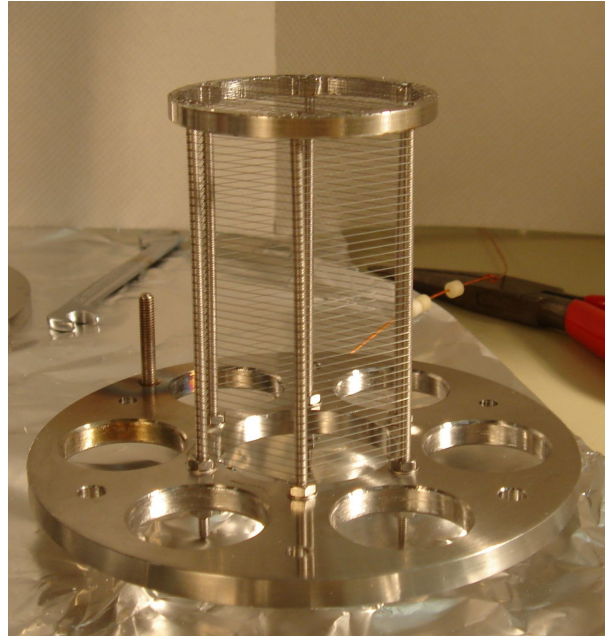


Figure 2.20: Photo of the Mesh used in EYE. [3]

Fig. 2.19 shows a CAD picture of the EYE setup, the cylinder symmetric setup consists of 2 pairs of deflection plates for correcting the flight path of the ions and an einzel lens for focusing the beam before the collision chamber. Just outside the collision chamber is a suppressor electrode that holds back electrons in the chamber to avoid losing emitted electrons through the opening for the ion beam.

The collision chamber has a cylindrical collector as outer wall. Inside this cylinder there is the cylindrically shaped mesh (Fig. 2.20) and the targetholder (Fig. 2.21). The target holder can be moved out of the chamber into a 2nd position where a sputter gun is mounted for cleaning of the target. The original targetholder also included a filament based heating and a thermocouple for measuring the target temperature. This targetholder was used with thin round targets of the material under investigation which were fixed on the targetholder with 2 screws.

The collision chamber was designed to work either on ground potential or to be put on a higher potential to allow deceleration of the ions for measurements with slower ions.

The chamber is pumped to UHV by a turbomolecular pump, additionally there is a titan sublimation pump available for faster pumping after ventilation. The typical pressure within this chamber at working temperature is below 10^{-9} mbar when the beamline valve is closed and no ion beam is inside the chamber. When the valve is open and ions are accelerated into the collision chamber the pressure increases a bit into the low 10^{-9} range.

This setup allows rather fast changing of the target, or other smaller parts as long as the new parts are well cleaned. When the experiment is ventilated with nitrogen to a slight over pressure, and then only opened shortly for replacing the parts, a good enough vacuum for first testing can be reached within a few hours. With the use of the titanium sublimation

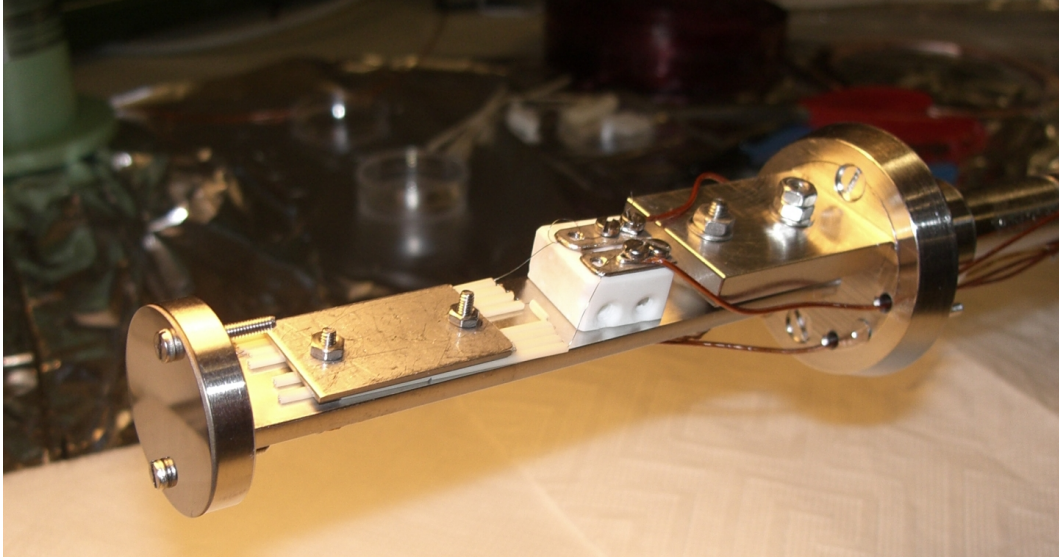


Figure 2.21: Targetholder originally used in EYE. [3]

pump, and nitrogen cooling we reached a pressure in the low 10^{-8} mbar range in less than a day after replacing the complete targetholder, with smaller changes like only changing the target crystal this can be even faster.

The ISA control software which is also used for EYE works with 3 voltage states for collector and mesh in the measurements (see Fig. 2.22).

- During the state plus (+) mesh and collector are both set to positive voltage compared to the target (collector on a higher potential than the mesh). Emitted electrons are accelerated by the mesh and after passing the mesh further accelerated to the collector. Backscattered ions or neutral atoms which hit the collector can produce secondary electrons (SE), but since the mesh is on negative potential compared to the collector they are pushed back to the collector.
- In the state minus (-) mesh and collector are both on negative potential compared to the target (mesh more negative than the collector). Electrons emitted from the target are repelled back to the target. SE produced on the collector by backscattered ions or neutral particles are repelled back to the collector since the mesh is more negative than the collector. SE produced on the mesh move either to the target or to the collector.
- In the last state (e) the mesh is set to negative potential, the collector to positive potential. Electrons produced on the target are repelled back to the target. SE produced on the mesh are accelerated to either the collector or to the target, but with the collector being closer and on higher positive potential the majority of these electrons should move to the collector and less of them to the target. SE produced on the collector stay there because of the negative potential on the mesh.

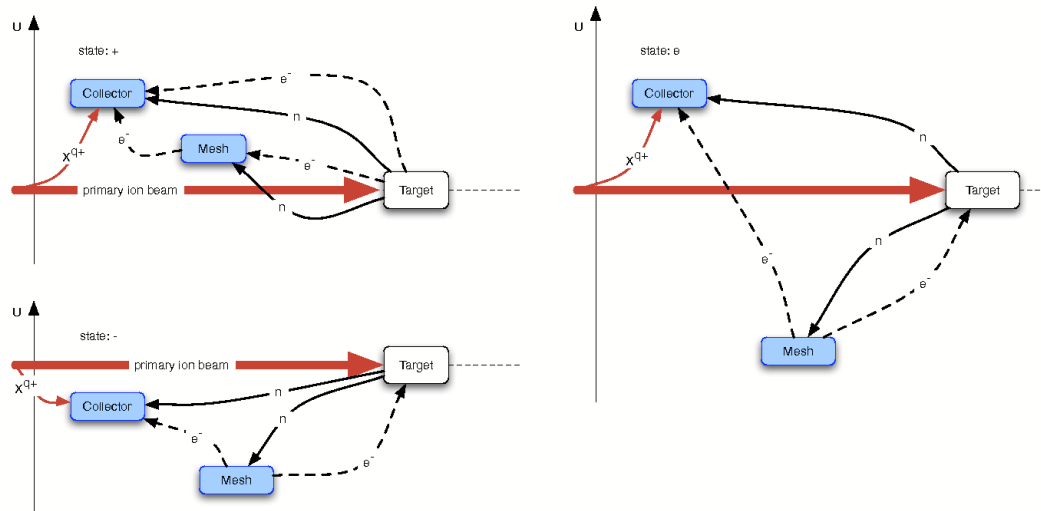


Figure 2.22: The 3 different potential states in ISA and EYE measurements as explained in the text. [44]

In all 3 states the collector is on a more positive potential than the mesh, which should ensure that the SE produced on the collector by impinging neutral particles or backscattered ions stay there, so they should not influence the measurements. The state (e) was introduced to get a better indication on the size of the currents produced by SE.

2.5.3 Changes made during this work

The goal of this thesis was to test the EYE with a sample from a $LiF(100)$ single crystal. For the start a simple metallic plate that holds the crystal on the target holder was designed and then created in the workshop. The piece of the crystal (approx 1 cm x 1cm big and 1 mm thick) was mounted on the targetholder and the heating was tested.

We soon found out that we could reach temperatures of about 350°C , but when exceeding approximately 250°C we measured blind currents up to a few μA , which would be orders of magnitude higher than the currents we want to measure. Therefore we had to replace the heating. The first try was just replacing the filament with a coaxial heating cable, which already improved things a bit but the blind currents were still there and still too big.

We then identified the problem to be caused by the heavily reduced resistivity of the commonly used Al_2O_3 insulators at these high temperatures. So we decided to design a completely new target holder. We now knew that the resistance between the inner and outer surfaces of the coaxial heater cable is too low for our applications.

The base design idea for the new design was to use heat radiation originating from a coil wound from a coaxial heating cable (three windings) surrounded by 2 polished radiation

shields to heat the copper holder plate on the other side. The coil is held in position by two clamps outside the heat shield, that are insulated against the target. This gives us double insulation between the heating coil and the target, also the insulation between the clamps and the target holder is in an area that is not that hot (the temperature simulations showed a temperature of less than 200°C for these insulators), so the insulation should be better than with the hotter insulators inside the heat shield. The heat shields are held in place and insulated against the target by Alumina (Al_2O_3) split bushes. A K-type thermocouple is mounted onto the holder plate to measure the temperature. (See Fig. 2.23 and Fig. 2.24 for Pictures of it).

The design of the target holder in CAD was done in a collaboration with Elisabeth Gruber and Gregor Kowarik (I mainly worked on the design of the front part of the holder including the heating, the other two designed the mounting clamps for the heating spiral and the part that connects the new holder to the original holder). To make sure we can reach the needed temperatures Elisabeth made some basic calculations which can be found in her bachelor thesis [1], and I verified the final design in temperature simulations in Solidworks (see Fig. 2.25).

After the successful simulations the target holder was built and installed inside the EYE vacuum chamber. The 2 heat shields are just held in place by the insulator split bushes which give them a little room for movement. After moving the target holder into the position inside the collision chamber it should be checked that the inner heat shield does not touch the heating spiral, which would lead to noticeable blind currents (the split bushes are at a rather hot temperature so their insulation is not good enough to be really sufficient).

In case that the heater touches the heat shield this usually can be fixed again by carefully moving the target holder a bit with the manipulator, and checking the target currents while doing it. If there is no contact between the heating wire and the heat shield the blind currents should be lower than 0.1 nA. (Typical blind currents on the target at temperatures around 360°C were in the 0.02 - 0.03 nA range with this setup).

2.5.4 Validation of the Measurements

To validate that there is no influence of the measurements by the charge built on the surface, we first made a few simulations in SIMION to see how much influence a potential distribution on the surface will have on the flight paths of the emitted electrons (we approximated a Gaussian distribution by a few circles of different potentials). The first simulations showed that increasing the potentials of the mesh and the collector will reduce the effect of a small charge. So in all measurements we used $U_M = 70V$ and $U_C = 96V$ for the mesh and collector voltages in the + state.

These simulations (see Fig. 2.26) showed that a potential of approx 5V on the target has near to no effect on the electrons reaching the collector, a potential of 10V already

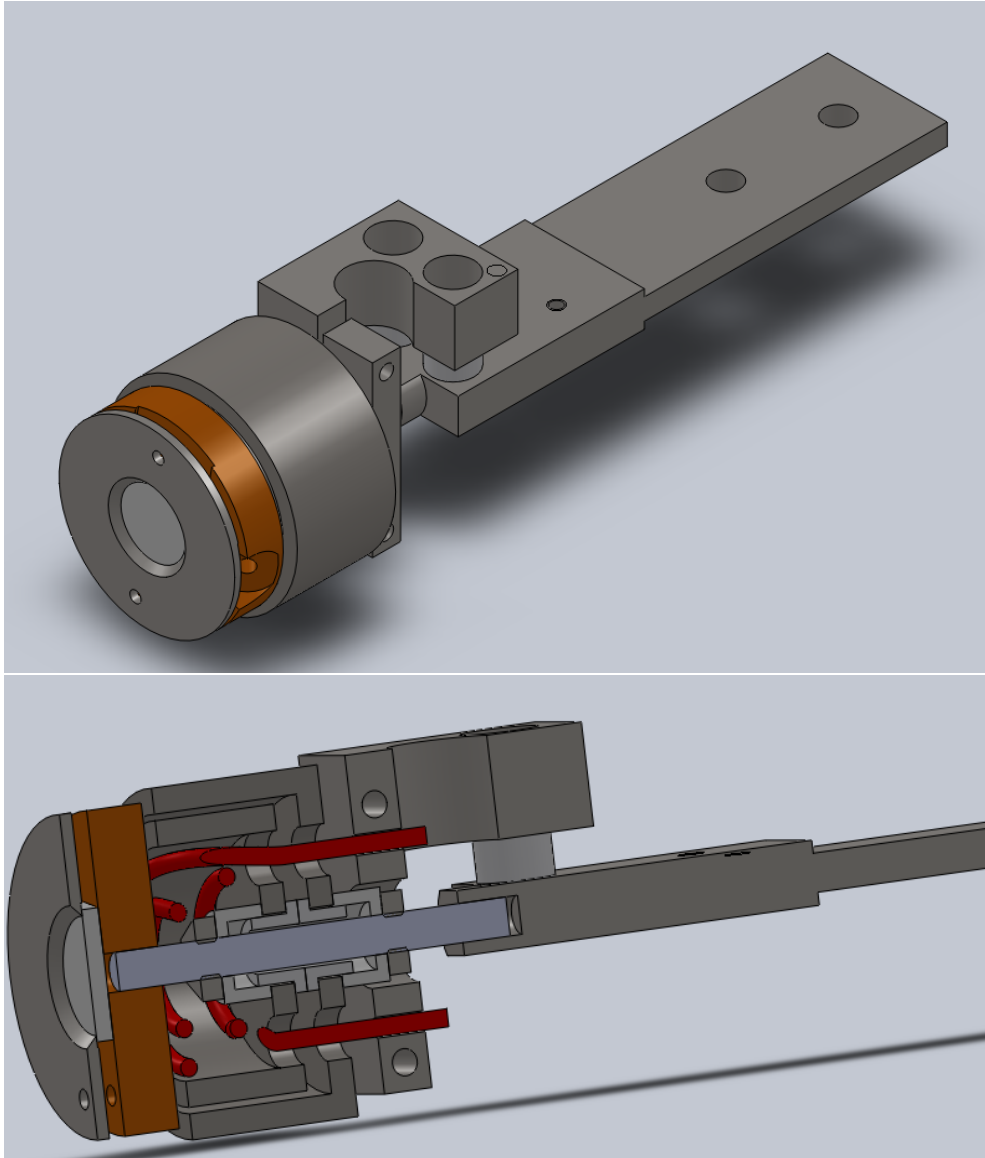


Figure 2.23: New targetholder CAD images

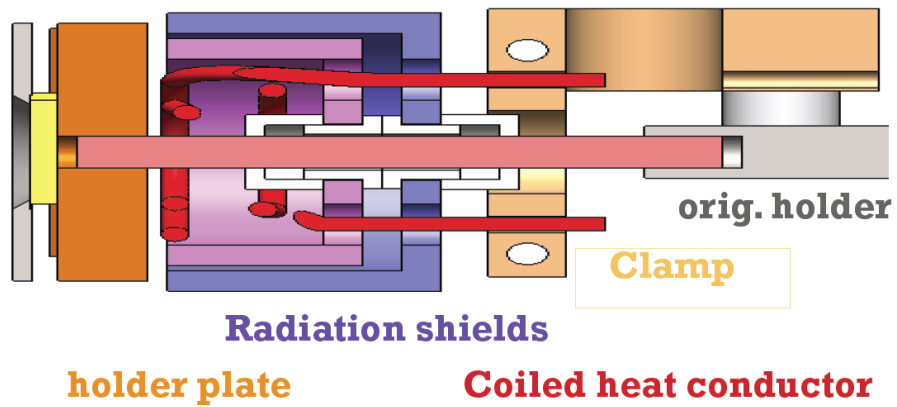


Figure 2.24: Schematic picture of the targetholder [2]

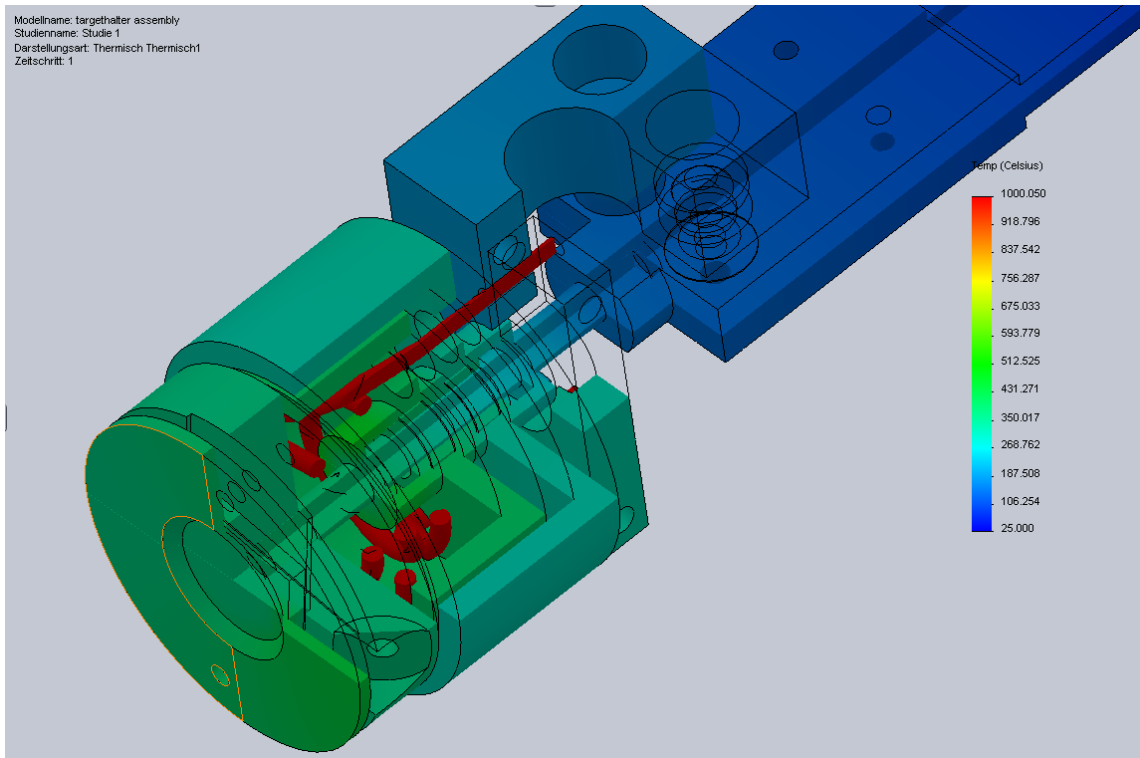


Figure 2.25: Temperature simulation of the new targetholder design

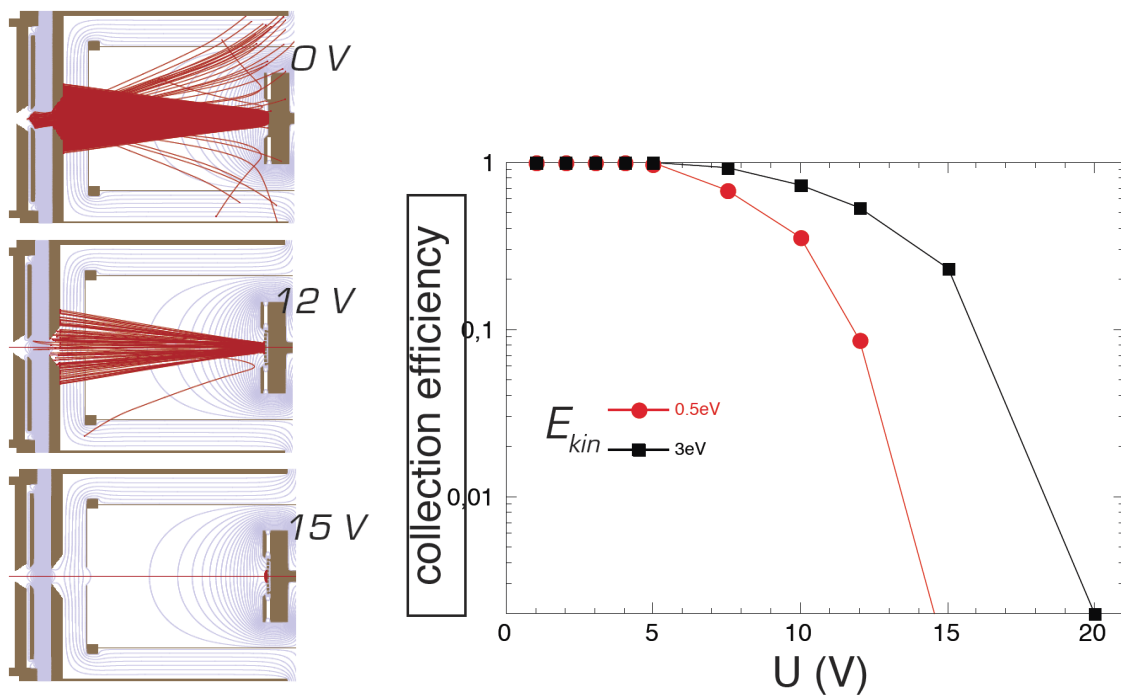


Figure 2.26: Influence of increasing charge on the Target - The left pictures show the potential and the trajectories of the electrons, for no target potential and approximated Gaussian potential distribution on the target with a maximum at 12V and 15V. The graph on the right shows the percentage of electrons reaching the collector for increasing target potential. [2]

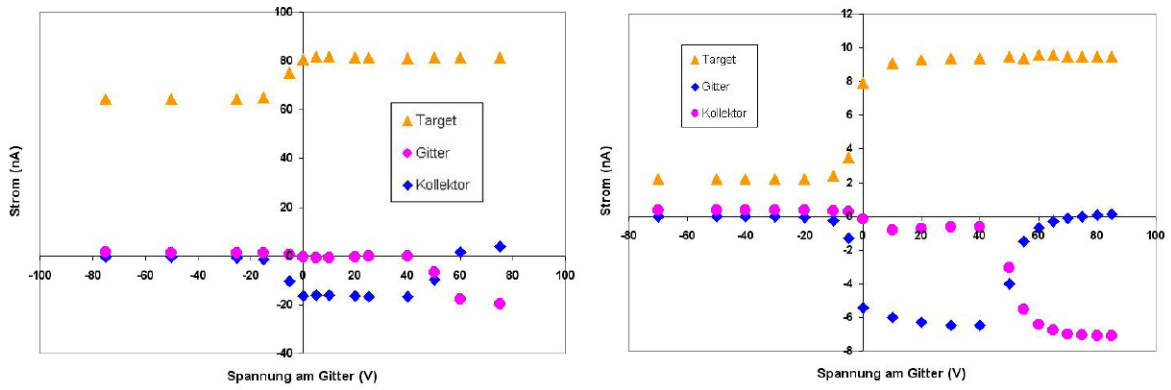


Figure 2.27: Currents measured for the variation of the mesh potential, with the collector potential fixed at 50V. The Graph on the left shows similar measurements for tungsten compared to measurements with *LiF*. [1]

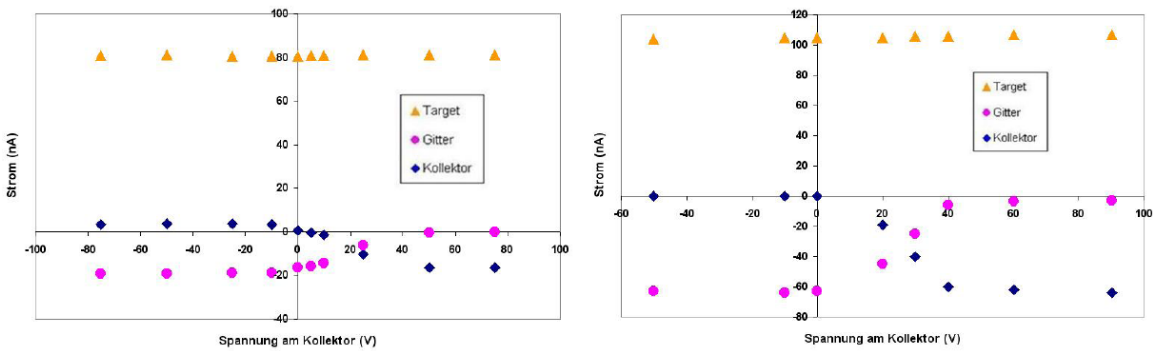


Figure 2.28: Currents measured for the variation of the collector potential, with the mesh potential fixed at 25V for *W*, 30V for *LiF*. The Graph on the left shows similar measurements for tungsten compared to measurements with *LiF*. [1]

holds back about 50% of the electrons and with a target potential of 15 to 20V almost no electrons can escape the target.

We also found the existence of a lens effect for a charged target in the simulations. This effect increases with the target potential and was studied in more details by Elisabeth Gruber in her bachelor thesis [1].

We also measured the voltage dependency of the target-, mesh- and collector-currents in relation to the collector and mesh voltages to compare them with older measurements on conductors (see Fig. 2.27 and Fig. 2.28). The shapes of these graphs look very similar to the tungsten measurements but these measurements already show the much higher yields γ for *LiF*. The *LiF* measurements were all done using an Ar^+ beam with 2keV energy and a low ion current.

Charging effects can also be verified by studying the time and ion current dependency of the yield γ . The Graph Fig. 2.29 shows the dependency of the yield γ on target temperature and ion current. The small graph in the top right shows that γ stays constant for currents up to 20nA (for a temperature of approx 360°C). With further increasing ion currents the

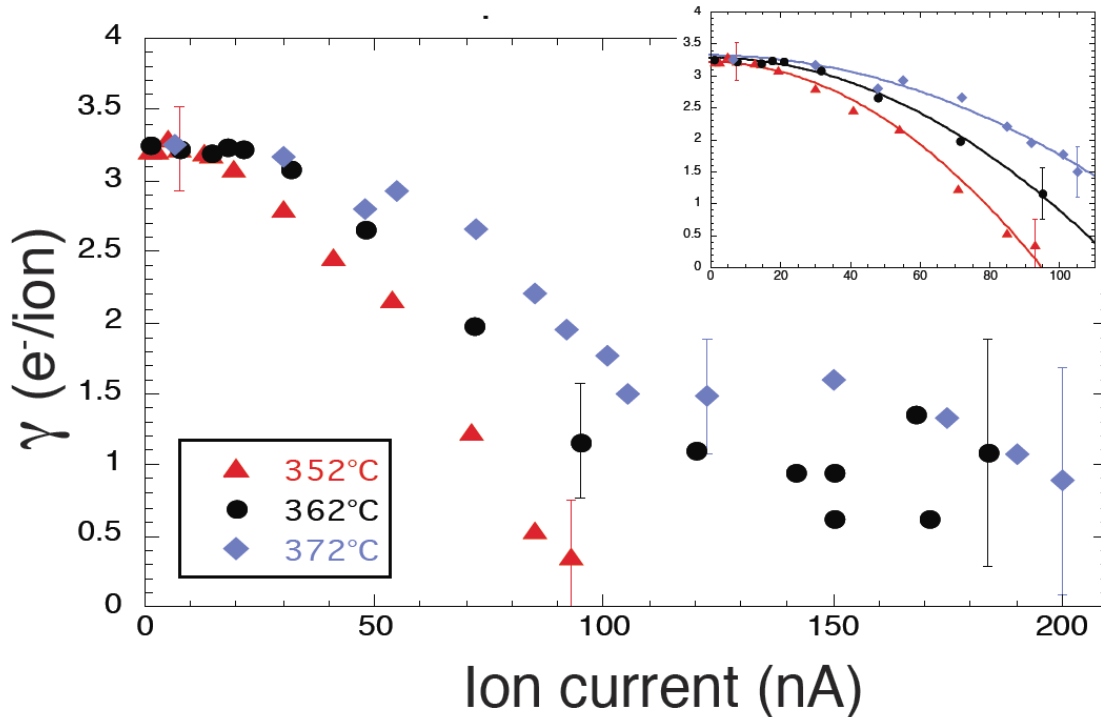


Figure 2.29: Yield dependency on ion current for different temperatures. [1]

yield starts to drop. As expected this also shows a temperature dependency so with higher temperatures the currents could be higher before the measured yield starts dropping, but for our setup we cannot increase the temperature much more without getting higher blind currents (which would reduce the accuracy of the measurement).

Studying the time dependency of the yield is another way to investigate the charging effects, during the charging phase the yield should be dropping over time, because the increased potential results in more electrons being held back at the target and less electrons reaching the collector. Fig. 2.30 shows yields over time for different ion currents. For the 14nA current the yield stays stable over time, while it drops over time for 170nA ion current. These measurements were all performed at a temperature of approx 360°C.

For lower currents the non existing time dependency of the yield has also been verified by interrupting the measurement by closing the beamline valve for different periods of time (which should allow any existing target charge to decay), on all these checks the yield stayed the same after reopening the valve.

In summary there are a two major indicators that under the right conditions the measurements are not influenced by charging effects. The yields do not show any current dependency below a threshold current (the threshold depends on the temperature), and the time dependency of the ion yields also shows no indication of charging effects for beams with a low enough current. This leads to the assumption that measurements with sufficiently low ion currents (15nA or less) at temperatures of approx 360°C should give valid results.

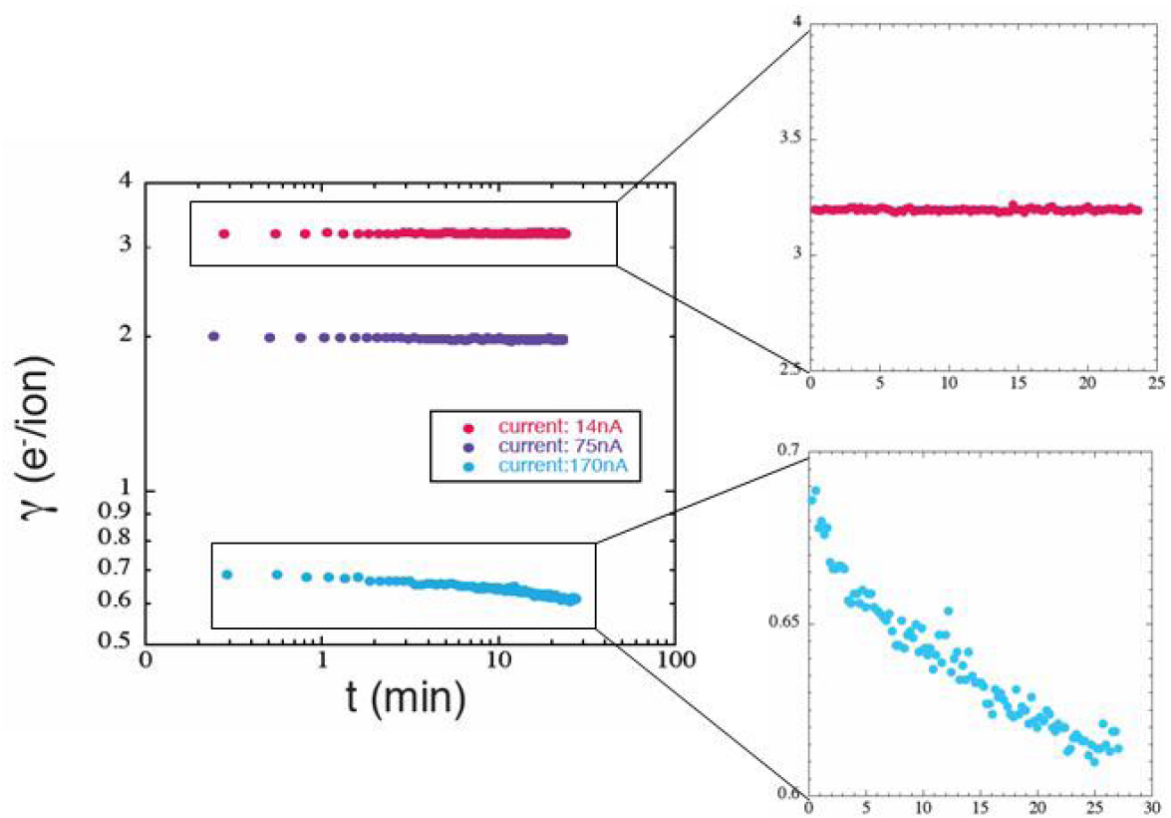


Figure 2.30: Yields over time for different ion currents at a constant temperature of 362°C. [1]

3 Results

3.1 Ar^{q+} on LiF

The IIEE from LiF under impact of Ar ions was measured in order to validate the method and setup, since data already exists for this process in [23, 24]. The previous measurements were done with a statistics detector setup using a thin layer of polycrystalline LiF as a target, while in the new measurements a 1mm thick piece of a LiF (100) single crystal was used. The sample was already prepared by cleaving and we only had to mount it on our targetholder and insert it into the collision chamber.

The measurements were done with the heating current set to 3A, the voltage changed a bit over time due to a changing resistivity of the heater, but ended up in the 5V range, which gives us approximately 15W of heating power and a target temperature in the range of approximately 360°C. The ion beams were optimised for stability and then usually defocused a bit with the quadrupole and the einzel lens to get sufficiently small intensities (typical beam currents used for measuring were in the 5-10nA range).

For all measurements the blind currents were measured first (at least once per day) using a closed beamline valve. These blind currents were used as calibration values in the ISA evaluator.vi software to subtract them from all measured currents.

The impact angle for all measurements with EYE is fixed to 90° by the geometry of the experimental setup.

Especially during the first measurements on the crystal a slow surface modifying effect (probably cleaning by sputtering) at the start of the measurement could be detected. During this phase the yield was increasing, which made it easy to differentiate it from a charging effect that should reduce the yield. Depending on the ion current used for the measurement this effect could last for hours. After some time the yield stabilises and a real measurement is possible. This effect was only visible with the fresh crystal or when there were no measurements for a longer time (multiple days or even weeks). When changing ions or energy after the initial cleaning it did not reappear.

During the yield measurements for Ar on LiF the mesh transparency c' , which the software automatically calculates from the measured currents as an indicator for the plausibility of the values, was higher than expected and showed a dependency on the projectile energy. (cf. Fig. 3.1) (The energy dependency was not noticed until it was found in the

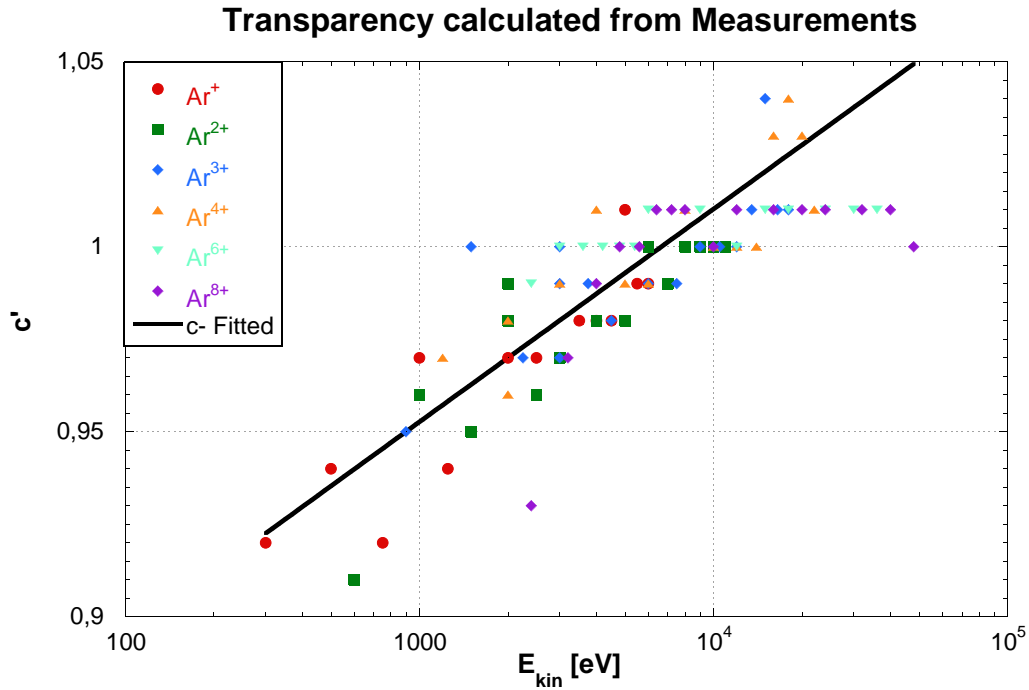


Figure 3.1: Apparent transparency c' for the different Ar projectile energies as evaluated from the ratio of the yields γ_1 and γ_2 (cf. equations 2.7 and 2.8).

Xe measurements, where it is a more clear and pronounced effect. A later re-evaluation of the already measured Ar data showed that for Ar^{q+} c' is also dependent on the impact energy). Compared to this the measurements on conductors that were performed in the past showed a stable transparency of approx 0.91 which would be much more in line with the real geometry.

A possible explanation for this increased and energy dependent transparency are secondary electrons produced on the mesh. In all 3 states (cf. Chapter 2.5.2, Fig. 2.22) these secondary electrons will leave the mesh and in the $+$ state they will move to the collector, while in the other 2 states they will partially move to the target and the collector. This would lead to an increased electron current on the collector in the $+$ state I_C^+ , while in the minus state only a part of these SE would move to the collector while the other part moves to the target. This results in a higher difference in the collector currents between these 2 states and so increases the yield γ_2 calculated from the collector currents. And this again increases the transparency factor c' which is calculated from the ratio of γ_1 and γ_2 .

The effects of c on the calculated yields can be seen in 3.2. For consistent data with the lower statistic error, which γ_2 has compared to γ_1 , but still eliminate the error caused by the SE which are created on the mesh during the measurement, we decided to use γ_2 (from Equation 2.8) with an energy fitted mesh transparency c (from Fig. 3.1) for the evaluation of the data.

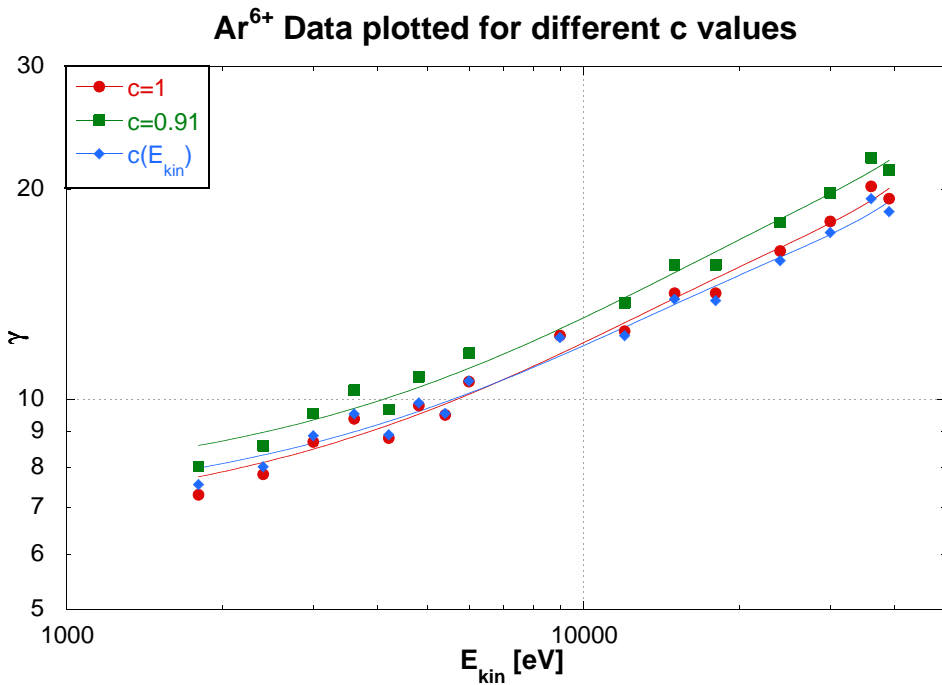
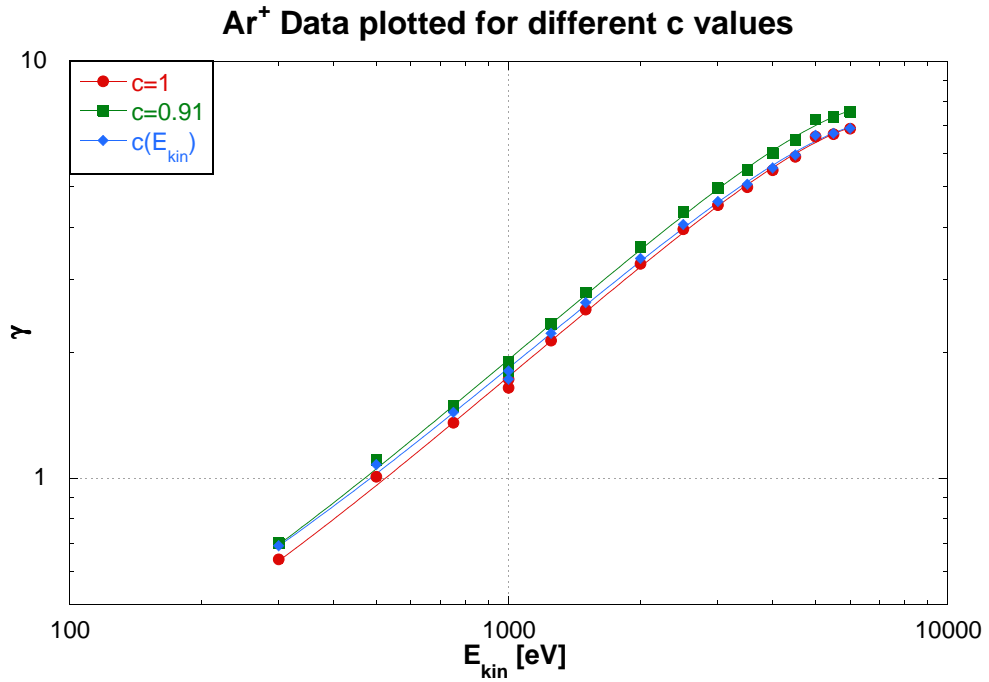


Figure 3.2: Dependency of the yield γ_2 on apparent mesh transparency c . The same measured data is evaluated with different values for c in equation (2.8). The blue curve shows the energy dependent c that is used for the evaluation of the results in this work.

The deceleration by setting the collision chamber to a positive potential was also tested, but the insulation of the chamber again made of Al_2O_3 is at rather high temperatures when the target is heated. This again leads to the problem we already had with the old targetholder design, and we observed huge blind currents already when only using a deceleration potential of 100V. The changes to improve this situation would have required redesigning major parts of the EYE chamber, so we decided to measure as much as possible without decelerating the ions. This put a hard limit on the lowest energy of ions we could use for our measurements, since it is not possible to extract a stable ion beam from SOPHIE for source potentials below 400V.

With 500V extraction voltage it is still possible to get stable ion currents for all investigated charge states, which allowed reliable measurements between 500 and 6500V extraction voltage. Using the relation $E_{kin} = q * e * U_{extraction}$ (where q is the ion charge state and E_{kin} the kinetic energy of the ion) this leads to the possible impact energy range for the ions.

However measurements with an extraction voltage of 300V and 400V were also attempted, but in these measurements the ion currents were significantly lower and therefore the signal to noise ratio decreased, since the blind currents stayed the same. These measurements at the lowest energies therefore are affected by larger errors.

The upper part of Fig. 3.3 shows the newly measured IIEE yields for the impact of singly and multiply charged Ar ions on LiF (1 0 0). In the lower part results for Ar^{q+} impact on polycrystalline LiF measured by the electron statistics technique are shown for comparison. Both graphs share the same qualitative trends.

For low impact energies the curves split up based on the projectile charge states. This equals a split based on E_{pot} and indicates that PE starts playing a bigger role for the higher charge states in this low impact energy regime. Ar ions in the lowest charge states carry very little E_{pot} so their behaviour is characteristic for mainly KE. E_{pot} for Ar^{6+} on the other hand already exceeds 300eV (see Fig. 3.4) so PE plays a more prominent role for measurements at low impact velocities. Without the option of decelerating the ions we were not able to reach an impact energy range where solely PE is responsible for IIEE.

For intermediate impact energies an interesting “anomaly” in the yield plots can be observed in both sets of data. The electron emission yields for Ar^{+} exceed yields for Ar^{2+} and Ar^{3+} . The possible reasons for this strange behaviour has been a source for some discussion when the older data were presented, but the existence of this effect is confirmed by the new measurements. A charge state dependent KE was presented by Vana et al. [24] as a possible mechanism leading to the observed “crossing” of the electron yields.

At the highest impact energies both graphs show an “asymptotic” behaviour where all curves for the different ions approximate the one curve dominated by E_{kin} .

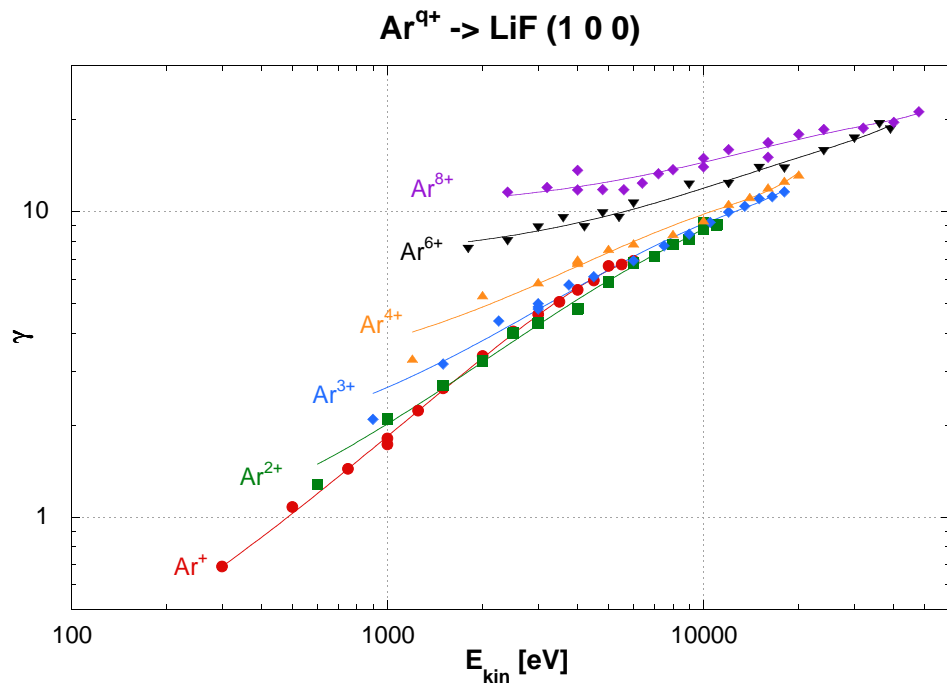


Figure 3.3: IIEE yields γ for singly and multiply charged *Ar* ion impacting on *LiF*. The upper graph shows the new data measured with the current method during the present work on single crystal *LiF* (1 0 0). In the lower graph existing data measured by the electron statistics method [24] on polycrystalline *LiF* are shown for comparison

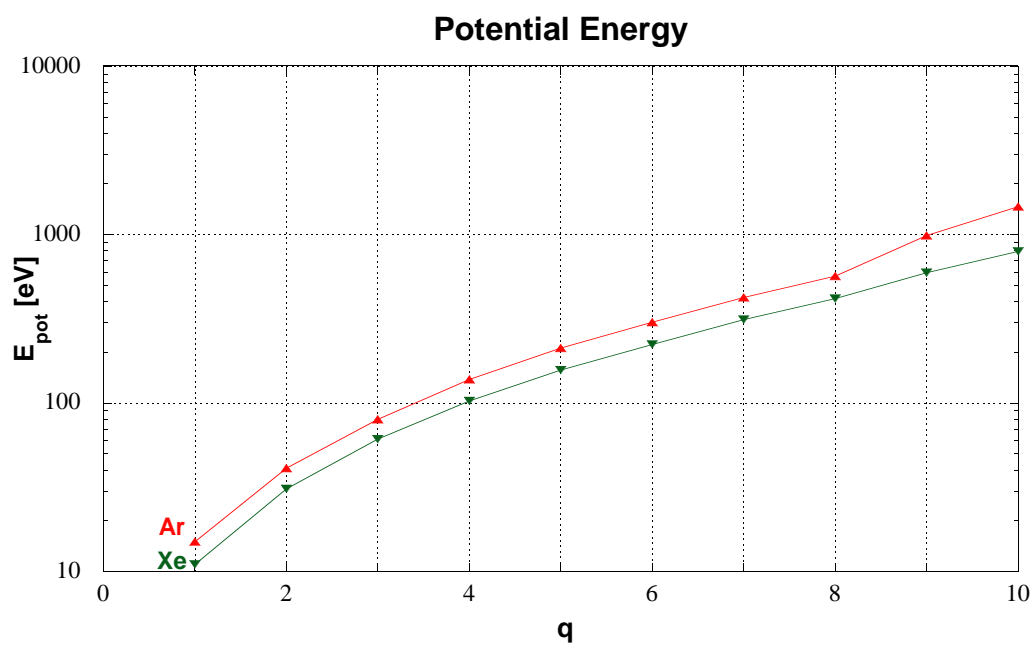
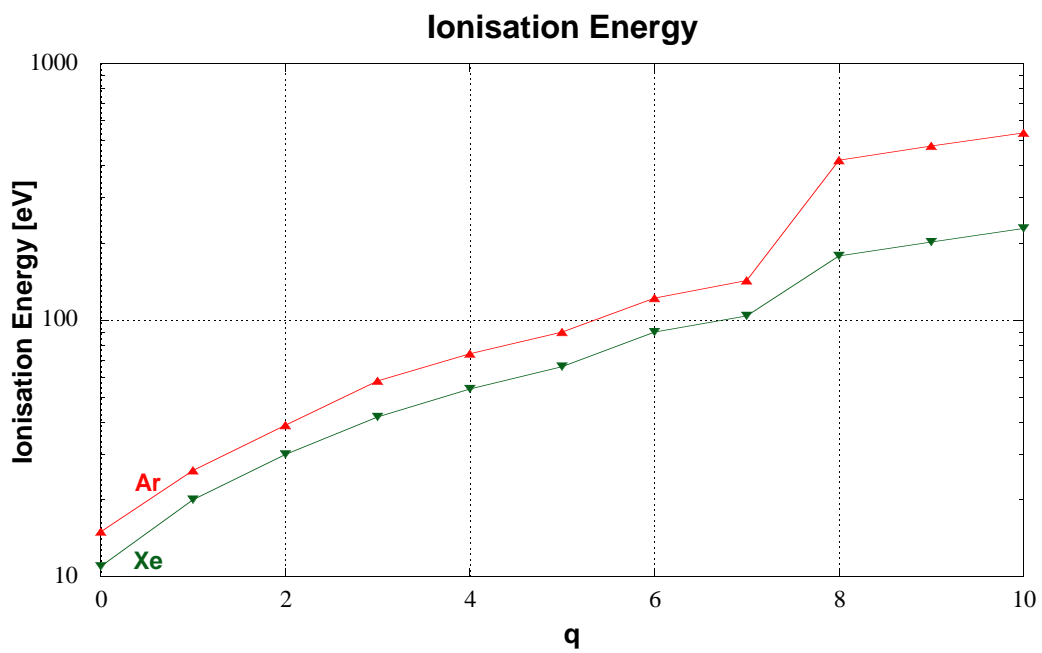


Figure 3.4: Ionisation energies and potential energies for the first ten charge states q of *Ar* and *Xe*. Graphs created with data from [45].

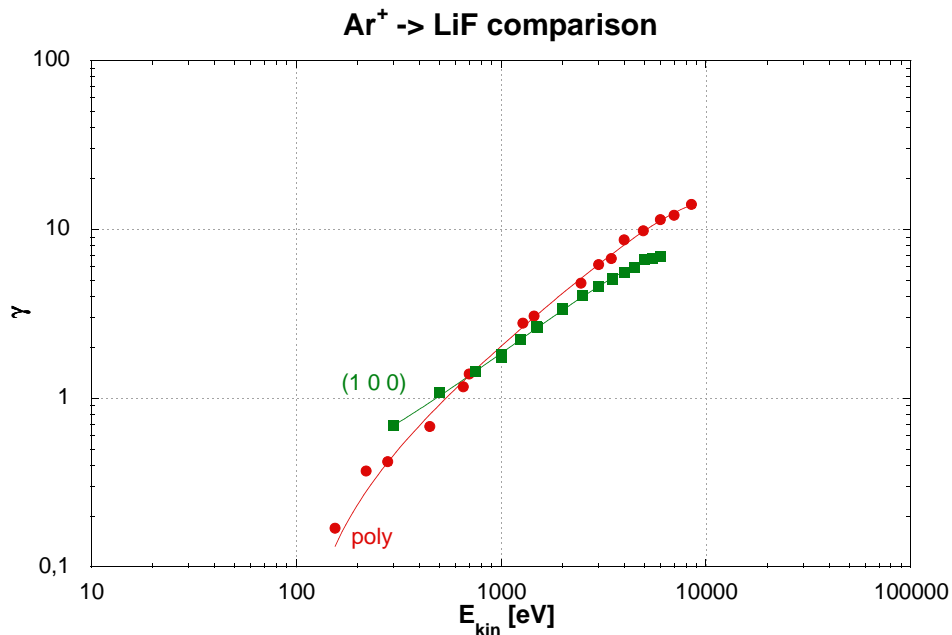


Figure 3.5: Direct comparison of the yields from LiF for Ar^+ . The newly measured Ar^+ yields are plotted for comparison together with the existing data from [24]. Red points show the existing data (polycrystalline LiF , statistics method), green points the new measurements (single crystal LiF (1 0 0), current method).

The energy range for the newly measured data was limited at the lower end by the minimum extraction voltage of SOPHIE (without the option to use a deceleration voltage), and on the top end by the power supply for the source potential which allowed a maximum of 6.5 kV extraction voltage. The highest charge state that could be produced with currents high enough for reliable measurements was Ar^{8+} . In particular measurements at lower E_{kin} would have been desirable to reach areas where PE plays the dominant role for electron emission and KE can be neglected. For higher impact energies a better study of the Ar^+ yields and the behaviour of this curve after it intersects the curves for higher charge states might have been interesting too.

For a better comparison of the absolute yields to the older data, separate graphs for Ar^+ , Ar^{3+} and Ar^{6+} are presented in Fig. 3.5 to Fig 3.7. While in the lower energy range even the absolute values for the yield γ are in good agreement between both sets of measurements, the slope of the curve in the old data was somewhat steeper than in the new measurements. This leads to a difference between the 2 datasets which increases with energy.

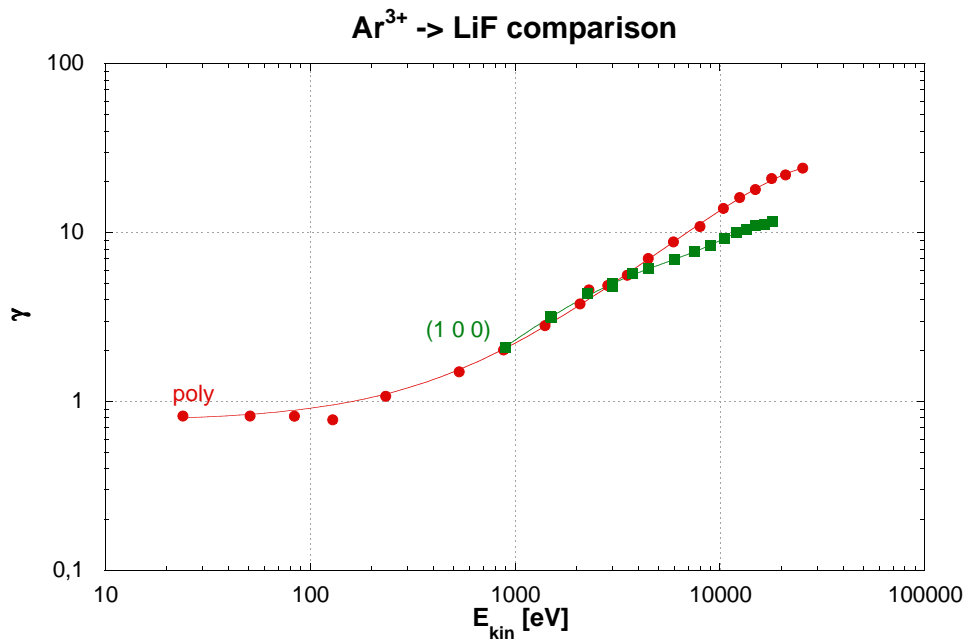


Figure 3.6: Direct comparison of the yields from *LiF* for Ar^{3+} . The newly measured Ar^{3+} yields (green) are plotted for comparison together with the existing data from [24] (red).

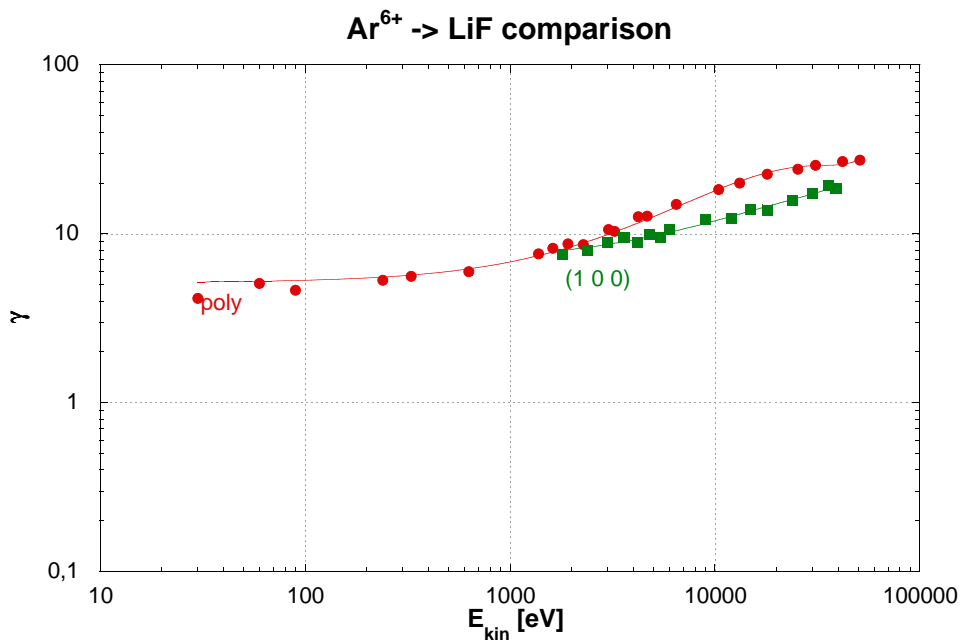


Figure 3.7: Direct comparison of the yields from *LiF* for Ar^{6+} . The newly measured Ar^{6+} yields (green) are plotted for comparison together with the existing data from [24] (red).

Possible explanations for this difference are:

- (a) While Vana et al [23, 24] used a thin polycrystalline LiF film, the target in our case consisted of a single crystal LiF (1 0 0). It is well known that EE yields can show a dependency on impact angles in respect to the orientation of the crystal lattice in the target [46].
- (b) Charging effects have to be considered also as a possible cause for the difference. We used a 1mm thick target and an intense ion beam (approx 10nA which equals some 10^{10} ions/sec) to measure the current, while Vana et al. used a thin film target (about 200nm thick) and single ions ($< 10^3$ ions/sec). The number of ions in the beam and the longer distance for charge transport in the insulator, which are both higher by multiple orders of magnitude in our experiment, lead to a highly increased probability for charging effects in our setup.
- (c) Other effects of the setup and the experimental technique could also play a role e.g. can all emitted electrons be collected by the detectors, are SE generated somewhere in the setup and influence the measurement. Furthermore the different target temperature could influence the yields too (we used a target heated to approx 360°C, while the target in the older data was at room temperature).

The only reliable way to validate this would be to use the same target with both measurement methods and then compare the results again.

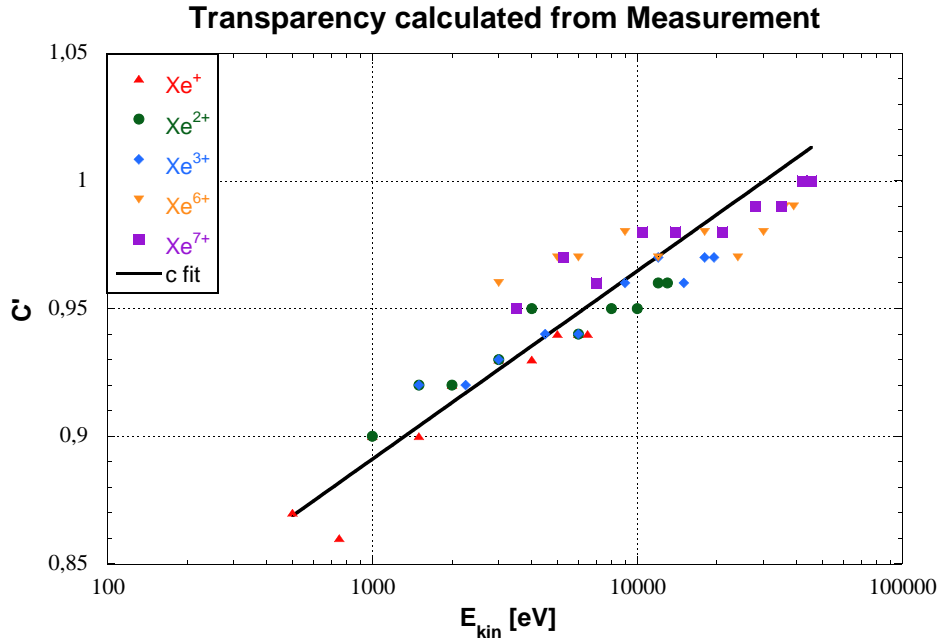


Figure 3.8: Apparent transparency c' for the different Xe projectile energies as evaluated from the ratio of the yields γ_1 and γ_2 (cf. equations 2.7 and 2.8).

3.2 Xe^{q+} on LiF

After finishing the measurements with Ar ions the next step was to measure IIEE with Xe ions. The setup and measurement conditions were not changed, only the gas bottle at the ion source had to be replaced.

An interesting behaviour was observed for the transparency c' calculated from the measured currents. (see Fig. 3.8) At low impact energies a value in the range of the real mesh transparency (as observed in measurements with conductors) was found. But with increasing impact energy (both E_{kin} and E_{pot} seemed to play a role in this) the transparency started to increase slowly to an approximate value of 1 (similar to the case of most Ar projectiles). After this I rechecked the Ar Data and found also an energy dependency for c' . In the Argon data it was just less obvious because at low projectile energies c' values were already higher than the real mesh transparency and the increase with energy was not so pronounced.

The fact that the electron yield increases with both E_{kin} and E_{pot} is a strong indicator that this “apparent” change in mesh transparency is caused by SE created on the mesh. At lower projectile energies less backscattered ions or neutral particles with high enough energies to produce SE hit the mesh, and with increasing projectile energy this starts to play a bigger role.

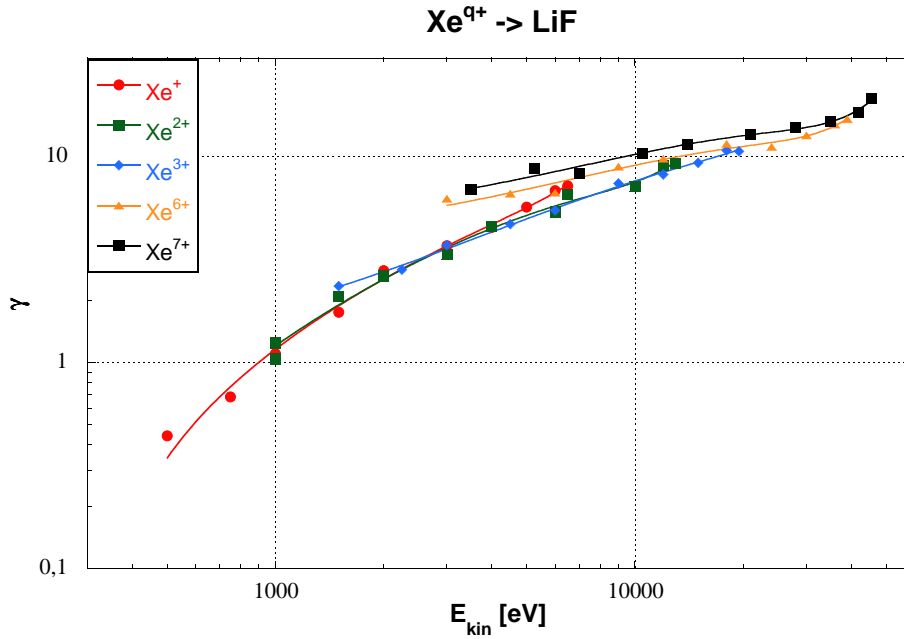


Figure 3.9: IIEE yields for Xe^{q+} ion impact on LiF

For the calculation of the yields presented in this work, again a mesh transparency depending on the projectile energy was used (see the fit in Fig. 3.8)

Fig. 3.9 shows the measured IIEE yields γ for Xe^{q+} projectiles impacting on LiF . A similar trend as in the results for Ar^{q+} impact on LiF is found, e.g. a separation of the curves for different projectile charge states in the low impact energy range, and an asymptotic behaviour of all curves at higher energies. However the splitting between the different charge states at lower energies is not as pronounced as in the case of Argon projectiles. Xe has lower ionisation energies than Ar (see Fig. 3.4) at the same charge state, which could explain why PE is not as pronounced as in the case of Ar .

Fig. 3.10 shows a direct comparison of the yields for Argon and Xenon projectiles of the same charge states. Practically all measured yields for Xe projectiles are slightly lower than the yields for Ar projectiles of the same charge state and kinetic energy.

For Ar^{+} and Xe^{+} the gap between the two yields seems to be closing at roughly 6keV. These singly charged ions have potential energies of only 15 electron Volt (eV) (Ar^{+}) and 11 eV (Xe^{+}), so KE should be the dominant emission mechanism for these ions. The binding energy of LiF is 12eV, which is higher than the potential energy of Xe^{+} and makes PE for Xe^{+} impossible. While E_{pot} of Ar^{+} is larger than the binding energy of LiF the energy difference is so small that PE should also play no role for Ar^{+} too.

For ions with $q = 3$ and $q = 6$ the differences in γ are getting smaller with increasing energy too, but the point where both yields coincide is beyond the highest impact energy measured.

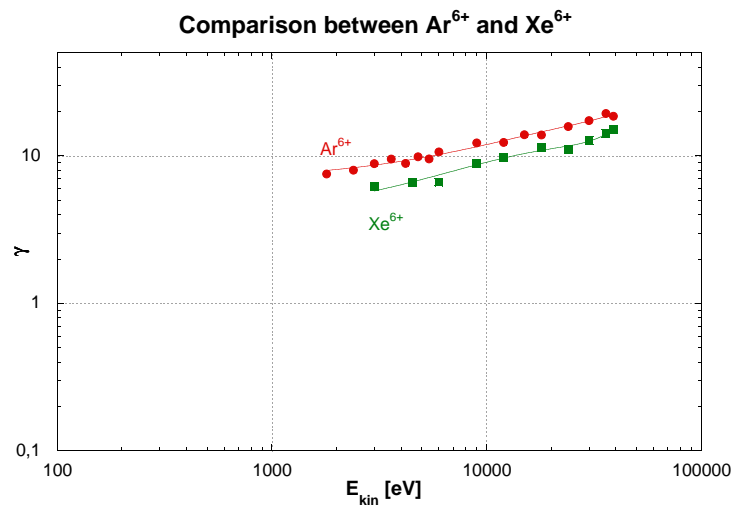
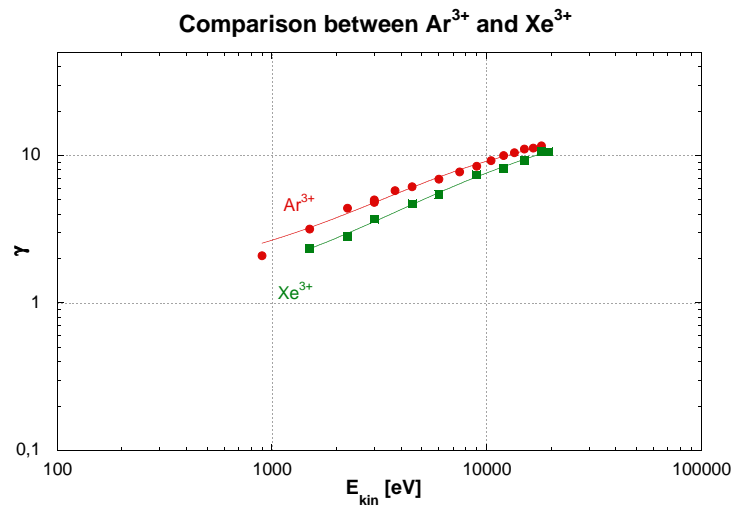
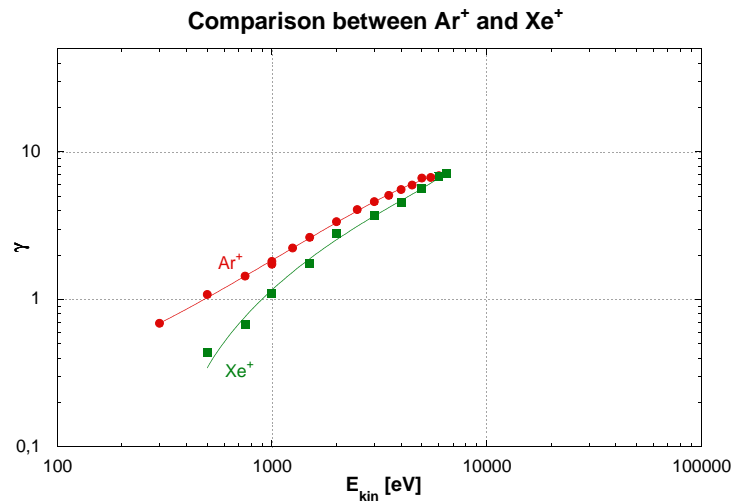


Figure 3.10: Comparison of the measured yields γ between Ar and Xe projectiles of the same charge state.

3.3 Estimation of the Error

Compared to the measurements on conducting surfaces which used the same setup [3] the following changes to the error estimation presented there have to be added. The blind currents from the heating are adding a contribution to the systematic error that critically depends on the ratio of the ion current to the blind currents. The usual blind currents were in the 0.02-0.03nA range, while the currents measured from ions and from the emitted electrons were usually in the 5-10nA range so their contribution to the total error should be below 1%. However for the measurements with an extraction potential below 400V the ion currents and especially the measured current on the collector were smaller than 1nA, which makes this contribution bigger, but the error still remains below 5%.

Also the statistical errors from repeated measurements were usually higher than on conducting surfaces. For some measurements the γ_2 yield was rather “unstable”, while for other measurements the statistical error was comparable to the measurements on conductors. But even in the worst case (low energy measurements with low yield and high instability) the statistical error always stayed below 10% (for conducting surfaces this was 5%).

For typical measurements where we could use an ion current of at least 5nA and yields were higher than $2 \frac{e^-}{ion}$ the total error should therefore be close to the value estimated for conducting surfaces. Only in special cases (low impact energies, high instabilities, low ion current) the total error can reach 20-25%.

4 Conclusions and Outlook

During this work a new control software for the ECR ion source SOPHIE at the IAP, TU-Wien was developed, put into operation, was tested and the known problems were fixed. Faraday cups that can be automatically moved into the ion beam were designed and one of these was installed and tested at BL1. Some other smaller changes to the lab setup (like the replacement of the magnet power supplies) were planned and executed too.

As the second big part of this work the EYE setup was modified to allow current measurements of the ion induced electron yield on insulating surfaces. First measurements were executed with a LiF target and singly and multiply charged Ar and Xe ions as projectiles. The possible charging-up of the target was investigated by simulations, and by watching the behaviour of different parameters of the experiment. Additionally the data obtained for Ar projectiles could be compared to available data obtained by the statistics technique. Good agreement between the datasets was found. The data for Xe impact were measured for the first time.

Plans for the close future include getting the remaining 2 Faraday cups installed, and the rest of some small tasks on the SOPHIE Setup finished. For the software the first ideas for improvement already exist, like an automatic mode, which would automatically measure a spectrum, and then identify the peak of interest in it and try optimising the settings for this ion. For EYE everything is ready for further measurements with other targets and projectiles to get more data on the IIEE yields for insulators.

Acknowledgements

I would like to thank the following people for their support during this work.

Professor Friedrich Aumayr for giving me the chance to do this work, and for all the support beginning from help with the ordering of the bigger and smaller parts needed (sometimes its harder to order some small parts like that USB to Serial hub than the big ones), to the chance to join the ITS-LEIF Winterschool.

DI Gregor Kowarik my direct supervisor who helped me a lot with the problems in the design phases, and for all the discussion that we had during this work.

Also thanks to the rest of workgroup AG Aumayr for the nice working atmosphere and the fun times.

Paul Berlinger our electronics engineer for building the needed electronics and always being helpful when I needed help with different electronic problems.

Wolfgang Beck, Rainer Gärtner and *Herbert Schmidt* the staff of our workshop for building the parts for the moving Faraday cups and the indirectly heated target holder for me.

Werner Hübner the head of the IT-Development department at my work, for a great working atmosphere, all the nice discussions we had over the years during work and at other events, for the visits in the hospital, and for allowing me to change to a 2 days a week work schedule without which I would never have been able to write this thesis.

Last but not least huge thanks to my family and friends for all the fun times but also for the support during my studies, and for all the motivation that you gave me to continue with them. Also lots of thanks for all the visits in the hospital in the time after my accident, especially during the time that I spent awake in the intensive care unit, when I was happy about any distraction.

Bibliography

- [1] E. Gruber. Experimentelle Untersuchung ioneninduzierter Elektronenemission von Isolatoren, Bachelors thesis, Institut für allgemeine Physik, TU Wien.
- [2] G. Kowarik, E. Gruber, K. Iskratsch, and F. Aumayr. Using a current method for measuring ion induced kinetic electron emission from LiF . Poster: 4th Annual Meeting of the EU network ITS-LEIF, Platja d'Aro, Girona/Spain, May 2009.
- [3] M. Brunmayr. Experimentelle Untersuchungen zur ioneninduzierten Elektronenemission aus Kernfusions-relevanten Oberflächen. Master's thesis, Institut für allgemeine Physik, TU-Wien, Feb 2008.
- [4] E. Galutschek. *Development of a 14.5 GHz All-Permanent Magnet Multicharged ECR Ion Source for Remote Operation*. PhD thesis, Institut für allgemeine Physik, TU-Wien, Mar 2005.
- [5] XDMCP. HOWTO, 2007. URL <http://tldp.org/HOWTO/XDMCP-HOWTO/intro.html>.
- [6] E Galutschek, R Trassl, E Salzborn, F Aumayr, and HP Winter. Compact 14.5 GHz all-permanent magnet ECRIS for experiments with slow multicharged ions. *Journal of Physics: Conference Series*, 58:395–398, 2007.
- [7] J. Bundesmann. Das Kontrollsystem Codian - Steuerung und Visualisierung eines Ionenquellen-Teststands. In *Begleitband zum Kongress VIP2001 - "Virtuelle Instrumente in der Praxis"*, pages 125–131. Hüthig Verlag Heidelberg, 2001.
- [8] T. Neidhart, F. Pichler, F. Aumayr, HP Winter, M. Schmid, and P. Varga. Potential sputtering of lithium fluoride by slow multicharged ions. *Physical review letters*, 74 (26):5280–5283, 1995.
- [9] M. Sporn, G. Libiseller, T. Neidhart, M. Schmid, F. Aumayr, HP Winter, P. Varga, M. Grether, D. Niemann, and N. Stolterfoht. Potential Sputtering of Clean SiO_2 by Slow Highly Charged Ions. *Physical Review Letters*, 79(5):945–948, 1997.
- [10] G. Kowarik, M. Brunmayr, and F. Aumayr. Electron emission from tungsten induced by slow, fusion-relevant ions. *Nuclear Inst. and Methods in Physics Research, B*, 267 (16):2634–2637, 2009.

- [11] R. Heller, S. Facsko, RA Wilhelm, and W. Möller. Defect mediated desorption of the KBr (001) surface induced by single highly charged ion impact. *Physical Review Letters*, 101(9):96102, 2008.
- [12] AS El-Said, R. Heller, W. Meissl, R. Ritter, S. Facsko, C. Lemell, B. Solleder, IC Gebeshuber, G. Betz, M. Toulemonde, et al. Creation of Nanohillocks on CaF_2 Surfaces by Single Slow Highly Charged Ions. *Physical Review Letters*, 100(23):237601, 2008.
- [13] N. Stolterfoht, JH Bremer, V. Hoffmann, R. Hellhammer, D. Fink, A. Petrov, and B. Sulik. Transmission of 3 keV Ne^{7+} Ions through Nanocapillaries Etched in Polymer Foils: Evidence for Capillary Guiding. *Physical Review Letters*, 88(13):133201–133900, 2002.
- [14] RJ Bereczky, G. Kowarik, F. Aumayr, and K. Tőkési. Transmission of 4.5 keV Ar^{9+} ions through a single glass macro-capillary. *Nuclear Inst. and Methods in Physics Research, B*, 267(2):317–320, 2009.
- [15] G. Kowarik, RJ Bereczky, F. Aumayr, and K. Tőkési. Production of a microbeam of slow highly charged ions with a single microscopic glass capillary. *Nuclear Inst. and Methods in Physics Research, B*, 267(12-13):2277–2279, 2009.
- [16] R. A. Baragiola, E. V. Alonso, and A. Oliva Florio. Electron emission from clean metal surfaces induced by low-energy light ions. *Phys. Rev. B*, 19(1):121–129, Jan 1979.
- [17] J. Lörinčík, Z. Šroubek, H. Eder, F. Aumayr, and HP Winter. Kinetic electron emission from clean polycrystalline gold induced by impact of slow C^+ , N^+ , O^+ , Ne^+ , Xe^+ , and Au^+ ions. *Phys. Rev. B*, 62(23):16116–16125, Dec 2000.
- [18] W. Meissl, M.C. Simon, J.R. Crespo López-Urrutia, H. Tawara, J. Ullrich, HP. Winter, and F. Aumayr. Highly charged ion-induced potential electron emission from clean $Au(111)$: Dependence on the projectile angle of incidence. *Nuclear Instruments and Methods in Physics Research Section B: Beam Interactions with Materials and Atoms*, 256(1):520–523, 2007.
- [19] H. Winter and H. P. Winter. Classical model of kinetic electron emission near threshold induced by impact of atomic projectiles on a free-electron gas metal. *EPL (Europhysics Letters)*, 62(5):739–745, 2003.
- [20] J. Burgdörfer, P. Lerner, and F. W. Meyer. Above-surface neutralization of highly charged ions: The classical over-the-barrier model. *Phys. Rev. A*, 44(9):5674–5685, Nov 1991.

- [21] HP Winter, F. Aumayr, C. Lemell, J. Burgdörfer, S. Lederer, and H. Winter. Kinetic electron emission by grazing atom scattering from clean flat metal surfaces. *Nuclear Instruments and Methods in Physics Research Section B: Beam Interactions with Materials and Atoms*, 256(1):455–463, 2007.
- [22] W. Meissl, D. Winklehner, F. Aumayr, M. C. Simon, R. Ginzl, J. R. Crespo López-Urrutia, J. Ullrich, B. Solleder, C. Lemell, and J. Burgdörfer. Electron Emission from Insulators Irradiated by Slow Highly Charged Ions. *e-Journal of Surface Science and Nanotechnology*, 6:54–59, 2008.
- [23] M. Vana, F. Aumayr, P. Varga, and HP Winter. Electron Emission from Polycrystalline Lithium Fluoride Induced by Slow Multicharged Ions. *EPL (Europhysics Letters)*, 29(1):55–60, 1995.
- [24] M. Vana, F. Aumayr, P. Varga, and HP. Winter. Electron emission from polycrystalline Lithiumfluoride bombarded by slow multicharged ions. *Nucl. Instrum. Meth. Phys. Res. B*, 100:284–289, 1995.
- [25] D. Hasselkamp. *Kinetic electron emission from solid surfaces under ion bombardment*, volume 123 of *Springer Tracts in Modern Physics*, pages 1–95. Springer Berlin / Heidelberg, 1992.
- [26] F. Aumayr and HP Winter. *Potential Electron Emission from Metal and Insulator Surfaces*, volume 225 of *Springer Tracts in Modern Physics*, pages 79–112. Springer Berlin / Heidelberg, 2007.
- [27] H. Eder, M. Vana, F. Aumayr, and H. P. Winter. Precise total electron yield measurements for impact of singly or multiply charged ions on clean solid surfaces. *Review of Scientific Instruments*, 68(1):165–169, 1997.
- [28] F. Aumayr, H. Kurz, D. Schneider, M. A. Briere, J. W. McDonald, C. E. Cunningham, and HP. Winter. Emission of electrons from a clean gold surface induced by slow, very highly charged ions at the image charge acceleration limit. *Phys. Rev. Lett.*, 71(12):1943–1946, Sep 1993.
- [29] H. Kurz, F. Aumayr, HP. Winter, D. Schneider, M. A. Briere, and J. W. McDonald. Electron emission and image-charge acceleration for the impact of very highly charged ions on clean gold. *Phys. Rev. A*, 49(6):4693–4702, Jun 1994.
- [30] D. Hasselkamp, H. Rothard, K. O. Groeneveld, J. Kemmler, P. Varga, and HP. Winter. *Particle induced electron emission*, volume 123 of *Springer tracts in modern physics*. Springer, 1992.

- [31] HP Winter, H. Eder, F. Aumayr, J. Lörincik, and Z. Sroubek. Slow-ion induced electron emission from clean metal surfaces: “Subthreshold kinetic emission” and “potential excitation of plasmons”. *Nuclear Instruments and Methods in Physics Research Section B: Beam Interactions with Materials and Atoms*, 182(1-4):15–22, 2001.
- [32] M. C. Simon. Elektronen Emission bei Beschuss von Isolator- und Metall-Oberflächen mit hochgeladenen Ionen. Master’s thesis, Institut für allgemeine Physik, TU-Wien, Aug 2006.
- [33] HP Winter and J. Burgdörfer, editors. *Slow heavy-particle induced electron emission from solid surfaces*. Springer tracts in modern physics ; 225. Springer, Berlin, 2007.
- [34] A. Arnau, F. Aumayr, P. M. Echenique, M. Grether, W. Heiland, J. Limburg, R. Morgenstern, P. Roncin, S. Schippers, R. Schuch, N. Stolterfoht, P. Varga, T. J. M. Zouros, and HP Winter. Interaction of slow multicharged ions with solid surfaces. *Surface Science Reports*, 27(4-6):113–239, 1997.
- [35] J. P. Briand, L. de Billy, P. Charles, S. Essabaa, P. Briand, R. Geller, J. P. Desclaux, S. Bliman, and C. Ristori. Production of hollow atoms by the excitation of highly charged ions in interaction with a metallic surface. *Phys. Rev. Lett.*, 65(2):159–162, Jul 1990.
- [36] C. Lemell, J. Stöckl, J. Burgdörfer, G. Betz, HP. Winter, and F. Aumayr. Multicharged Ion Impact on Clean Au(111): Suppression of Kinetic Electron Emission in Glancing Angle Scattering. *Phys. Rev. Lett.*, 81(9):1965–1968, Aug 1998.
- [37] AG Drentje. Techniques and mechanisms applied in electron cyclotron resonance sources for highly charged ions. *Review of Scientific Instruments*, 74:2631, 2003.
- [38] D. Leitner, C.M. Lyneis, S.R. Abbott, D. Collins, R.D. Dwinell, M.L. Galloway, M. Leitner, and D.S. Todd. Next generation ECR ion sources: First results of the superconducting 28 GHz ECRIS - VENUS. *Nuclear Instruments and Methods in Physics Research Section B: Beam Interactions with Materials and Atoms*, 235(1-4):486–493, 2005.
- [39] R. J. Goldston and P. H. Rutherford. *Introduction to Plasma Physics*. Institute of Physics Publishing, 1995.
- [40] A. Girard, D. Hitz, G. Melin, S. Gammino, G. Ciavola, and L. Celona. Utilization of gyrotrons in the field of ECRIS for accelerators, first results and perspectives. *Nuclear Fusion*, 43(11):1520–1525, 2003.
- [41] R. Geller. *Electron cyclotron resonance ion sources and ECR plasmas*. Institute of Physics Publishing, 1996.

- [42] I.G. Brown. *The physics and technology of ion sources*. Wiley-VCH Verlag GmbH, 2004.
- [43] NX. Getting Started with NX, 2007. URL <http://www.nomachine.com/documents/getting-started.php>.
- [44] G. Kowarik. Investigations on ion induced electron emission from fusion-relevant surfaces. Master's thesis, Institut für allgemeine Physik, TU-Wien, Jan 2007.
- [45] FZ Dresden-Rossendorf. Calculator for the potential energy of a highly charged ion. URL http://www.dreebit.com/en/highly_charged_ions/data/index.php.
- [46] S. Cernusca, M. Fursatz, HP. Winter, and F. Aumayr. Ion-induced kinetic electron emission from HOPG with different surface orientation. *EPL (Europhysics Letters)*, 70(6):768–774, 2005.

A Appendix

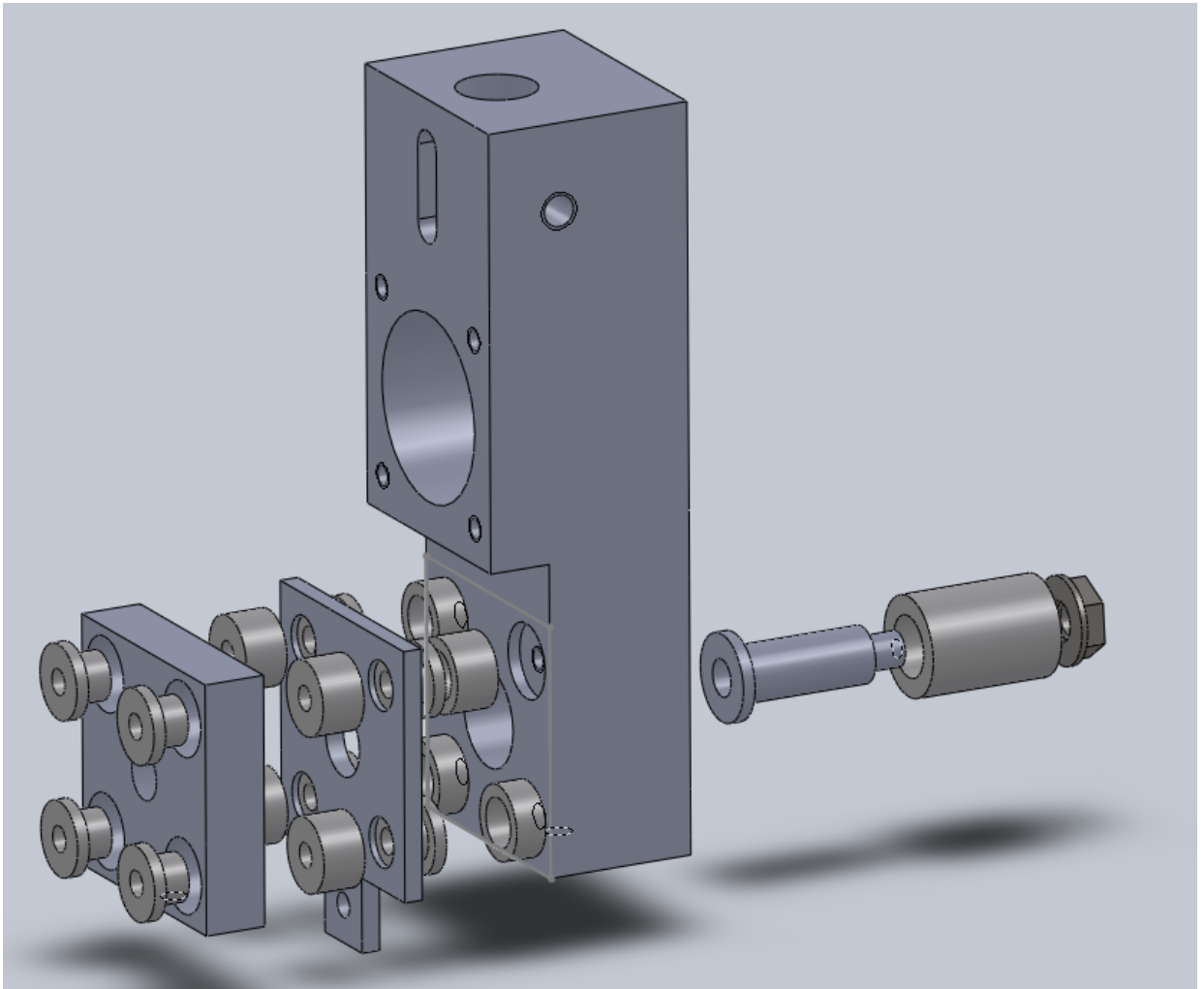
A.1 List of used or reserved I/O Connectors

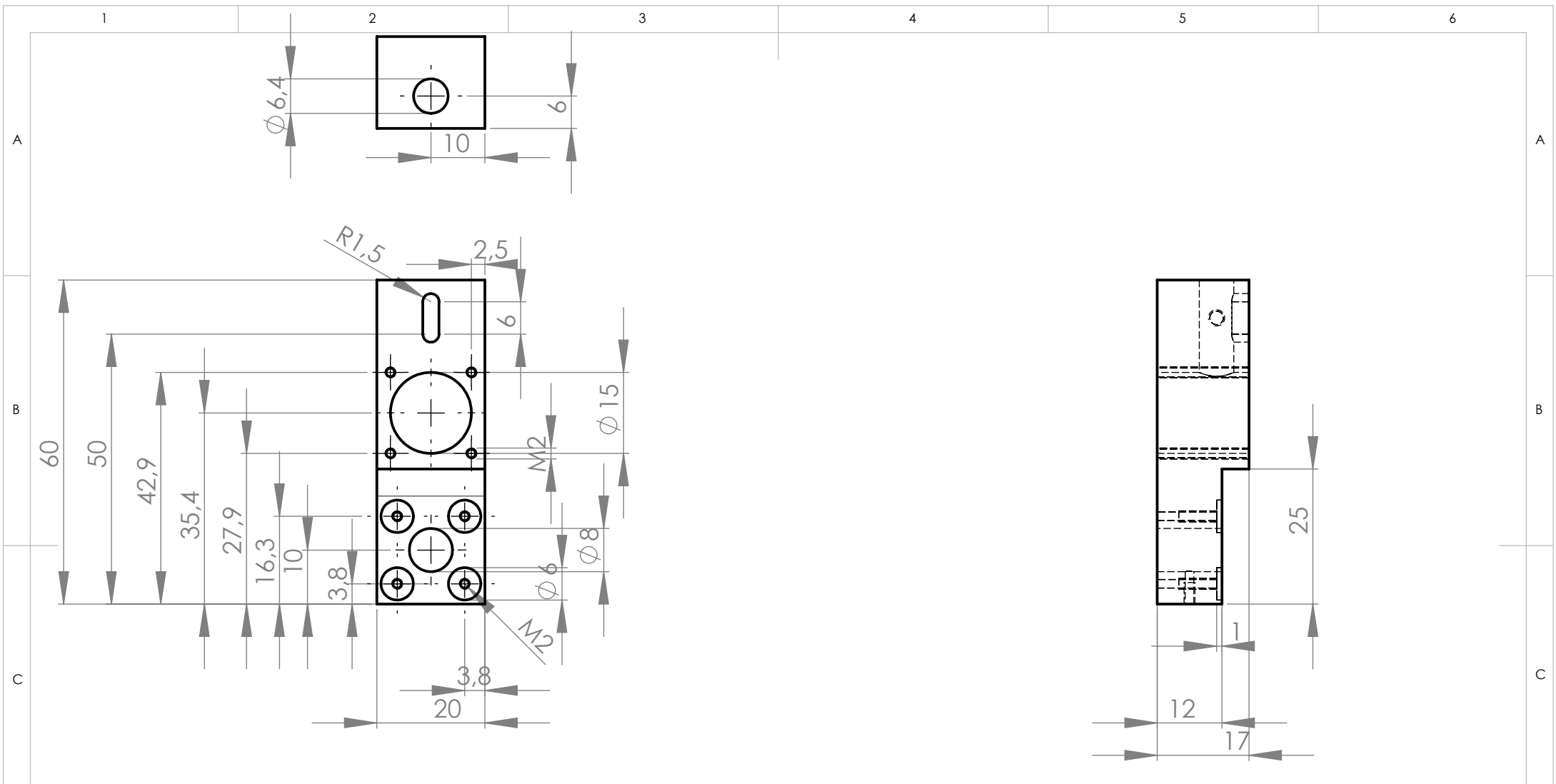
Serial RS232	
VISA Device Id	Connected to
ASRL1	Microwave Amplifier
ASRL2	Sector Magnet 1 Power Supply
ASRL3	Quadrupole Power Supply One
ASRL4	Quadrupole Power Supply Two
Analogue Outputs	
Channel	Connected to
0	U Bias
1	U Source
2	U Suppressor
3	
4	
5	Sector Magnet 2
6	Microwave Frequency
7	Gas 1
8	Gas 2
9	
10	
11	
12	
13	User 1
14	User 2
15	User 3

Analogue Inputs	
Channel	Connected to
0	User 1
1	User 2
2	User 3
3	
4	
5	Pressure Beamline 1
6	Pressure Beamline 2
7	Pressure Beamline 3
8	I Source
9	I Suppressor
10	I Sector Magnet 2
11	Pressure Main Chamber
12	Pressure Gas 1
13	Pressure Gas 2
14	I Faraday Cup
15	Magnetic Field Signal
Digital IO on AO card	
Channel	Connected to
0	Polarity Sector Magnet 1
1	Polarity Sector Magnet 2
2	Mover Faraday Cup 1
3	Mover Faraday Cup 2
4	Mover Faraday Cup 3
5	Valve Beamline 1
6	Valve Beamline 2
7	Valve Beamline 3
Digital IO on AI card	
Channel	Connected to
0	Flow Cooling Water SM 1
1	Flow Cooling Water SM 2
2	
3	
4	
5	
6	
7	

A.2 CAD Drawings

A.2.1 CAD Drawings for the Faraday Cups





UNLESS OTHERWISE SPECIFIED:
 DIMENSIONS ARE IN MILLIMETERS
 SURFACE FINISH:
 TOLERANCES:
 LINEAR:
 ANGULAR:

FINISH:
 DEBUR AND
 BREAK SHARP
 EDGES

DO NOT SCALE DRAWING

REVISION

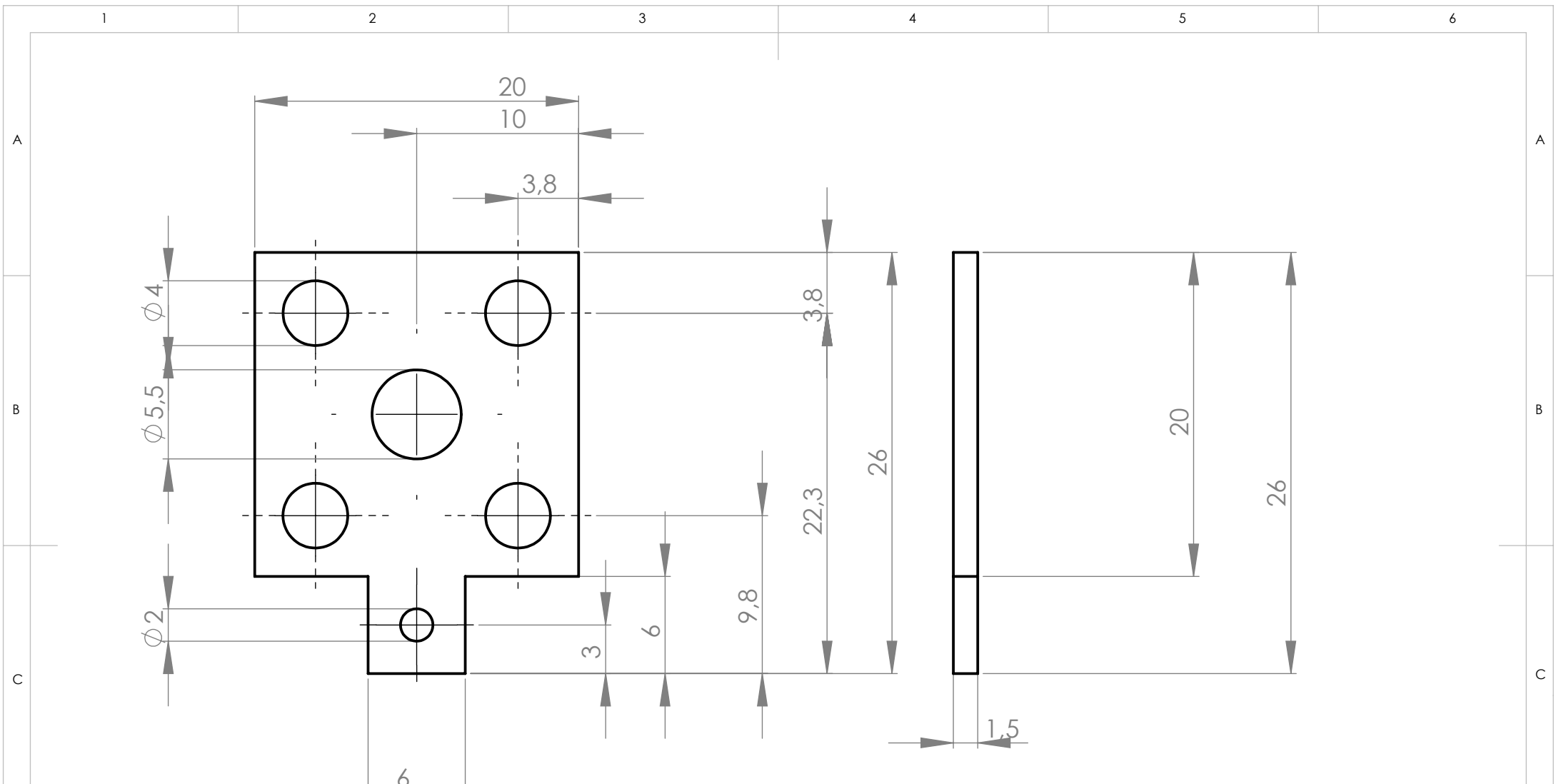
	NAME	SIGNATURE	DATE		
DRAWN					
CHK'D					
APPV'D					
MFG					
Q.A					
				MATERIAL:	
				WEIGHT:	

TITLE:

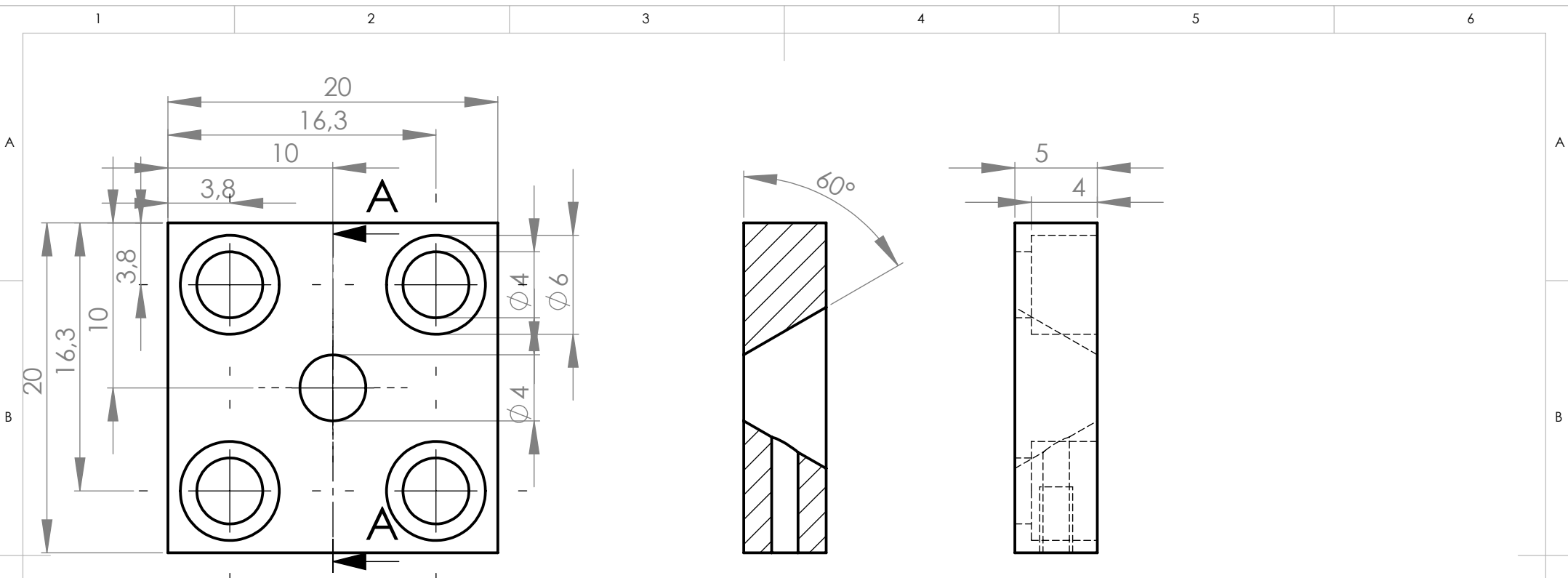
DWG NO. **Cup - Basepart** A4

SCALE:1:1

SHEET 1 OF 1



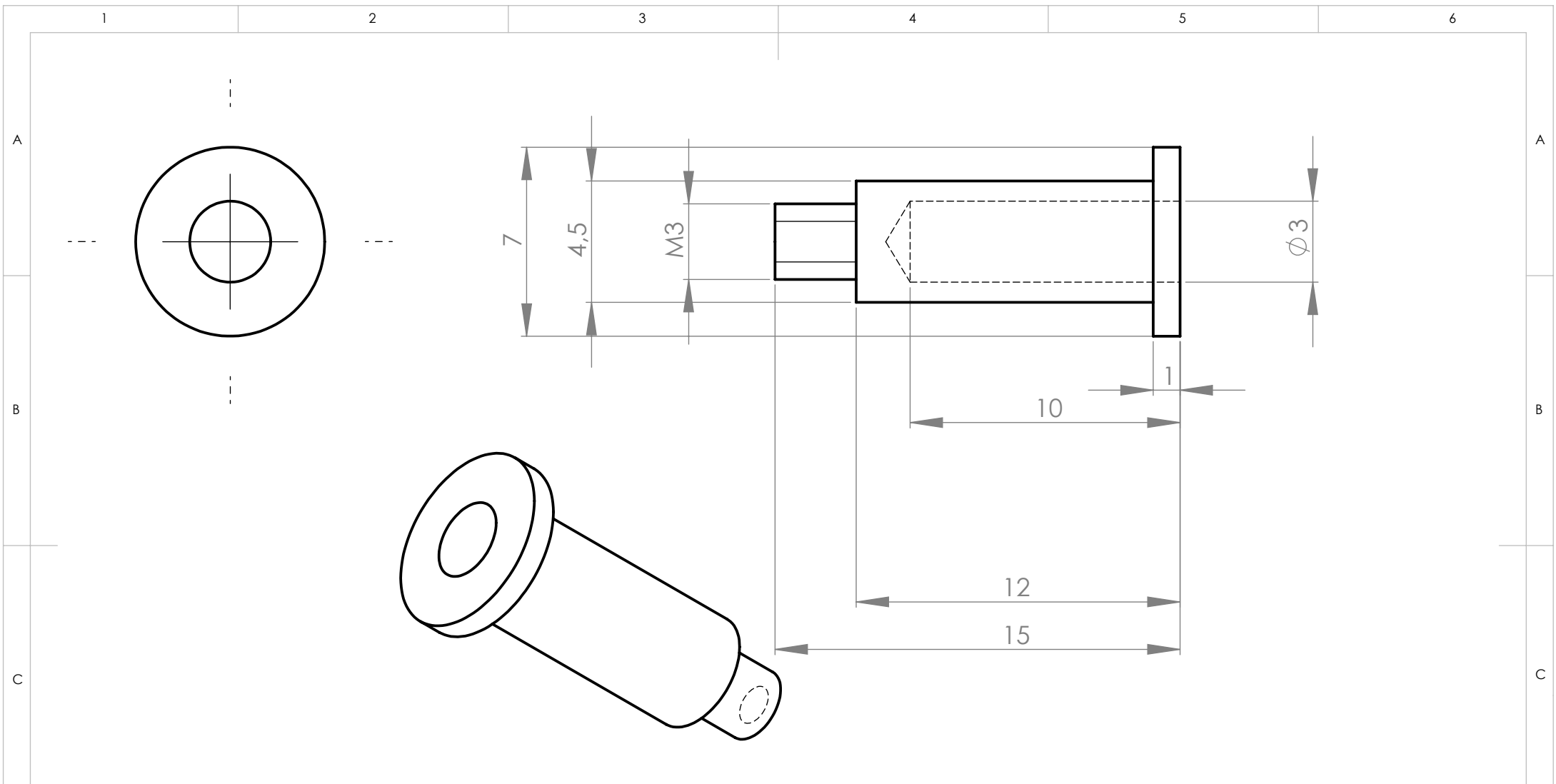
UNLESS OTHERWISE SPECIFIED: DIMENSIONS ARE IN MILLIMETERS SURFACE FINISH: TOLERANCES: LINEAR: ANGULAR:				FINISH:		DEBUR AND BREAK SHARP EDGES		DO NOT SCALE DRAWING		REVISION	
								TITLE:			
DRAWN				NAME		SIGNATURE		DATE			
CHK'D											
APPV'D											
MFG											
Q.A								MATERIAL:		DWG NO.	
										electrode	
								WEIGHT:		A4	
								SCALE: 3:1		SHEET 1 OF 1	



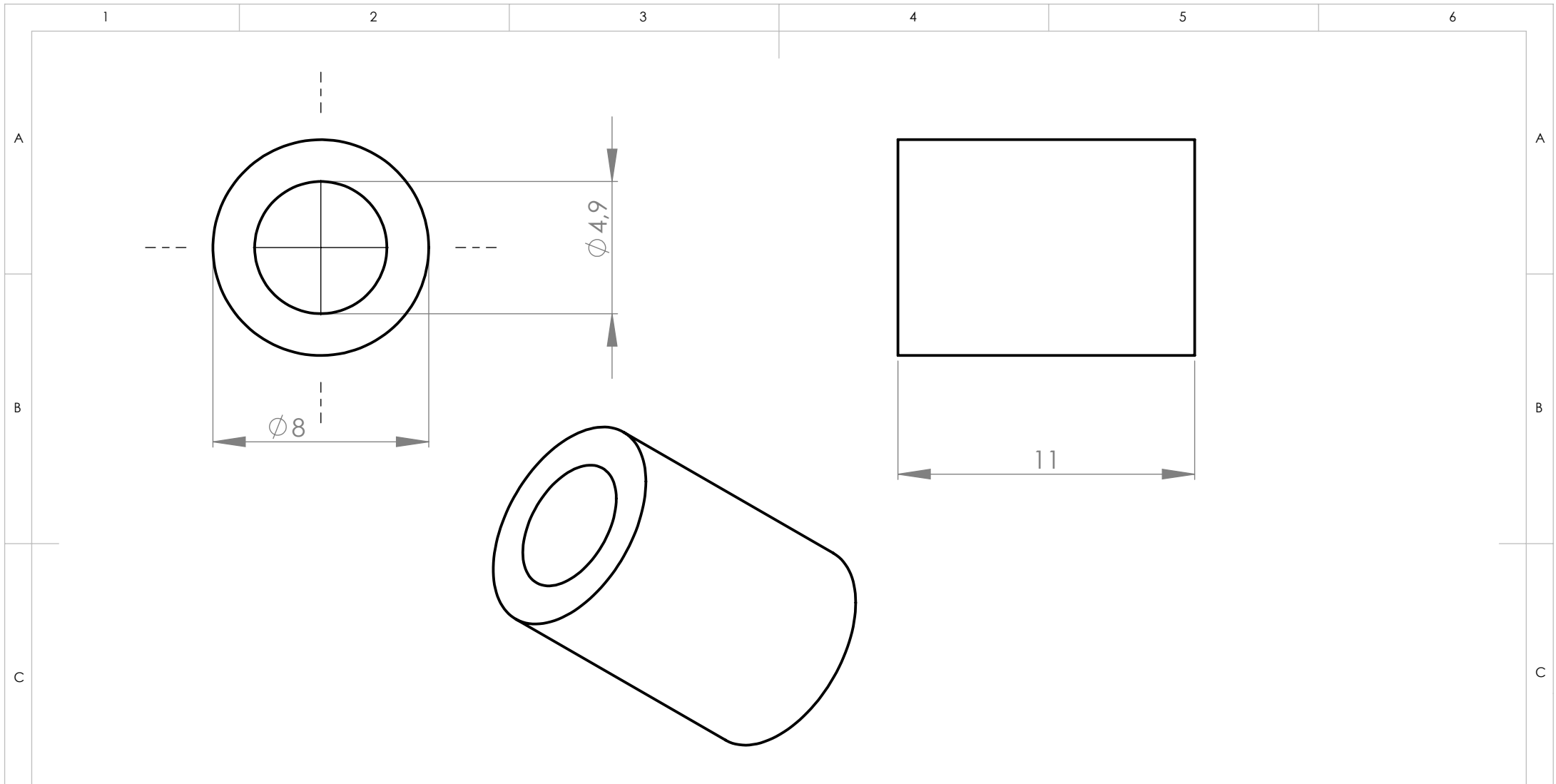
SCHNITT A-A
 MAßSTAB 3 : 1

M2x0.4

UNLESS OTHERWISE SPECIFIED: DIMENSIONS ARE IN MILLIMETERS SURFACE FINISH: TOLERANCES: LINEAR: ANGULAR:				FINISH:		DEBUR AND BREAK SHARP EDGES		DO NOT SCALE DRAWING		REVISION	
DRAWN				SIGNATURE		DATE		TITLE:			
CHK'D											
APPV'D											
MFG											
Q.A						MATERIAL:		DWG NO.		aperture	
								SCALE:3:1		SHEET 1 OF 1	
										A4	

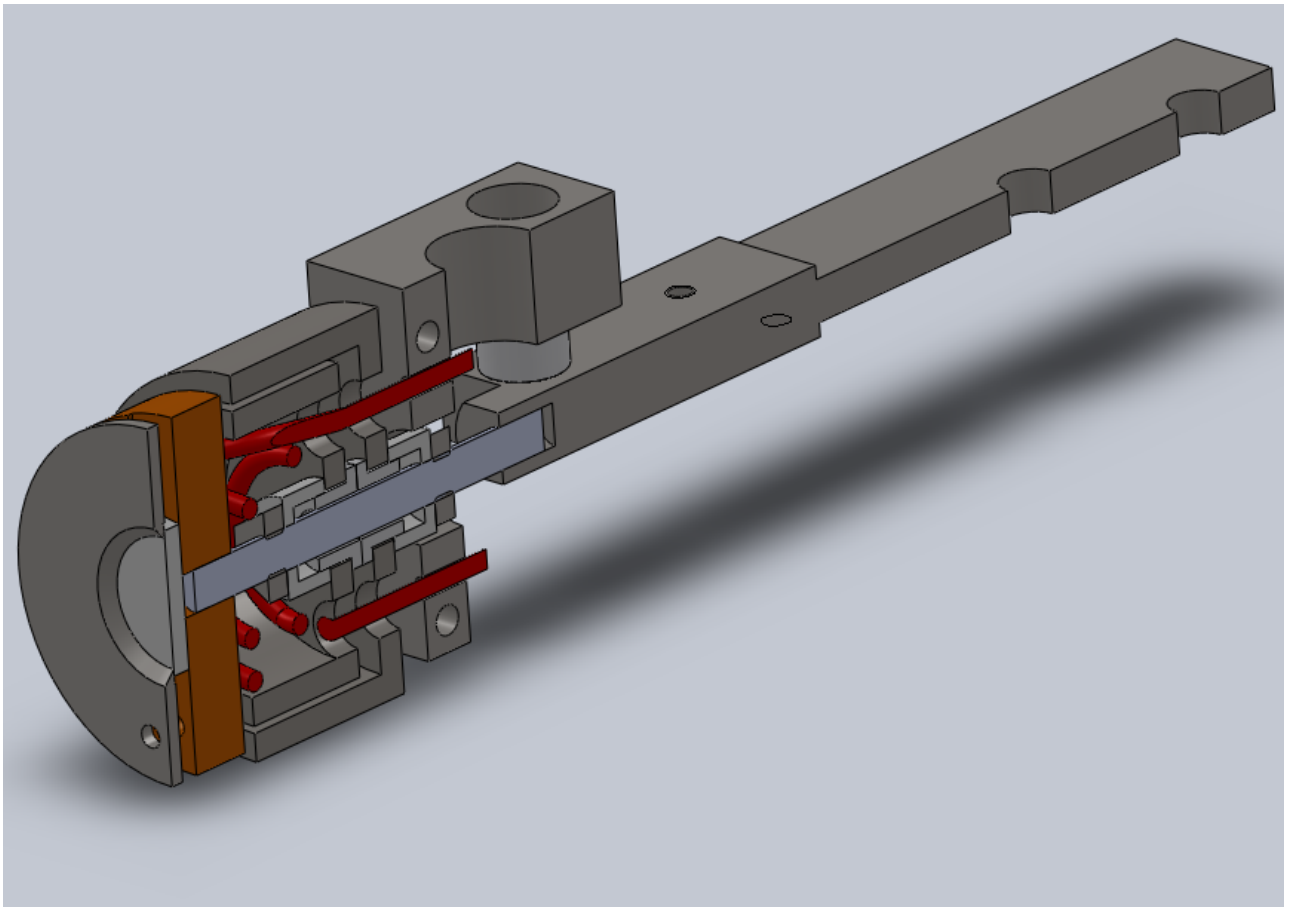


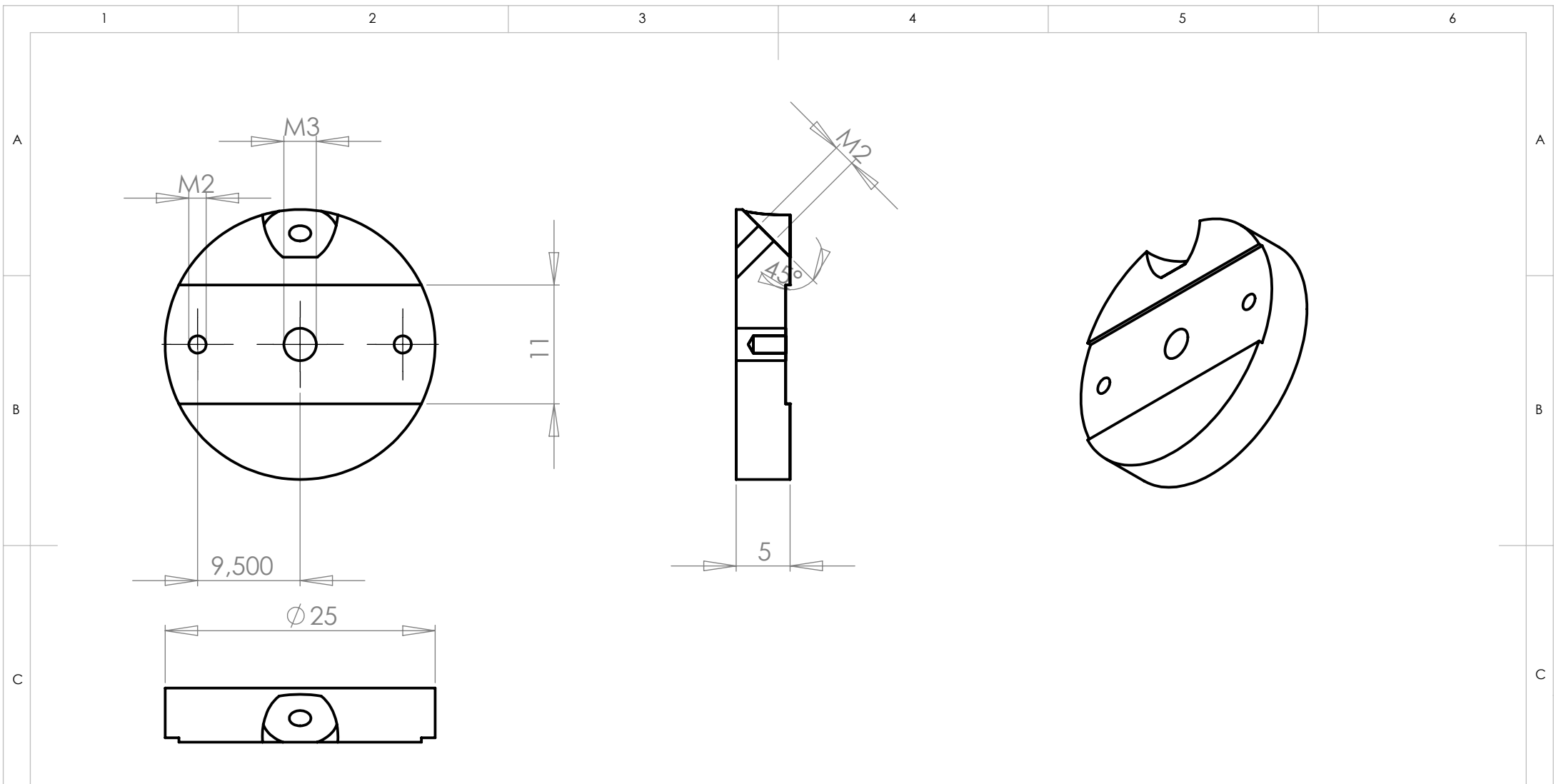
UNLESS OTHERWISE SPECIFIED: DIMENSIONS ARE IN MILLIMETERS SURFACE FINISH: TOLERANCES: LINEAR: ANGULAR:				FINISH:		DEBUR AND BREAK SHARP EDGES		DO NOT SCALE DRAWING		REVISION	
	NAME	SIGNATURE	DATE					TITLE:			
DRAWN											
CHK'D											
APPV'D											
MFG											
Q.A								MATERIAL:		DWG NO.	
										Cup	
								WEIGHT:		A4	
								SCALE:5:1		SHEET 1 OF 1	



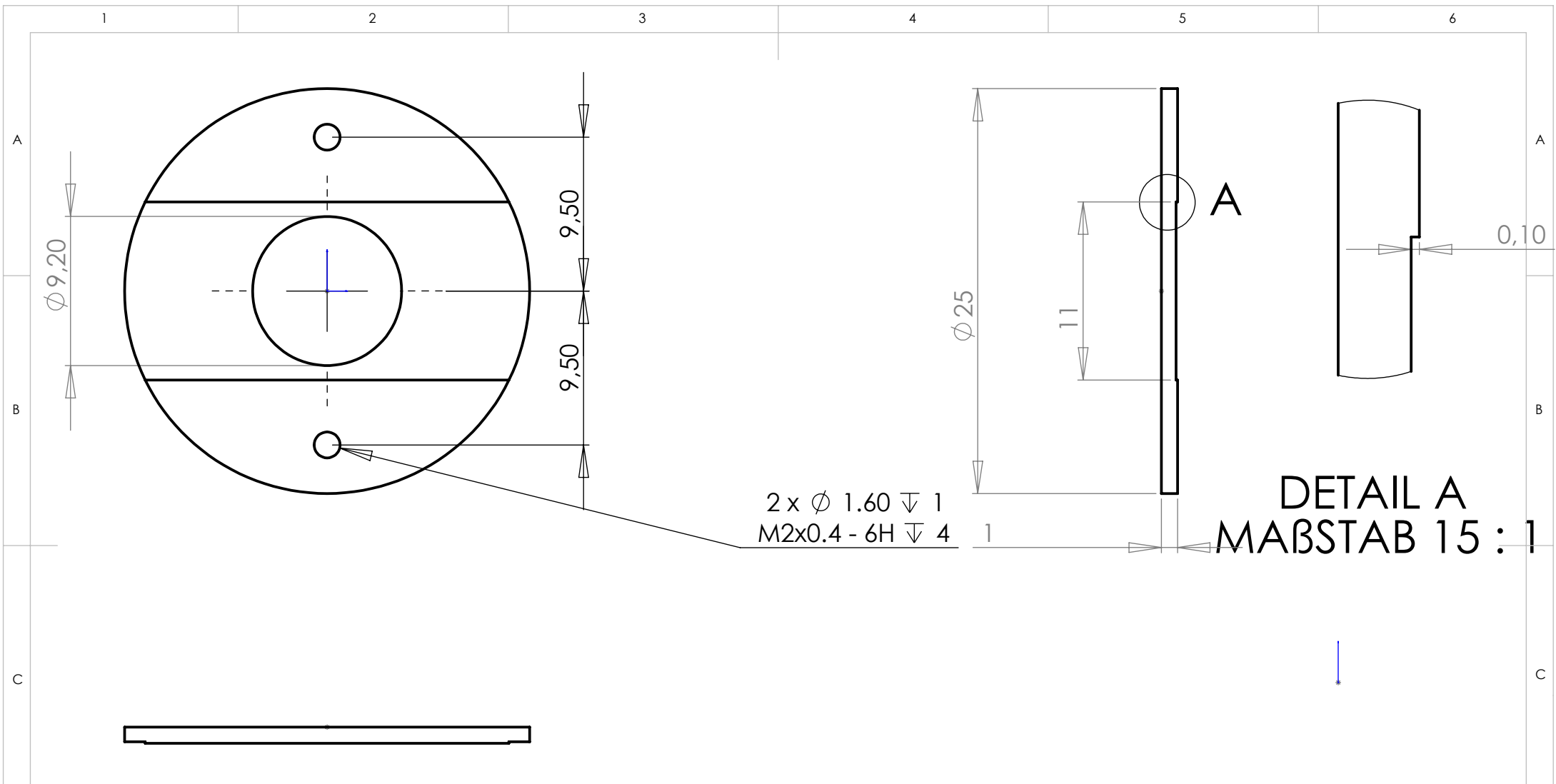
UNLESS OTHERWISE SPECIFIED: DIMENSIONS ARE IN MILLIMETERS SURFACE FINISH: TOLERANCES: LINEAR: ANGULAR:		FINISH:		DEBUR AND BREAK SHARP EDGES		DO NOT SCALE DRAWING		REVISION	
	NAME	SIGNATURE	DATE			TITLE:			
DRAWN									
CHK'D									
APPV'D									
MFG									
Q.A					MATERIAL:	DWG NO.		insulator	
								A4	
					WEIGHT:	SCALE:5:1		SHEET 1 OF 1	

A.2.2 CAD Drawings for the Indirect Heated Targetholder





UNLESS OTHERWISE SPECIFIED: DIMENSIONS ARE IN MILLIMETERS SURFACE FINISH: TOLERANCES: LINEAR: ANGULAR:		FINISH:		DEBUR AND BREAK SHARP EDGES		DO NOT SCALE DRAWING		REVISION	
	NAME	SIGNATURE	DATE			TITLE:			
DRAWN						DWG NO. Targetholder base A4			
CHK'D									
APPV'D									
MFG									
Q.A									
					MATERIAL:	WEIGHT:			
						SCALE:2:1		SHEET 1 OF 1	



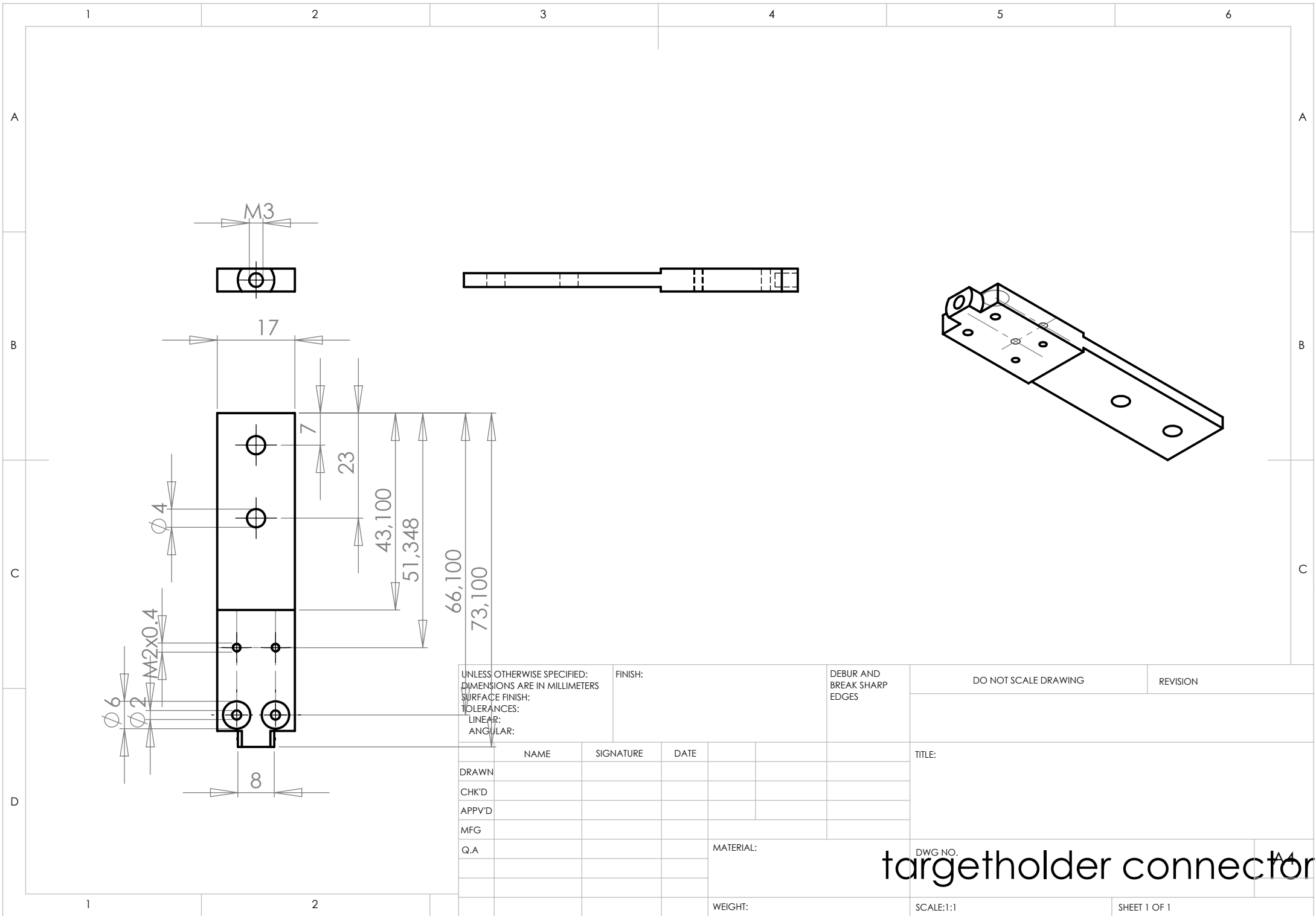
2 x \varnothing 1.60 ∇ 1
M2x0.4 - 6H ∇ 4

DETAIL A
MAßSTAB 15 : 1

UNLESS OTHERWISE SPECIFIED: DIMENSIONS ARE IN MILLIMETERS SURFACE FINISH: TOLERANCES: LINEAR: ANGULAR:		FINISH:		DEBUR AND BREAK SHARP EDGES		DO NOT SCALE DRAWING		REVISION	
DRAWN		SIGNATURE		DATE		TITLE:			
CHK'D									
APPV'D									
MFG									
Q.A						MATERIAL:		DWG NO. 14	
						WEIGHT:		SHEET 1 OF 1	

Targetholder Frontplate

SCALE:2:1



UNLESS OTHERWISE SPECIFIED:
 DIMENSIONS ARE IN MILLIMETERS
 SURFACE FINISH:
 TOLERANCES:
 LINEAR:
 ANGULAR:

FINISH:

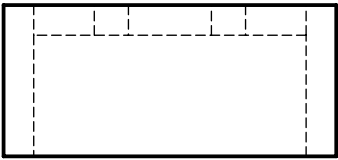
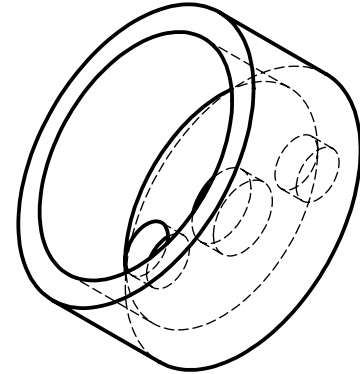
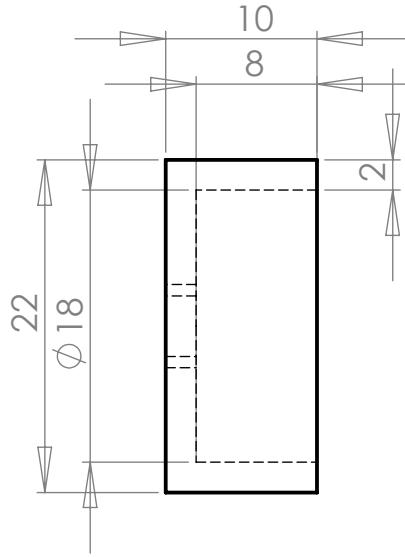
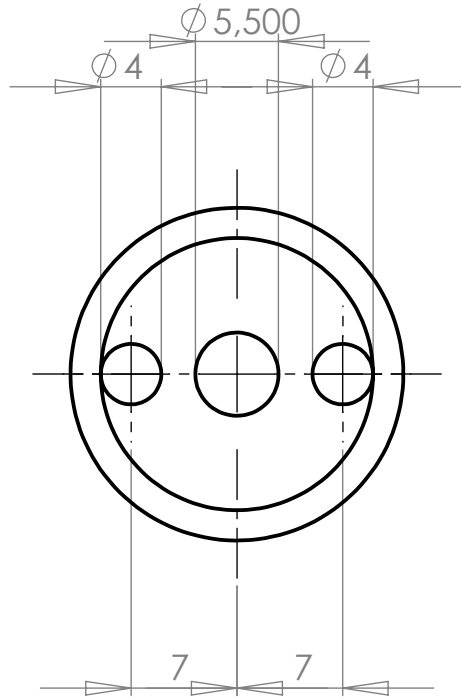
DEBUR AND
 BREAK SHARP
 EDGES

DO NOT SCALE DRAWING

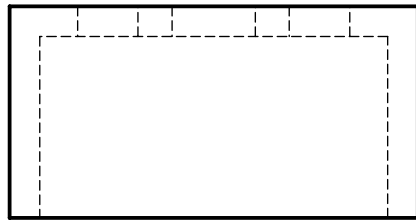
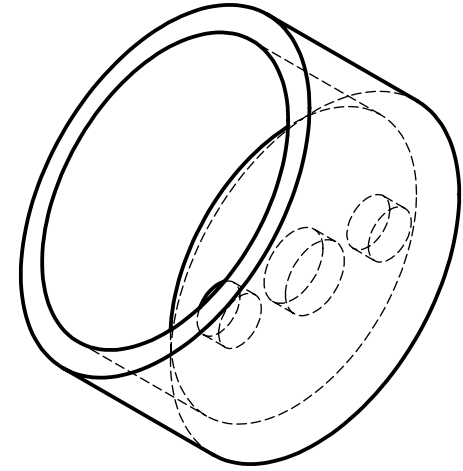
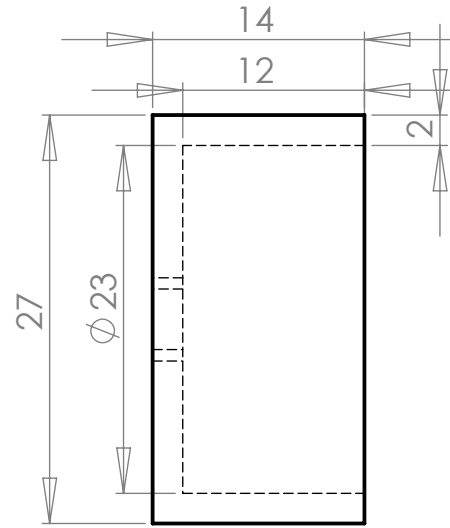
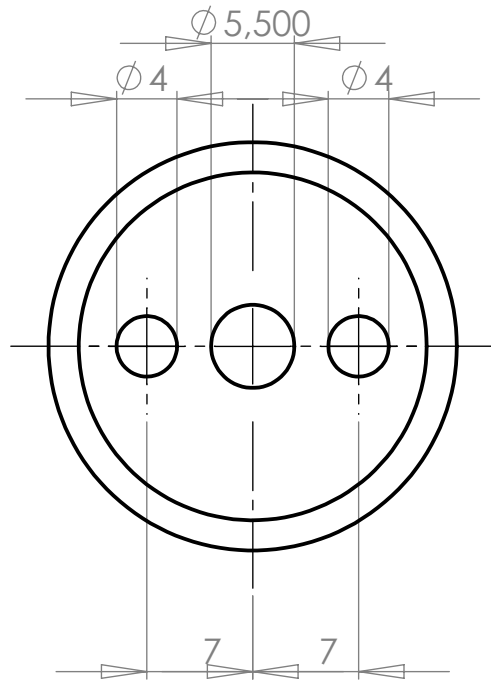
REVISION

	NAME	SIGNATURE	DATE		
DRAWN					
CHK'D					
APPV'D					
MFG					
Q.A					
				MATERIAL:	
				WEIGHT:	

TITLE:	DWG NO.	SCALE:	SHEET
targetholder connector		1:1	1 OF 1



UNLESS OTHERWISE SPECIFIED: DIMENSIONS ARE IN MILLIMETERS SURFACE FINISH: TOLERANCES: LINEAR: ANGULAR:			FINISH:		DEBUR AND BREAK SHARP EDGES		DO NOT SCALE DRAWING		REVISION	
DRAWN			SIGNATURE		DATE		TITLE:			
CHK'D										
APPV'D										
MFG										
Q.A					MATERIAL:		DWG NO.		inner Heatshield	
							SCALE:2:1		SHEET 1 OF 1	
					WEIGHT:				A4	



UNLESS OTHERWISE SPECIFIED:
 DIMENSIONS ARE IN MILLIMETERS
 SURFACE FINISH:
 TOLERANCES:
 LINEAR:
 ANGULAR:

FINISH:

DEBUR AND
 BREAK SHARP
 EDGES

DO NOT SCALE DRAWING

REVISION

	NAME	SIGNATURE	DATE		
DRAWN					
CHK'D					
APPV'D					
MFG					
Q.A				MATERIAL:	
				WEIGHT:	

TITLE:

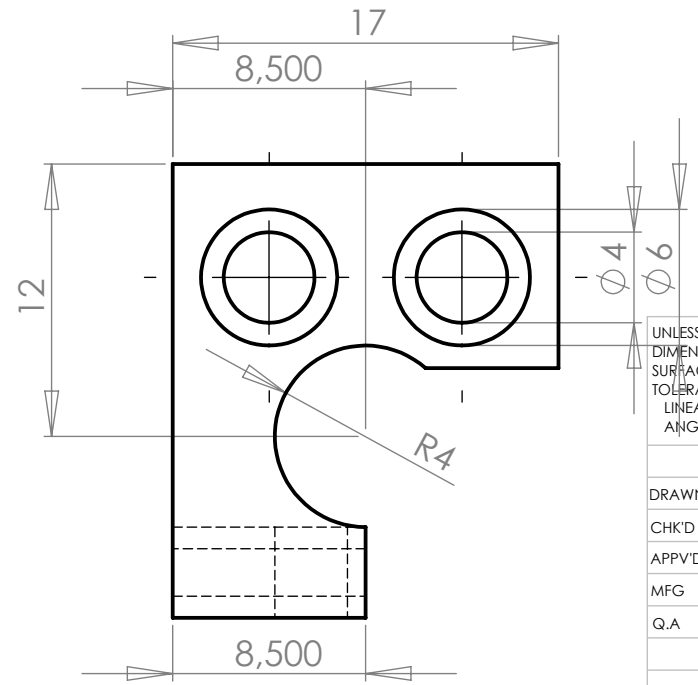
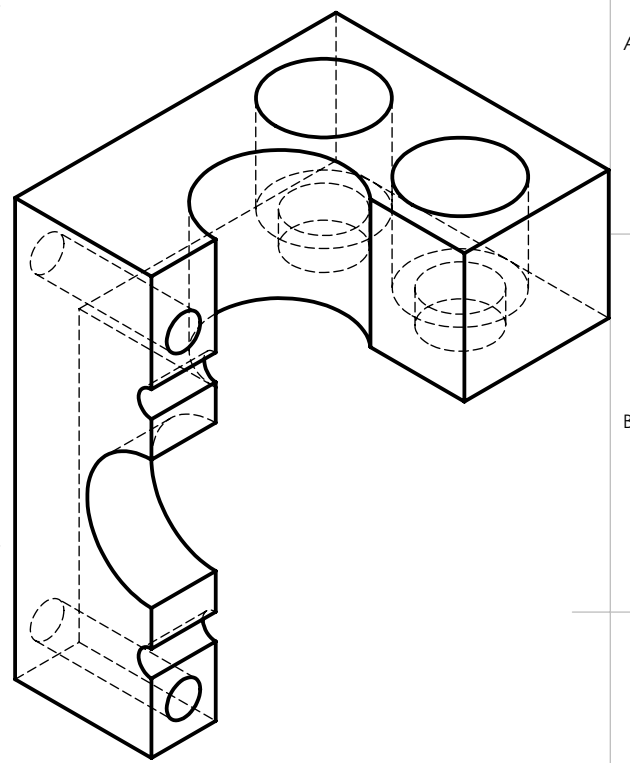
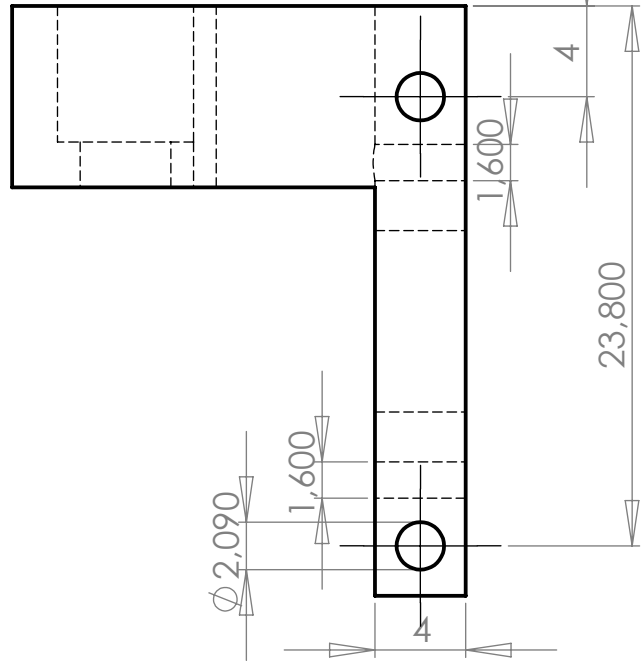
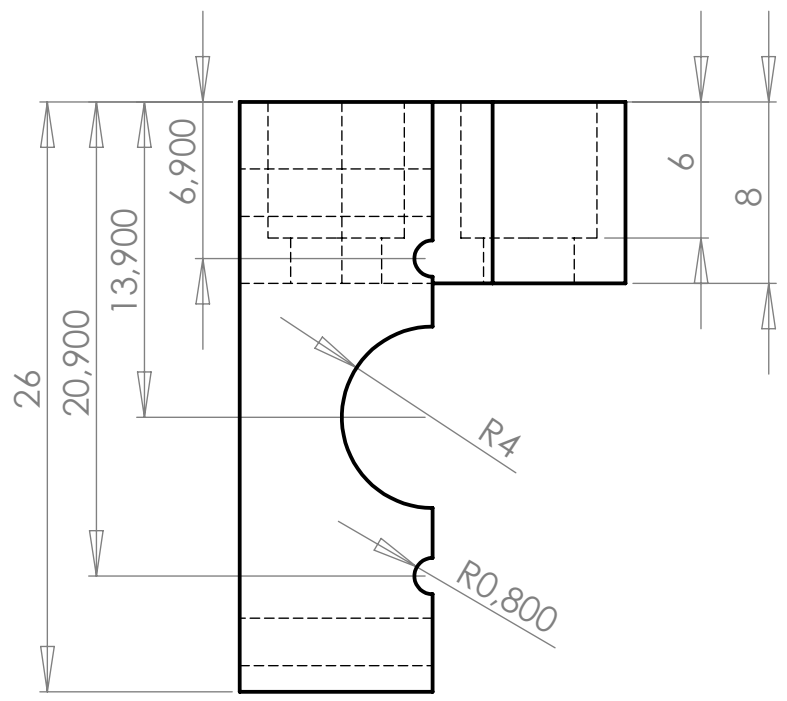
DWG NO.

outer Heatshield

A4

SCALE:2:1

SHEET 1 OF 1



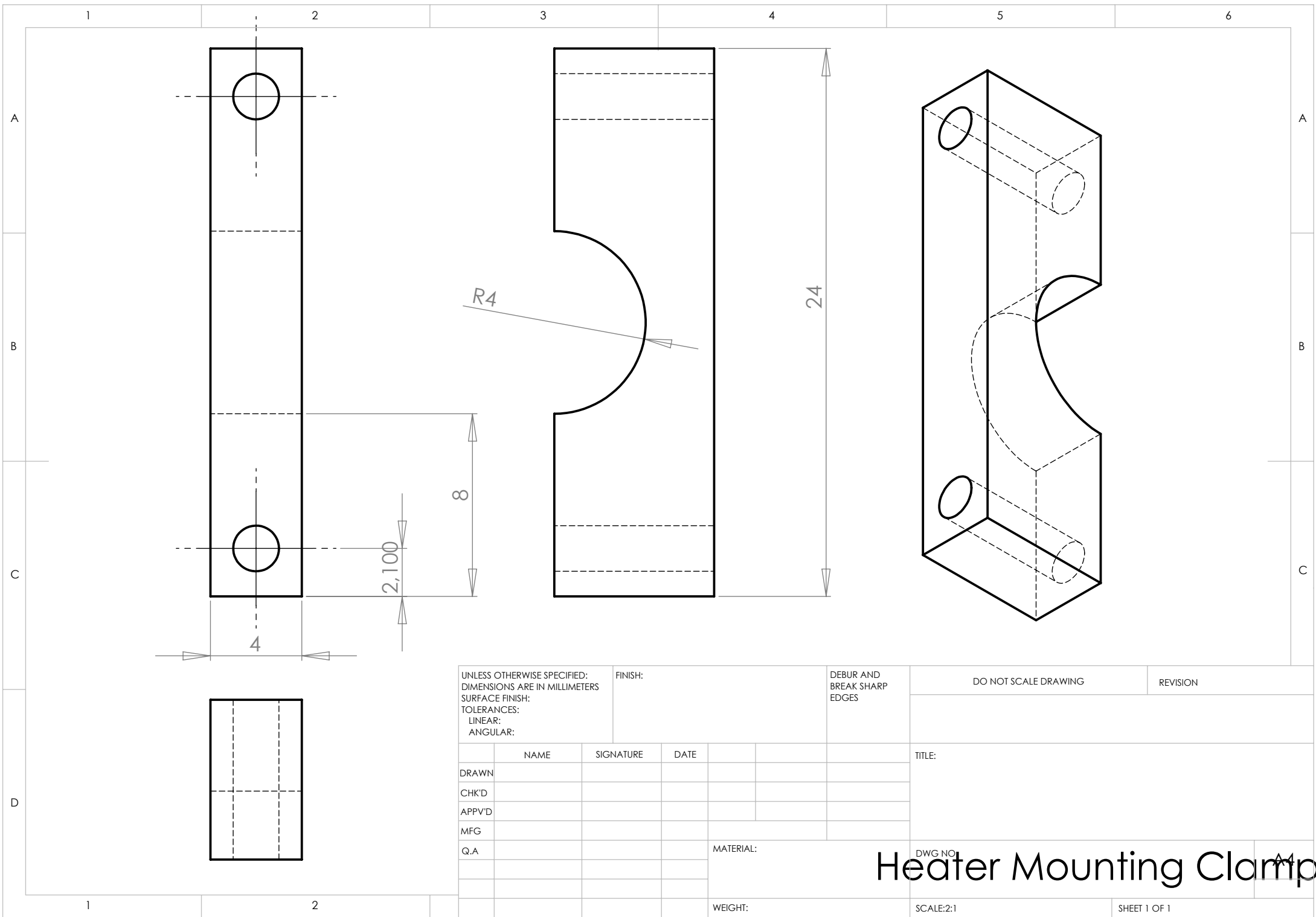
UNLESS OTHERWISE SPECIFIED:
 DIMENSIONS ARE IN MILLIMETERS
 SURFACE FINISH:
 TOLERANCES:
 LINEAR:
 ANGULAR:

FINISH:
 DEBUR AND
 BREAK SHARP
 EDGES

DO NOT SCALE DRAWING REVISION

	NAME	SIGNATURE	DATE		
DRAWN					
CHK'D					
APPV'D					
MFG					
Q.A					
				MATERIAL:	
				WEIGHT:	

TITLE:	
DWG NO.	Heater Mounting A4
SCALE:3:1	SHEET 1 OF 1



UNLESS OTHERWISE SPECIFIED:
 DIMENSIONS ARE IN MILLIMETERS
 SURFACE FINISH:
 TOLERANCES:
 LINEAR:
 ANGULAR:

FINISH:

DEBUR AND
 BREAK SHARP
 EDGES

DO NOT SCALE DRAWING

REVISION

	NAME	SIGNATURE	DATE		
DRAWN					
CHK'D					
APPV'D					
MFG					
Q.A					

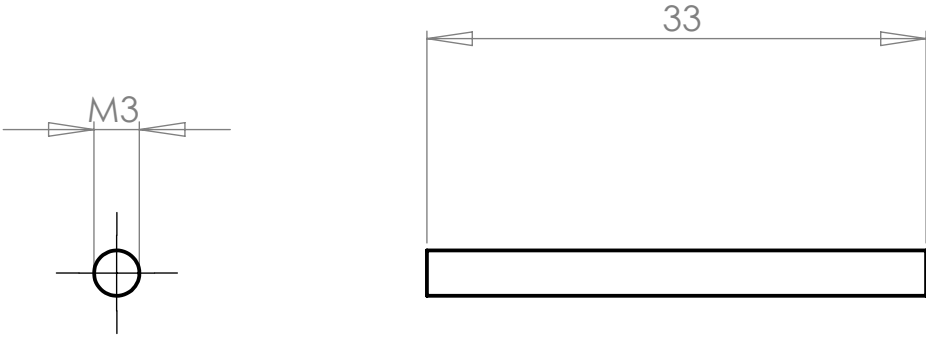
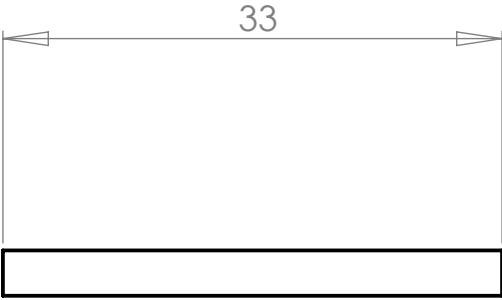
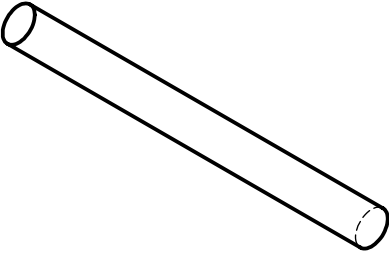
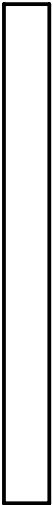
TITLE:

DWG NO:

Heater Mounting Clamp

SCALE:2:1

SHEET 1 OF 1

1		2		3		4		5		6	
A		B		C		D					
											
		<p>UNLESS OTHERWISE SPECIFIED: DIMENSIONS ARE IN MILLIMETERS SURFACE FINISH: TOLERANCES: LINEAR: ANGULAR:</p>		FINISH:		DEBUR AND BREAK SHARP EDGES		DO NOT SCALE DRAWING		REVISION	
		DRAWN		SIGNATURE		DATE		TITLE:			
		CHK'D									
		APPV'D									
		MFG									
		Q.A				MATERIAL:		DWG NO.		A4	
						WEIGHT:		SCALE:2:1		SHEET 1 OF 1	
								<h1>M3 Thread Rod</h1>			